PNAS RESEARCH ARTICLE | MICROBIOLOGY
ENVIRONMENTAL SCIENCES

Nutrient colimitation is a quantitative, dynamic property of microbial populations

Noelle A. Held[a,b,c,1], Aswin Krishna[a,d], Donat Crippa[a], Rachana Rao Battaje[e], Alexander J. Devaux[c], Anastasia Dragan[a], and Michael Manhart[a,b,e,f,1]

Affiliations are included on p. 10.

Edited by Alan Hastings, University of California, Davis, CA; received January 12, 2024; accepted November 5, 2024

Resource availability dictates how fast and how much microbial populations grow. Quantifying the relationship between microbial growth and resource concentrations makes it possible to promote, inhibit, and predict microbial activity. Microbes require many resources, including macronutrients (e.g., carbon and nitrogen), micronutrients (e.g., metals), and complex nutrients like vitamins and amino acids. When multiple resources are scarce, as frequently occurs in nature, microbes may experience resource colimitation in which more than one resource simultaneously limits growth. Despite growing evidence for colimitation, the data are difficult to interpret and compare due to a lack of quantitative measures of colimitation and systematic tests of resource conditions. We hypothesize that microbes experience a continuum of nutrient limitation states and that nutrient colimitation is common in the laboratory and in nature. To address this, we develop a quantitative theory of resource colimitation that captures the range of possible limitation states and describes how they can change dynamically with resource conditions. We apply this approach to clonal populations of *Escherichia coli* to show that colimitation occurs in common laboratory conditions. We also show that growth rate and growth yield are colimited differently, reflecting the different underlying biology of these traits. Finally, we analyze environmental data to provide intuition for the continuum of limitation and colimitation conditions in nature. Altogether our results provide a quantitative framework for understanding and quantifying colimitation of microbes in biogeochemical, biotechnology, and human health contexts.

microbial growth | biogeochemistry | nutrient limitation | marine microbes | colimitation

Significance

Much of what we know about microbes assumes a single nutrient limits growth, but does this reflect the ecological reality of microbes in nature? Understanding which nutrients limit growth, and by how much, is valuable for predicting and controlling microbial growth in environmental, biotechnological, and clinical contexts. We develop a framework that allows us to precisely quantify the extent of nutrient limitation in microbes. We show that nutrient availability differently affects how fast and how much microbes grow. Using our approach, we find evidence that multiple nutrients colimit microbial growth in typical laboratory experiments and that colimitation may be common for microbes in their natural habitats as well.

Resource availability is a fundamental control on microbial growth, physiology, and metabolic activity. Therefore, understanding which resources limit growth and by how much is both a core concept of microbiology as well as useful for predicting microbial contributions to biogeochemical cycles (1), inhibiting pathogens in the human body (2), and cultivating microbes in biotechnology (3). While limiting resources can be studied individually, there is evidence that microbes can be, and often are, limited by multiple resources simultaneously (colimitation) (4). For one thing, the elemental composition of the environment frequently reflects that of abundant microbes, suggesting a biogeochemical balance between supply and biological demand in nature (5–9). Furthermore, fundamental assumptions in ecology predict the possibility of colimitation; for instance, the coexistence of multiple species within a resource supply range, with each species depleting a specific resource, suggests a state of colimitation of the community as a whole (10–13). Accordingly, in situ experiments frequently find that adding multiple resources together enhances growth of microbial communities (1, 4, 14–19). Laboratory experiments have also found that microbial populations can completely deplete multiple resources simultaneously, suggesting the possibility of nutrient colimitation (3, 20).

Previous theoretical and empirical work on colimitation has largely considered limitation as a binary property of a resource (limiting or not) because of a principle known as the law of the minimum (3, 5, 21–24), which states that growth is solely determine by the scarcest resource relative to biological demand. As a result, empirical tests of colimitation, especially in natural samples, have primarily relied on factorial supplementation experiments, in which one measures the growth response to supplementing the population with multiple resources separately and in combination (1, 19). This approach has two major shortcomings. First, the outcomes of these experiments are usually interpreted only qualitatively, mainly by classifying the outcome as single limitation or colimitation (19, 23) (see *SI Appendix*, Fig. S1 *A* and *B* for a schematic

Author contributions: N.A.H. and M.M. designed research; N.A.H., A.K., D.C., R.R.B., A.J.D., A.D., and M.M. performed research; N.A.H., A.K., D.C., A.J.D., and M.M. analyzed data; and N.A.H. and M.M. wrote the paper.

The authors declare no competing interest.

This article is a PNAS Direct Submission.

[1]To whom correspondence may be addressed. Email: nheld@usc.edu or mmanhart@rutgers.edu.

This article contains supporting information online at https://www.pnas.org/lookup/suppl/doi:10.1073/pnas.2400304121/-/DCSupplemental.

Published December 18, 2024.

example). This binary approach neglects the possibility that populations occupy a continuum of limitation states rather than discrete categories. Furthermore, there has not been a common framework for quantifying these limitation outcomes, making them difficult to compare across studies. A similar ambiguity exists for laboratory experiments that attempt to designate a single limiting resource by keeping all other resources in excess, but without quantitatively determining what those concentrations must be to constitute single limitation. In both cases, this binary approach to limitation restricts our understanding and predictions of microbial growth in nature, where microbes experience a continuous range of resource concentrations and where many resources are simultaneously scarce (5, 8, 14, 19, 23, 25).

A second shortcoming of prior experiments, particularly supplementation experiments, is that these qualitative outcomes are very sensitive to the background resource conditions and the chosen concentrations of supplemented resources (*SI Appendix*, Fig. S1). Besides the fact that these experiments therefore cannot tell us about the general potential for colimitation in the system beyond the starting background conditions (23), we do not know a priori how to choose the supplemented concentrations; different choices can lead to completely different outcomes, even mistaking single limitation for colimitation (*SI Appendix*, Fig. S1 *C* and *D*).

Here, we address these issues by providing a quantitative theory of resource colimitation that goes beyond the binary law of the minimum perspective. In contrast to the chemical definition of colimitation used in some previous laboratory studies—whether multiple resources are simultaneously depleted to zero (20, 26, 27)—we suggest a biological definition (how is growth affected by the resources?) because 1) this allows precise identification of resource colimitation for different growth, activity, or physiological parameters of interest; 2) this strategy can be used in either batch or chemostat cultures, meaning also that growth rate and growth yield colimitation can be quantified separately; and 3) this allows instantaneous definitions of resource limitation and colimitation. We focus on independent resources, such as carbon and nitrogen sources, in clonal populations of microbes as a model case for untangling the fundamental principles of colimitation, but our results are generalizable to other types of resource combinations [substitutable or chemically dependent (5, 23)], multispecies communities (13, 28), and higher trophic levels (19, 23, 29, 30). We use this approach to test the hypothesis that microbes can experience a continuum of colimitation states and that these states are common enough to be observed in laboratory experiments and natural environments. We find that a wide range of laboratory conditions commonly used to study *Escherichia coli* have a significant degree of colimitation for glucose and ammonium and that growth rate and growth yield are colimited differently. We also find that data on microbes in their natural environments is consistent with a continuum of colimitation states. This work develops a theoretical foundation for more systematically testing whether colimitation is common in nature, whether there are distinct physiological states associated with colimitation, and how resource colimitation impacts ecological, clinical, biotechnological, and biogeochemical outcomes.

Results

A Quantitative Approach to Colimitation of Microbial Populations. In contrast with the qualitative types of limitation (single limitation, serial limitation, additive colimitation, etc.) usually obtained in factorial supplementation experiments (5, 6, 8, 14, 19, 23, 31), we introduce a framework for precisely quantifying limitation states of populations without choosing arbitrary thresholds and categories. While in this article we focus on single-species populations of microbes, the approach can be similarly applied to study colimitation in multispecies communities (13, 28) and other organisms such as plants (19) and animals (23, 29, 30).

The per-capita growth rate g of a population typically depends on a large number M of individual limiting processes, which include uptake and utilization of different resources from the environment as well as internal cellular processes such as transcription and translation. Let r_i be the rate of each process i. We define the limitation coefficient of growth rate for process i as the relative change in growth rate for a small relative change in the rate of that process (3, 32):

$$L_i^{\text{rate}} = \frac{r_i}{g}\frac{\partial g}{\partial r_i}. \quad [1]$$

The superscript "rate" indicates that this describes limitation of the growth rate, as opposed to other growth traits as we will discuss later. For example, $L_i^{\text{rate}} = 1$ means that a 1% increase in r_i entails a 1% increase in growth rate, whereas $L_i^{\text{rate}} = 0.5$ means that a 1% increase in r_i changes growth rate only by half as much, 0.5% (*SI Appendix*, section S1). For essential processes like uptake and utilization of carbon and nitrogen sources, we generally expect L_i^{rate} to range from 0 (when r_i is high and the growth rate no longer depends on it) to 1 (when r_i is low and the growth rate is proportional to it). However, other values are possible if growth rate depends superlinearly or negatively on r_i (for example, if an antibiotic reduces the growth rate).

Eq. **1** is analogous with control coefficients in metabolic control analysis (33), and as in that framework, we can prove that the sum of limitation coefficients over all limiting processes must equal 1 (*SI Appendix*, section S1):

$$\sum_{i=1}^{M} L_i^{\text{rate}} = 1. \quad [2]$$

This means that greater limitation for uptake of one resource or other process necessarily entails less limitation for other processes. Finally, we define the effective number of growth rate-limiting processes as a metric for colimitation:

$$M_{\text{eff}}^{\text{rate}} = \sum_i \frac{L_i^{\text{rate}}}{\max_j L_j^{\text{rate}}} = \frac{1}{\max_i L_i^{\text{rate}}}. \quad [3]$$

This quantity counts processes weighed by their limitation relative to the most limiting process. For example, if we have four processes with $L_1 = 0.4$, $L_2 = 0.3$, $L_3 = 0.2$, and $L_4 = 0.1$, then each counts as effectively 1, 0.75, 0.5, and 0.25 limiting processes, respectively, so that the total effective number of limiting processes is $M_{\text{eff}}^{\text{rate}} = 2.5$. For typical models of the limitation coefficients, values of $M_{\text{eff}}^{\text{rate}}$ will range from 1, when only one process is limiting at all, to M (the total number of processes) if all processes are equally limiting (*SI Appendix*, section S1 and Fig. S2).

How does the availability of resources in the environment limit growth? The uptake rate r of a resource is typically assumed to be proportional to the external concentration R according to the law of mass action (24, 34):

$$r = aR. \quad [4]$$

The proportionality constant a is sometimes known as the affinity for the resource (35). To model the dependence of growth rate on this variable resource, we must account for the role of all other resources and internal processes that growth depends on, such as the rate of transcription and translation. If we are only varying the one resource, then we can capture all these implicit limiting factors by a single rate $g_{\max}$, which describes the maximum growth rate when the uptake rate r for the variable resource is saturated; at this point, growth is limited by something else, whether it be availability of another resource or an internal cellular process such as the rate of transcription or translation. We refer to these other factors as implicit since we do not vary or measure them, and thus they cannot be distinguished from each other. One way to model the dependence of growth on both the variable resource and the implicit factors is to invoke the law of the minimum, so that the growth rate equals the rate of whichever process (uptake of the variable resource or all implicit processes combined) is slower:

$$g(R) = \min(aR, g_{\max}). \quad [5]$$

Eq. **5** is sometimes known as the Blackman model (36, 37). As shown by the solid lines in Fig. 1*A*, this model has binary limitation states: for resource concentrations $R < g_{\max}/a$, the limitation coefficient for the resource is 1, meaning that the implicit factors have zero limitation. For concentrations $R > g_{\max}/a$, the limitation flips and now the implicit factors are solely limiting. As a result, there can be no colimitation between the variable resource and the implicit factors. Conceptually, this situation arises if the uptake and utilization of the resource occur in parallel with the implicit factors (24, 28).

However, empirical measurements of growth rate dependence on resource concentration frequently support the Monod model (38, 39):

$$g(R) = g_{\max}\frac{aR}{aR + g_{\max}}. \quad [6]$$

While the Monod and Blackman models have similar asymptotic behavior, the Monod model entails a smooth transition between limitation regimes, meaning that the variable resource and the implicit factors are colimiting for a finite range of concentrations around $R = g_{\max}/a$ (Fig. 1*A*, dashed lines). Note that $g_{\max}/a$ is often denoted as K, the half-saturation concentration (39). In particular, the Monod dependence means that limitation and colimitation take on a continuum of values, rather than being discrete states of a population as often identified in previous colimitation studies using factorial supplementation experiments. For example, Fig. 1*A* shows that the number of limiting factors can take intermediate values such as 1.5 if the two process have unequal but nonzero degrees of limitation ($L = 2/3$ for one process and $L = 1/3$ for another). Conceptually, colimitation of growth rate arises when resource uptake and utilization occurs sequentially with the implicit processes (whether that is use of another resource or an internal cellular process), so that changes in either step affect the total rate (24, 28). Note that smooth models with colimitation such as the Monod model must always have lower growth rates than do models without colimitation for the same concentration conditions, assuming the models have the same asymptotic properties.

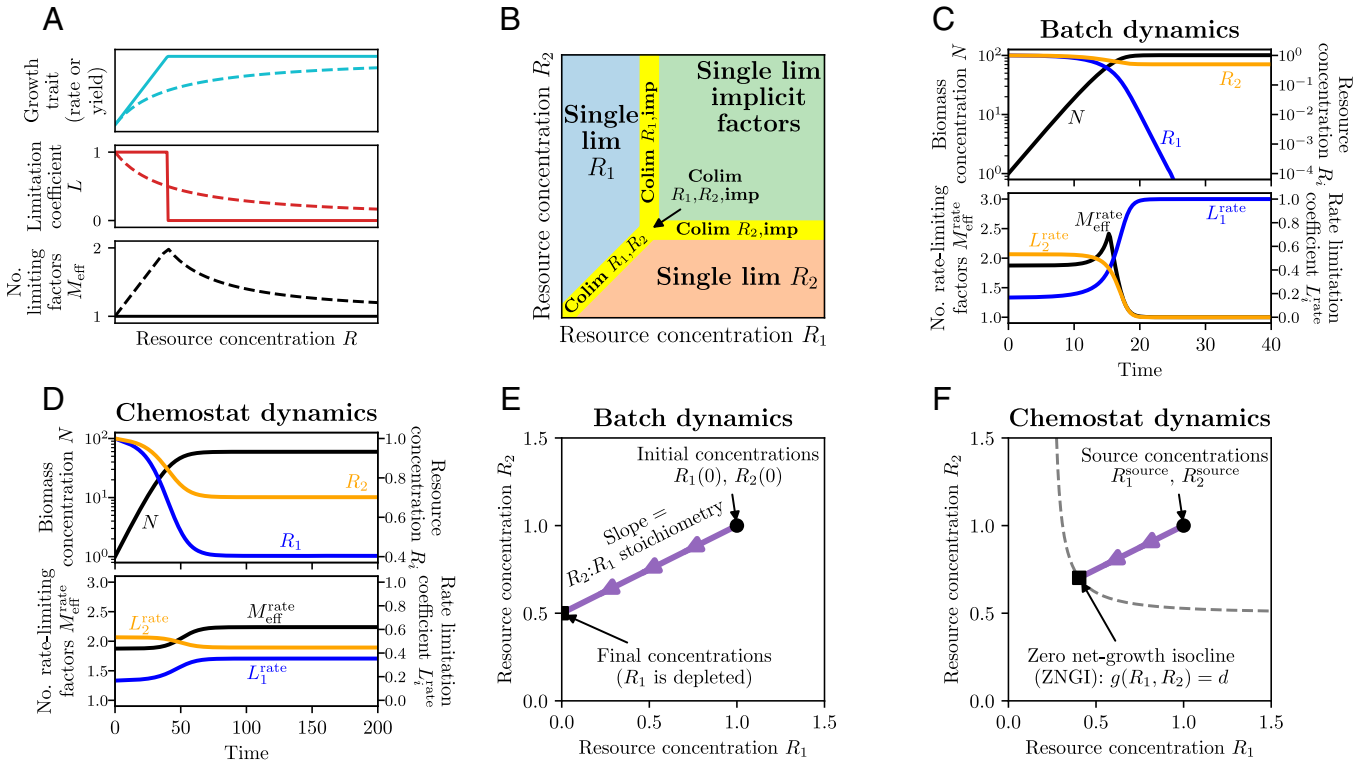

Fig. 1. Quantifying resource limitation and colimitation. (*A*) Schematics of how a growth trait (e.g., growth rate or growth yield) depends on a variable resource concentration. The solid lines show the Blackman model (Eq. **5**), which does not have colimitation of the resource and the implicit factors, while the dashed lines show the Monod model (Eq. **6**), which does have colimitation. (*B*) Schematic of limitation regimes over two resource concentrations. "Imp" denotes implicit limiting factors besides the two variable resources. (*C*) Simulation of batch culture dynamics and resource limitation for a population consuming two resources (blue and orange). (*D*) Same as (*C*) but for chemostat dynamics. (*E*) Trajectory of resource depletion for the batch dynamics in (*C*). (*F*) Same as (*E*) but for the chemostat dynamics in (*D*). Model parameters for (*C*)–(*F*) are $g_{\max} = 1$, $a_1 = 1$, $a_2 = 0.5$, $s_1 = 100$, $s_2 = 200$, $d = 0.2$ (*SI Appendix*, sections S2 and S3).

Since microbes rely on many resources to grow, it is important to generalize this approach to multiple variable resources. There are many models that generalize the Blackman (Eq. **5**) or Monod (Eq. **6**) dependence on multiple resources (*SI Appendix*, section S2), some of the most common being the Liebig Monod model (5, 23, 24, 28, 29, 34), the multiplicative Monod model (3, 5, 23, 28, 29, 40, 41), the Poisson arrival time/synthesizing-unit model (24, 29, 34, 42), and the additive model (29, 34). The limitation states predicted by these models almost all follow the schematic for two variable resources in Fig. 1*B* (*SI Appendix*, Fig. S3): there are regimes of single limitation for each of the variable resources, as well as for the implicit factors, separated by conditions of colimitation. This picture assumes both resources are independently essential and nonsubstitutable (e.g., a carbon source and a nitrogen source), but it can be generalized to substitutable (3, 5, 43) and chemically dependent resources (5) (*SI Appendix*, section S2 and Fig. S4). Note that while it is common to speak of limitation for individual elements like carbon and nitrogen, in general, we must specify the precise molecular forms of these elements since those forms can have distinct biological effects.

The quantitative nature of limitation means that it can rapidly change with the environment. For example, consider a population consuming two essential resources under batch dynamics, such that the two resources are supplied in an initial pulse (*SI Appendix*, section S3). Fig. 1*C* (*Top* panel) shows how the biomass concentration increases exponentially while the two resources are depleted. While the orange resource is more limiting initially, the blue resource becomes more limiting later before growth stops (*Bottom* panel of Fig. 1*C*). The degree of resource colimitation, measured by the number of rate-limiting factors $M_{\text{eff}}^{\text{rate}}$, peaks at an intermediate time when the two resources have equal limitation. In Fig. 1*D* we show the limitation dynamics of the same system but in a chemostat, where resources are supplied to the population at constant rate (*SI Appendix*, section S3).

Limitation of Growth Yield Is Distinct from Limitation of Growth Rate. Besides affecting how fast a population grows (growth rate), resource concentrations also determine how much biomass grows over a period of time, which we refer to as the growth yield. If the stoichiometry of biomass to each resource is constant (e.g., each gram of dry weight requires a fixed amount of glucose) and growth stops only when one resource concentration reaches zero, yield depends on resource concentrations according to the law of the minimum (similar to Eq. **5** for growth rates), since the total yield will be set by whichever resource produces the least amount of biomass (*SI Appendix*, section S3). Under these conditions, a single resource will therefore always be limiting, and there can be no colimitation for yield except when the resources are supplied in the exact stoichiometry that matches biological demand. For example, Fig. 1*E* shows the trajectory of resource depletion for the batch dynamics in Fig. 1*C*. The slope of the trajectory is the stoichiometry of resource use, so that constant stoichiometry means straight lines, with the length of the line being proportional to yield (*SI Appendix*, section S3 and Fig. S5*A*). Thus the yield will change if the initial concentration of resource 1 changes by a small amount (which shifts the line horizontally and increases its length), while small changes in the initial concentration of resource 2 will not change the yield (since that shifts the trajectory vertically and does not change its length).

However, the yield can depend smoothly on both resource concentrations, and hence display colimitation, if the biomass stoichiometry of one resource changes with the concentration of another resource (*SI Appendix*, section S3 and Fig. S5*B*), or if the resource concentrations at which growth stops depend on each other (*SI Appendix*, section S3 and Fig. S5*C*). The first case, variable stoichiometry, is possible through a variety of mechanisms, including resource consumption for biomass maintenance (*SI Appendix*, section S3 and Fig. S6 *A* and *B*) and proteome allocation that varies with growth rate (*SI Appendix*, section S3 and Fig. S6 *C* and *D*). The second case holds for chemostat dynamics if the zero net-growth isocline (43) (ZNGI, where growth rate equals the dilution rate; dashed line in Fig. 1*F*) is curved; even with fixed stoichiometry so that depletion trajectories are straight lines, their length to the ZNGI (which is proportional to the yield) will depend on the supplied concentration of both resources (Fig. 1*F*; *SI Appendix*, section S3 and Fig. S6 *E* and *F*).

We quantify growth yield limitation analogously with growth rate limitation, defining yield limitation coefficients L_i^{yield} (Eq. **1** but replacing growth rate with growth yield) and the number of yield-limiting factors $M_{\text{eff}}^{\text{yield}}$ (Eq. **3** but with L_i^{yield} instead of L_i^{rate}). We can also use equivalent mathematical models for describing how growth yield depends on resource concentrations (*SI Appendix*, section S2), leading to similar possibilities for colimitation as seen for growth rate (Fig. 1 *A* and *B*). However, growth rate and growth yield limitation are biologically distinct aspects of populations. In particular, resources may limit rate and yield differently—for example, in Fig. 1*C* the orange resource limits growth rate initially but the blue resource limits growth yield since it is depleted at the end. That being said, rate and yield limitation are coupled under certain circumstances. In batch dynamics, the yield-limiting resource (the one depleted when growth stops) is also necessarily the most rate-limiting resource at the end of batch growth. Under chemostat dynamics, growth rate limitation determines growth yield limitation because the former sets the shape of the ZNGI (13, 43). For example, if two resources obey a model without growth rate colimitation, then the ZNGI forms a right angle, in which case there is also no yield colimitation (28).

Growth Rate and Yield of *E. coli* Are Colimiting for Glucose and Ammonium Under Laboratory Conditions. To demonstrate our quantitative approach to colimitation, we measure the dependence of *E. coli* growth rate and yield on glucose and ammonium, two essential resources, under laboratory conditions. We also use these empirical measurements to address the second major shortcoming of traditional colimitation tests: instead of using only a single background condition and supplemented concentration for each resource, which cannot conclusively determine the extent of colimitation in a system (23) (*SI Appendix*, Fig. S1), we systematically scan a wide range of glucose and ammonium concentrations to determine the global potential for colimitation (*Materials and Methods*; Datasets S1 and S2; *SI Appendix*, Figs. S7–S11).

As expected, the data show a Monod-like dependence in which the growth rate depends on glucose and ammonium concentrations when they are low, but once they are sufficiently high, growth rate saturates as implicit factors become limiting (Fig. 2 *A* and *B*). To quantify colimitation in these data, we first fit the data to a range of models both with and without colimitation (*SI Appendix*, Table S1 and Figs. S12–S14). We find that while the fits favor a model with colimitation (Poisson arrival time model; *SI Appendix*, section S2) for two of the three experimental replicates, this result is not conclusive as the models without colimitation also fit the data fairly well (*SI Appendix*, Fig. S14).

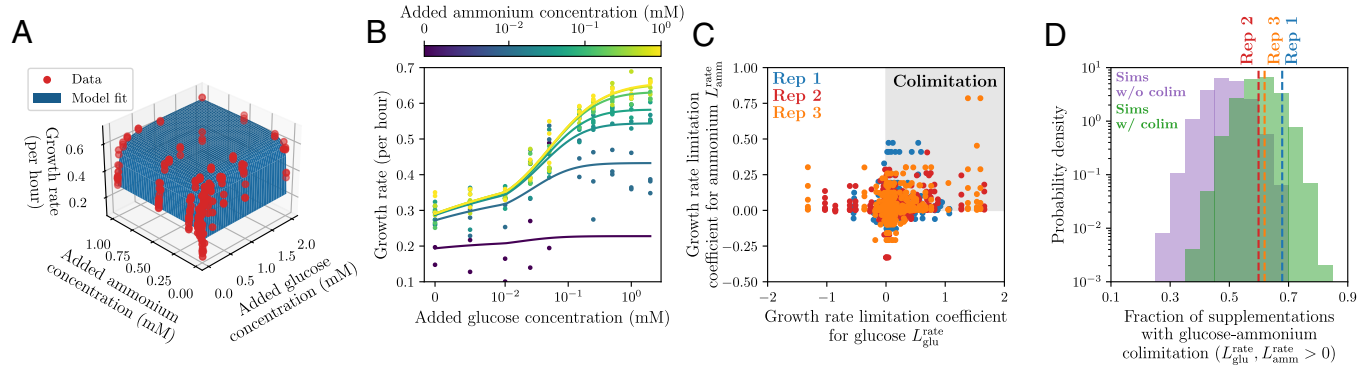

Fig. 2. Measuring growth rate colimitation in laboratory conditions. (*A*) Three replicate measurements of growth rate (red points) over glucose and ammonium concentrations for *E. coli* in minimal medium (*Materials and Methods*; Dataset S1; see *SI Appendix*, Figs. S7–S9 for growth curves). The blue surface is a model fit to all replicate measurements (Poisson arrival time model with $g_{max} \approx 0.66$ per hour, $a_{glu} \approx 23$ per hour per mM glucose, $a_{amm} \approx 90$ per hour per mM ammonium; $R_{glu,min} \approx 0.023$ mM, $R_{amm,min} \approx 0.0039$ mM; *Materials and Methods*; Dataset S1). (*B*) Same growth rate data as in (*A*) but plotted as a function of glucose concentration alone, with colors indicating ammonium concentrations. The lines are the same fitted model as in (*A*). (*C*) Growth rate limitation coefficients for glucose and ammonium from supplementations inferred from data in (*A*); the three replicate experiments are shown as different colors. The gray box marks the region of points with apparent colimitation of glucose and ammonium ($L^{rate}_{glu}, L^{rate}_{amm} > 0$). (*D*) Fractions of supplementations with growth rate colimitation between glucose and ammonium. The observed fractions from the three replicate experiments are marked with dashed lines of different colors. Compared to a null model without glucose-ammonium colimitation (purple, 10^4 simulations of the Liebig Monod model; *SI Appendix*, section S2), the probabilities of observing at least as much colimitation as in the data are $P = 0.0004$ for replicate 1, $P = 0.0338$ for replicate 2, and $P = 0.0135$ for replicate 3. Simulated datasets from a model with glucose-ammonium colimitation (green, Poisson arrival time model; *SI Appendix*, section S2) show levels of colimitation more consistent with the data. The simulations use parameters from the fits of these models to the experimental data and random noise estimated from the variation across experimental replicates (*Materials and Methods*).

However, these fits are based on an optimization that weighs all data points equally. Therefore, this approach may not be sufficiently sensitive to differences in the subset of concentrations where there is approximate balance of limitation between resources, such that colimitation can occur. An alternative approach is to measure the occurrence of apparent colimitation in the data directly and compare it to a null model without colimitation; therefore even if the number of colimitation conditions is too few to sway the overall outcome of a fit, it can still be distinguished from the null model to statistically indicate the presence of colimitation. To this end, we leverage the combinatorially complete set of concentration conditions in our data to infer the glucose and ammonium limitation coefficients of all possible supplementations on all background conditions contained within our data (*Materials and Methods*). This direct-from-data approach is independent of the fits as the limitation coefficients are estimated as finite differences in growth rates and resource concentrations. Fig. 2*C* shows these limitation coefficients for all supplementations across all three replicate datasets.

In principle, any points where L^{rate}_{glu} and L^{rate}_{amm} are both greater than zero indicate colimitation (Fig. 2*C*, gray box; *SI Appendix*, Fig. S15*A*). However, measurement noise could cause such observations to randomly appear even in the absence of true colimitation (*SI Appendix*, Fig. S15*B*). To determine whether the amount of observed glucose-ammonium colimitation is greater than would be expected from noise, we simulate a large number of datasets using models with and without colimitation but based on parameters and measurement noise fit to the data (*Materials and Methods*; *SI Appendix*, Figs. S16–S19). For each simulated dataset, we calculate the fraction of supplementations with glucose-ammonium colimitation. Compared to 10^4 simulations of a null model without glucose-ammonium colimitation (purple distribution in Fig. 2*D*; *SI Appendix*, Fig. S20), we find that the probabilities of generating colimitation levels at least as high as in each of our experimental replicates (*P*-values) are 0.0004, 0.0338, and 0.0135. In contrast, a null model that does have glucose-ammonium colimitation is largely consistent with the data (green distribution in Fig. 2*D*). These data therefore support the existence of growth rate colimitation between glucose and ammonium for *E. coli* under laboratory conditions. We perform an analogous analysis on our growth yield data and obtain similar results demonstrating the occurrence of yield colimitation for glucose and ammonium (*SI Appendix*, Figs. S21–S30).

Comparison of Growth Rate and Growth Yield Limitation in *E. coli*. Given the evidence of colimitation in our data, we can use the fitted colimitation models to quantitatively map different limitation states across resource concentrations. This is important for performing comparative measurements of cell physiology, ecology, or evolution across resource conditions; instead of simply postulating that a condition with low glucose and high ammonium is carbon-limiting, for example, we can precisely define how limiting that state really is. Fig. 3*A* shows limitation coefficients of glucose and ammonium for growth rate (*Top* panel) and growth yield (*Bottom* panel) across concentrations. We find that *E. coli* in typical M9 medium (0.2% ≈ 11.1 mM glucose, 18.7 mM ammonium) has growth rate limitation coefficients of $L^{rate}_{glu} \approx 3 \times 10^{-3}$ and $L^{rate}_{amm} \approx 10^{-4}$; this means that there is approximately single limitation for the implicit factors ($L^{rate}_{imp} \approx 0.997$, $M^{rate}_{eff} \approx 1.003$). On the other hand, the limitation coefficients for growth yield in these conditions are $L^{yield}_{glu} \approx 0.27$ and $L^{yield}_{amm} \approx 0.04$, which means there is an appreciable amount of colimitation, especially between glucose and the implicit yield-limiting factors ($L^{yield}_{imp} \approx 0.69$, $M^{eff}_{yield} \approx 1.5$).

Fig. 3*B* compares growth rate and growth yield colimitation across a broad range of glucose and ammonium concentrations (compare to Fig. 1*B*; *SI Appendix*, Fig. S31). The blue region marks conditions of significant colimitation (where neither glucose nor ammonium nor the implicit factors individually has more than 95% of total limitation for growth rate), while the red region marks the analogous conditions for growth yield.

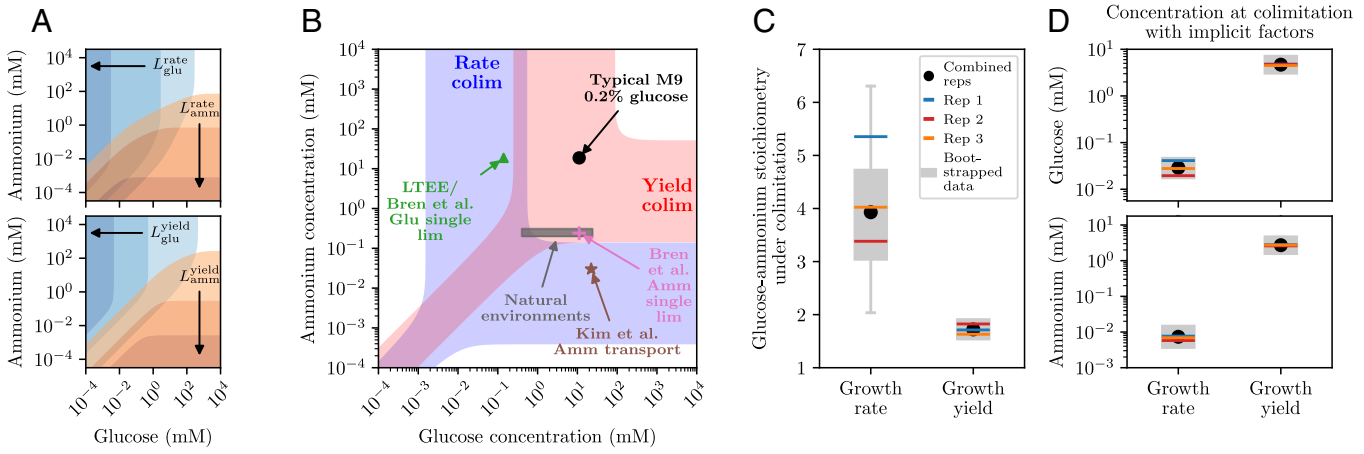

Fig. 3. Comparison of growth rate and growth yield colimitation in *E. coli*. (*A*) Using models fitted to measurements of growth rate (*Top*) and growth yield (*Bottom*), contours of limitation coefficients for glucose (blue) and ammonium (orange). From lightest to darkest, the contours show limitation coefficients above 10^{-4}, 0.01, and 0.9 for growth rate (*Top*), and above 0.01, 0.9, and 0.999 for growth yield (*Bottom*). (*B*) Diagram of rate and yield colimitation regimes in *E. coli* across glucose and ammonium concentrations in M9 medium. The blue shaded region shows concentrations of glucose and ammonium with significant colimitation (between glucose, ammonium, and implicit factors), where no one factor is limiting more than 95% of growth rate ($M_{\text{eff}}^{\text{rate}} > 1.05$). The red shaded region is the analogous concentration range for growth yield colimitation. Symbols mark reference concentrations of glucose and ammonium used in other studies: typical M9 medium (0.2% ≈ 11.1 mM glucose, 18.7 mM ammonium); putative single limitation condition for glucose (0.14 mM glucose, 18.7 mM ammonium) used by Bren et al. (44), which is very similar to the concentrations used in the long-term evolution experiment (45) (but with ≈15.2 mM ammonium in Davis–Mingioli medium); putative single limitation condition for ammonium (11.1 mM glucose, 0.24 mM ammonium) used by Bren et al. (44); conditions at which Kim et al. (46) found that *E. coli* activates its ammonium transporter (22.2 mM glucose, 0.03 mM ammonium); and the estimated range of natural environments for *E. coli* (0.4–24 mM glucose, 0.2–0.31 mM ammonium; Dataset S3). (*C*) Stoichiometry of glucose to ammonium in glucose-ammonium colimitation for growth rate and growth yield. For growth rate colimitation, this is calculated as the ratio of ammonium to glucose affinities fitted by the models to the data; for growth yield, this is calculated as the ratio of ammonium to glucose biomass stoichiometries fitted to the data (*SI Appendix*, section S2). The black point shows the stoichiometry from the fit to all three experimental replicates combined, while the colored bars represent the fits to each replicate individually. The gray boxes (first to third quartiles, with the whiskers extending to 1.5 times the interquartile range above and below) show the distributions of fitted stoichiometry across 100 datasets bootstrapped from the three replicates (*Materials and Methods*). (*D*) Same as (*C*) but for the concentrations of glucose (*Top* panel) and ammonium (*Bottom* panel) at which they are colimiting with the implicit limiting factors (such as another resource or an internal cellular process).

Together they demonstrate that a wide range of conditions—from approximately 1 μM to 100 mM of either glucose or ammonium—have some degree of colimitation for either growth rate or growth yield. We also find that the conditions of glucose and ammonium colimitation for growth rate overlap significantly with those for growth yield, but growth rate and growth yield have largely nonoverlapping conditions for colimitation between the implicit limiting factors and either glucose or ammonium. Besides typical M9 medium, we also compare our colimitation map to several other reference media conditions, including the long-term evolution experiment (45) (green triangle, with the caveat that that experiment uses Davis–Mingioli rather than M9 medium and a different strain of *E. coli*); conditions for putative single limitation for glucose and for ammonium used in a study by Bren et al. (44) (green triangle and pink cross); conditions at which *E. coli* activates its ammonium transporter (46) (brown star); and the estimated range of glucose and ammonium in *E. coli*'s natural environment (gray box; *Materials and Methods*; Dataset S3).

It is also valuable to quantitatively compare the colimitation conditions between growth rate and growth yield. We find that the glucose-ammonium stoichiometry needed for growth rate colimitation between glucose and ammonium is approximately 4 (C:N = 24), while it is approximately 1.7 (C:N = 10.2) for growth yield colimitation (Fig. 3*C*). Both values suggest that the environment under these apparently balanced conditions must have a C:N ratio much higher than the typically observed *E. coli* biomass C:N ratio (47) (4.33 to 5.17 depending on the growth conditions). This may be due to the requirement that some carbon is respired for energy production. The conditions for colimitation between implicit factors and glucose or ammonium are also quite different between growth rate and growth yield, with the concentrations being approximately 100-fold higher for growth yield colimitation than for growth rate colimitation (Fig. 3*D*). This suggests that the implicit limiting factors for growth rate and growth yield are different, which is not surprising, but this may also be indicative of the different selection pressures on rate versus yield limitation. For example, stronger selection on rate limitation compared to yield limitation may have driven rate limitation toward much lower resource concentrations.

Quantifying Colimitation of Growth Rate and Growth Yield in Natural Environments. While we have shown that colimitation can occur in the laboratory, an important but more complex problem is to test whether colimitation occurs for microbes in their natural environments (4). We now demonstrate our quantitative approach by estimating limitation and colimitation in several natural ecosystems. To quantify colimitation of growth rate, we collected measurements of half-saturation resource concentrations K_i [measured from the dependence of growth rate on that resource concentration according to the Monod model (39)] and environmental concentrations R_i for those same resources across many organisms (Fig. 4*A*; *Materials and Methods*; Dataset S3). Note that some strains with laboratory measurements are different from those in the natural environments and hence may have different trait values (39).

We use these data to estimate limitation for each resource, assuming all other resources for these organisms are present at very high concentrations (*SI Appendix*, section S1). Since the true dependence of growth rate on multiple resources is unknown for these organisms and resources, we consider four common growth rate models (Liebig Monod, multiplicative Monod, Poisson arrival time, and additive; *SI Appendix*, Table S1 and section S2)

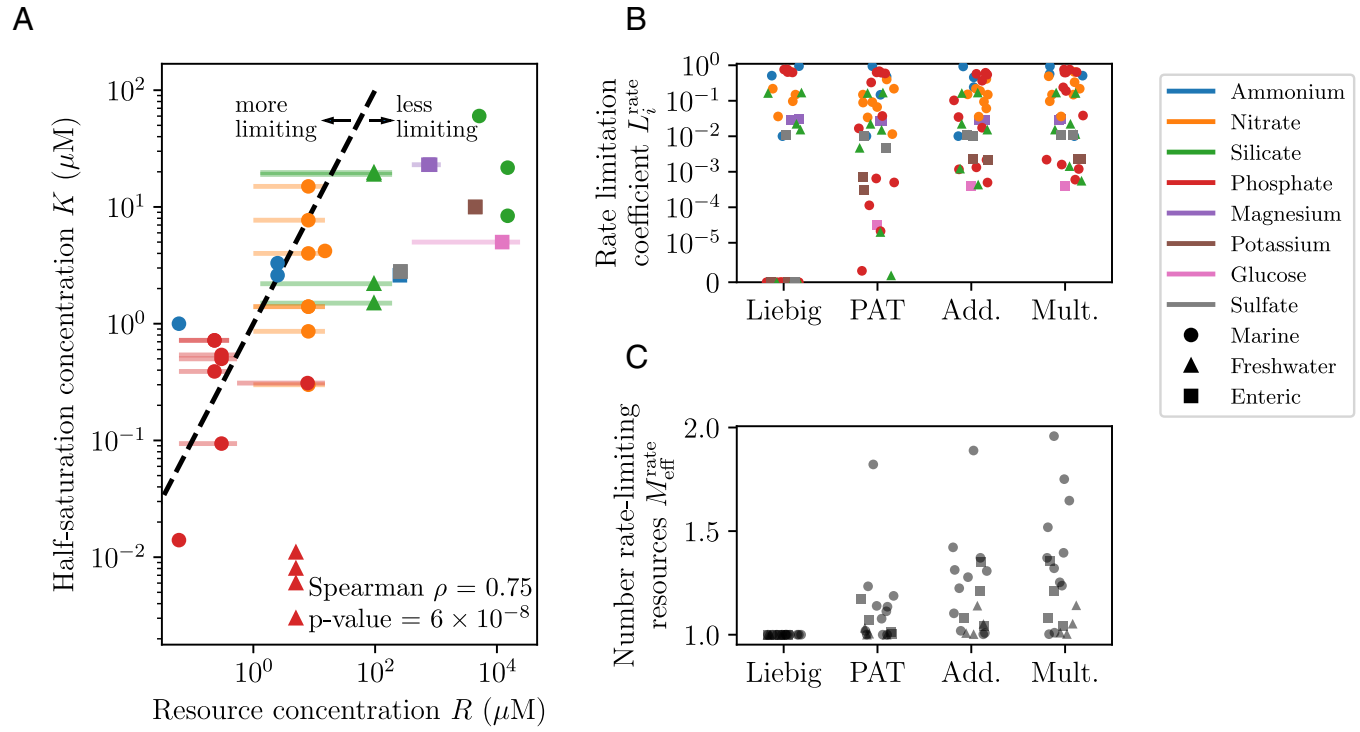

Fig. 4. Applying limitation concepts to empirical growth rate data across species and resources. (*A*) Half-saturation concentrations *K* versus representative estimates of environmental concentrations *R* from various organisms, resources, and environments collected from the literature (*Materials and Methods*; Dataset S3). When we found estimates of environmental concentrations *R* as ranges, we indicate this in the plot by horizontal bars attached to the symbol. Symbol color indicates resource, and shape indicates habitat. (*B*) Rate limitation coefficients (L_i^{rate}) calculated from the data shown in (*A*); we calculated limitation coefficients for individual resources in all organism/resource combinations, considering four common growth rate models (horizontal axis: Liebig = Liebig Monod model, PAT = Poisson arrival time model, Add. = additive model, Mult. = multiplicative Monod model; *SI Appendix*, Table S1 and section S2). (*C*) Number of rate-limiting resources $M_{\text{eff}}^{\text{rate}}$ among the resources in the data shown in (*A*), also considering the same growth rate models as in (*B*). Each organism has data for a pair of resources, such that the maximum number of limiting resources is 2 (we exclude implicit factors since we do not have sufficient data for them in the natural environments; *SI Appendix*, section S1) .

to calculate limitation coefficients in Fig. 4*B*. The analysis reveals the necessity of our quantitative approach: the data show a continuum of limitation coefficients, rather than a dichotomy of high and low limitation (*SI Appendix*, Fig. S32). In particular, we find significant intermediate limitation coefficients for many of the marine species, but low limitation for the freshwater and enteric species. This is evident from the *R* and *K* data itself; most half-saturation concentrations *K* are less than their corresponding environmental concentrations *R*, which means low limitation, with the exceptions being several marine strains on phosphate, nitrate, and ammonium (Fig. 4*A*). The lack of large growth rate limitation coefficients is not surprising given the strong selection to reduce the half-saturation concentration relative to the environment (39). We moreover see a continuum of growth rate colimitation states between these resources according to the number of rate-limiting resources $M_{\text{eff}}^{\text{rate}}$ (Fig. 4*C* and *SI Appendix*, Fig. S32). The degree of colimitation seems to be linked to habitat; several of the marine species show high colimitation, and some enteric species show intermediate colimitation as well.

To demonstrate quantification of colimitation for growth yield, we apply our approach to elemental resources for marine phytoplankton. Using the abundance of each element in the ocean and its stoichiometry in phytoplankton biomass (6), we calculate the maximum potential growth yield of each element (Fig. 5*A*); this is the maximum amount of biomass that could grow from that element's concentration in the ocean, if all other elements were unlimited. This shows roughly three tiers of resources, separated by orders of magnitude: the trace metals iron, cobalt, and manganese have the lowest potential yields, followed by another set of similar potential yields for nitrogen, phosphorus, and other metals. The remaining elements all have much higher potential yields.

From these potential yields, we can calculate yield limitation coefficients for each elemental resource. Since we do not know how phytoplankton growth yield depends on multiple resources, we use a phenomenological model that generalizes the additive model, with a variable parameter that captures interactions between resources in determining the yield (*SI Appendix*, section S2). For weak interactions between resources, limitation is strongly concentrated in the resource most rare relative to its biomass requirements, especially iron (Fig. 5*B*), and hence there is little colimitation (Fig. 5 *B*, *Inset*). For stronger resource interactions, we see greater colimitation for yield across resources.

This analysis reflects known patterns of oceanic nutrient limitation, such as the prevalence of iron limitation as well as nitrogen and phosphorus limitation, and the possibility of limitation by trace metals such as cobalt and manganese (1, 6). While the data we used are coarse-grained and do not account for temporal, spatial, and biological variability (including plasticity in resource use), nor the full suite of nutrients that can potentially limit phytoplankton, they do indicate that to determine the true level of colimitation for these populations, we would need to measure the dependence of phytoplankton biomass across many resources simultaneously.

Discussion

What Are the Consequences of Colimitation? At the cellular scale, colimitation has been known to alter traits such as cell

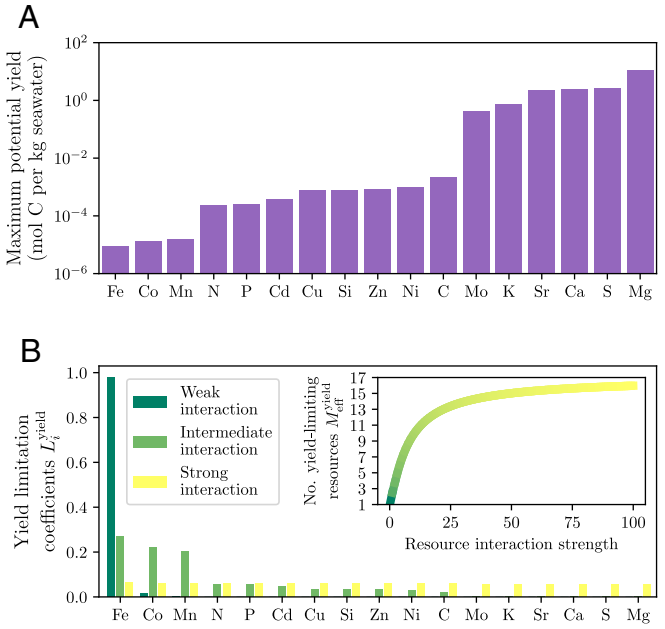

Fig. 5. Applying limitation concepts to empirical growth yield data for marine phytoplankton. (*A*) Maximum potential growth yield for phytoplankton (measured in moles of carbon) per kg of seawater that can be produced by each elemental resource's environmental concentration. Data is from Moore et al. (6) (Supplementary Table S1 therein). (*B*) Using potential yields from (*A*), we calculate growth yield limitation coefficients L_i^{yield} for each elemental resource. Since we do not know the underlying model for how multiple resources contribute to growth yield, we calculate limitation using a generalized-additive model with variable strength of resource interaction that tunes the degree of colimitation (*SI Appendix*, section S2). *Inset*: Number of yield-limiting resources $M_{\text{eff}}^{\text{yield}}$ as a function of the resource interaction strength, using data from (*A*).

size (48), raising the possibility that our knowledge of physiology is distorted by laboratory measurements with limitation for only one resource. This problem has been discussed since the 1970s, notably in works by Droop (49) and by Valdkamp and Jannasch (50), who pointed out that laboratory experiments provide artificially high concentrations of resources besides a focal limiting resource. We also observe that growth is less efficient under models with colimitation (e.g., Monod) compared to models without (e.g., Blackman; compare lines in *Top* panel of Fig. 1*A*) (29), suggesting a fundamental physiological difference between single limitation and colimitation.

At the scale of populations and communities, resource colimitation has been linked to evolutionary outcomes distinct from those under single nutrient limitation (51). In microbial communities, colimitation could increase susceptibility to invasion, because there are multiple potential niches for an invader to exploit. The competitive exclusion principle says that the number of species cannot exceed the number of limiting resources, but when "limiting" is no longer a binary state of a resource, the concept must be reexamined. Consideration of colimitation could therefore enhance the ability to predict and engineer microbial communities in environmental and human health contexts. For instance, knowing which nutrients are limiting and by how much would be useful in the design of probiotics and prebiotics. There is also the possibility that colimitation plays a role at larger ecological and biogeochemical scales, based on the notion that microbial life and the composition of its surroundings coevolve with one another (52, 53).

This raises the question of whether the many models used to describe growth under colimitation (*SI Appendix*, section S2) have meaningful differences in their biological consequences. Experimental data, from both this work and from previous studies (24, 29, 41), generally favors colimitation models (e.g., Poisson arrival time/synthesizing unit, additive) over law of the minimum–type models without colimitation (e.g., Blackman and Liebig models), but distinctions among colimitation models are difficult to resolve with these data. On one hand, the quantitative behavior of these models is broadly similar; theoretical work has argued that some models are just different approximations of the same underlying process (24, 28). In this case the chosen formalism may not matter for some outcomes such as stability of a microbial community (54). On the other hand, the models differ primarily at low resource concentrations, which is why they are hard to differentiate in laboratory experiments but also suggests that the consequences of these different models may be realized, and thus detectable, in contexts where low concentrations matter. This may include biogeochemical processes, evolution (where small differences between models can lead to large differences over time), or when resources are consumed for maintenance as well as growth (*SI Appendix*, section S3).

What Mechanisms Might Cause Colimitation? Intuitively, resource colimitation implies an interaction between resources such that their limitation states align (4). The most direct examples include biochemically dependent resource colimitation and substitutable resource colimitation (*SI Appendix*, section S2 and Fig. S4); however, indirect mechanisms are also possible, including metabolic bottlenecks and tradeoffs due to constraints on molecular composition, resource uptake, and energy utilization that are exacerbated when multiple resources are rare. Systems biologists have predicted the possibility of resource colimitation resulting from fine-scale molecular networks and especially stoichiometric flexibility, which could be a direct result of growth optimization in resource-colimited conditions (23, 40, 55). In microbial communities, colimitation could also result from heterogeneity in resource preferences and biomass stoichiometries, such that different organisms are limited for different resources, causing community-level colimitation (13). This mechanism could be an indirect result of community formation, or it could involve direct metabolic dependencies among organisms (12). Similar biological heterogeneity could occur even in clonal populations if there is phenotypic heterogeneity (56), for instance, if a subset of the population is primarily limited for one resource while another subset is limited for another resource. Environmental heterogeneity can also be a factor, as it has been suggested that microscale environmental "patchiness" could reduce the chance that cells encounter both necessary resources quickly. Stochasticity may be a cause of either biological or environmental heterogeneity even if this averages out at larger scales, as our consistent observations of colimitation in laboratory populations show. Our quantitative framework can be applied to all of these scenarios since it is agnostic to the mechanism of the colimitation.

Are Microbes Actually Colimited in Nature? Our evidence of colimitation in *E. coli* for two essential resources at naturally relevant concentrations (Fig. 3*B*), as well as our estimates of colimitation from environmental data (Figs. 4 and 5), highlight a need for closer attention to resource colimitation in nature. Our example shows that it can be difficult to access growth rate limitation in laboratory experiments due to the difficulty of reducing background contamination as well as biological adaptation to low resource concentrations. In our case, expression of the ammonium transporter AmtB likely helped *E. coli* to maintain high growth rates across a wide range of ammonium

concentrations (46). Therefore it may be more effective to directly test colimitation in nature using in situ incubation experiments where the full environmental context can be considered, including implicit factors that may not be represented in the laboratory (*SI Appendix*, section S1). Many studies have attempted these measurements and reported evidence of colimitation across a range of systems (4); for example, factorial supplementation experiments have suggested that colimitation frequently occurs in the surface ocean (1, 5). However, so far it has been challenging to assess the results of these datasets because of the shortcomings of supplementation experiments (as described in the Introduction; *SI Appendix*, Fig. S1), and because the data are biased toward certain ecosystems (marine and freshwater) and metabolic types (photosynthetic organisms) (4, 19, 57). Thus, it is not yet possible to statistically test the hypothesis that resource colimitation is common across organisms, environmental contexts, and outside of specific biochemical dependencies.

One alternative to factorial supplementation experiments is to develop molecular biomarkers of colimitation to measure in situ. These are already being explored in marine biogeochemistry and human microbiome contexts for single resource limitation (1, 58, 59). If resource colimitation represents a distinct physiological state of cells, it is possible that specific biomarkers for resource colimitation can also be identified. The biomarker approach has the benefit of avoiding experimental artifacts of laboratory or in situ perturbations, and may be able to identify how strain and even substrain level resource limitations vary in the community (60). Our quantitative definitions of limitation coefficients L will help to more rigorously calibrate limitation conditions for biomarker identification.

Comparing Colimitation of Growth Rate Versus Growth Yield. Our results demonstrate that different resources may be limiting for growth rate versus growth yield [also known as kinetic versus stoichiometric limitation in other work (3)], and that resources become rate- or yield-limiting at different concentrations (with growth rate limitation usually occurring at lower resource concentrations; Fig. 3*B*). For microbes, growth rate limitation is likely to be more important to evolution, since growth rate is under direct selection while growth yield is often not [depending on spatial structure and privatization of resources (61)]. Yield limitation, on the other hand, can be an important parameter in situations where we care about environmental and ecological composition, like elemental cycling in the ocean or total production in biotechnology (62–64). Since the possibility of tradeoffs between growth rate and growth yield has received significant attention in the past [despite limited empirical evidence (65, 66)], we note here that distinct resources limiting rate versus yield will not cause these tradeoffs to evolve in the first place [since yields evolve neutrally in the absence of spatial structure (61)], but an existing tradeoff could maintain distinct resources limiting rate and yield.

Growth Limitation Beyond Resources. In this work, we focus on chemical resources such as carbon and nitrogen sources, but the availability of physical resources such as light and space can also limit population growth (67–69). In the ocean, predators and viral lysis kill a substantial number of cells per day and have quantitative effects on growth rates and standing stocks of microbes (70, 71). In host-associated microbiomes, such as the human gut, viral lysis also plays a role, as does the host immune system (72, 73). In all of these contexts, there is also the possibility of intermicrobial warfare such as toxin release, as well as the opposite, promotion of growth through quorum-sensing behaviors due to the presence of other bacteria (74, 75). While the dependence of growth on these other factors is likely more complex than it is on chemical resource availability (e.g., nonmonotonic dependence), it is possible to extend the limitation metrics we present here to these cases as well, such that one can consider multiple factors at once (e.g., resource availability and virus concentrations).

Goals for Future Work. One of the most pressing questions is whether resource colimitation is a common or rare state; we propose performing systematic scans of field samples across gradients of multiple resource concentrations to estimate L and M_{eff}, and performing these experiments in a variety of natural systems. We note that this approach is applicable not just to microbes, but across biological systems. The time is also ripe to identify underlying mechanisms of colimitation, which is possible by performing precise physiological comparisons of limitation conditions. For instance, such experiments could address at which level to coarse-grain mechanisms (e.g., whole proteome allocation versus specific biochemical reactions) and identify biomarkers of colimitation that could be leveraged in natural contexts, including potentially in higher trophic-level organisms. At the same time, it will also be important to identify how these molecular mechanisms within individual cells and populations are layered to determine colimitation in microbial communities. Last, we believe it is important to test the effect of colimitation in experimental evolution, ecosystem, and biogeochemical models to understand the extent to which this phenomenon impacts broader outcomes for the prediction, management, and use of microbial growth.

Materials and Methods

Numerical Methods. We performed all numerical calculations in Python version 3.10.9, using tools from NumPy (76) version 1.24.1 and SciPy (77) version 1.10.0. We used the Python `random` module with seed = 0 for analyses with random number generation (bootstrapping and noisy data simulation). We prepared all figures using Matplotlib (78) version 3.9.1. Code for reproducing all analyses and figures is available at: https://github.com/proteoceanLab/Heldetal2024_Nutrient_Colimitation_Theory (81).

Measurement of Growth Rates from Luminescence Growth Curves. For luminescence growth curves we used the *E. coli* strain K-12 MG1655 pCS-λ (79), which contains a plasmid under kanamycin selection with a luciferase protein expressed under the constitutive lambda CS promoter, and a modified M9 minimal medium base without nitrogen: 12.8 g/L Na_2HPO_4 heptahydrate (Sigma Aldrich BioXtra grade lot SLBV4967, CAS S9390-500G), 3 g/L KH_2PO_4 monobasic (Sigma Aldrich ACS grade lot SZBF350AV CAS P0062-500G), 0.5 g/L NaCl (Sigma Aldrich BioXtra grade lot SYBG1530V CAS S7653-250G), 2 mM $MgSO_4$ hexahydrate (Sigma Aldrich ACS grade lot BCBT5460), and 50 μg/mL kanamycin (Sigma Aldrich CAS 70560-51-9 lot 0000130025). We selected three colonies of the strain from an agar plate to serve as biological replicates. We grew separate overnight cultures of each replicate in the base medium along with 10 mM D(+)glucose (Sigma Aldrich BioXtra grade lot SLBW5196 CAS G7528-1Kg) and 20 mM ammonium chloride (Sigma Aldrich ACS Reagent lot STBH3180 CAS 31107-500G). After 16 h of overnight growth, we collected the cells by centrifugation and washed each replicate culture three times in the base medium without glucose and ammonium, then adjusted the OD at 600 nm of each culture to 0.01 by diluting into the base medium. We prepared gradients of glucose (0 to 2 mM) and ammonium chloride (0 to 1 mM) in the base medium and aliquoted them into three white-walled, flat-bottom 96-well plates (Corning). We then diluted each replicate culture at a 1:100 ratio into the wells of its corresponding plate, resulting in a final OD of 10^{-4} in 200 μL at time zero for the growth curve experiments. We grew the cells at 37 °C for 22 h in three separate Biotek Synergy H1 plate readers (Agilent Technologies, Inc.), with measurements of luminescence every

10 min (orbital shaking of 15 s prior to each measurement, luminescence integration time of 3 s). We analyzed the growth curves by 1) performing a background correction of the data using media blanks with no cells added, 2) selecting a time interval of approximate exponential growth, 3) performing linear regression of the log-luminescence in that interval, and 4) quality control based on R^2 for the linear regression and manual inspection of the fit (Dataset S1; *SI Appendix*, Figs. S7–S9).

Measurement of Growth Yields from Optical Density Growth Curves. For OD growth curves we used the *E. coli* strain K-12 MG1655 (also containing a chromosomal GFP not used in this experiment) and a modified M9 minimal medium base without nitrogen: 6 g/L Na_2HPO_4 (VWR Life Science, 0404, CAS: 7558-79-4), 3 g/L KH_2PO_4 (VWR Chemicals, BDH9268, CAS: 7778-77-0), 0.5 g/L NaCl (VWR Chemicals, BDH9286, CAS: 7647-14-5), 1 mM $MgSO_4$ (J.T. Baker, 2506-01, CAS: 7487-88-9), and 0.1 mM $CaCl_2$ (VWR Life Science, 1B1110, CAS: 10043-52-4). We selected three colonies of the strain from an agar plate to serve as biological replicates. We grew separate overnight cultures of each replicate in the base medium along with 40 mM glucose (VWR Chemicals, BDH9230, CAS: 50-99-7) and 40 mM ammonium chloride (VWR Life Science, 0621, CAS: 12125-02-9). After 16 h of overnight growth, we collected the cells by centrifugation and washed each replicate culture five times in the base medium without glucose and ammonium, then adjusted the OD at 600 nm of each culture to 0.02 by diluting into the base medium. We prepared gradients of glucose (0 to 40 mM) and ammonium chloride (0 to 40 mM) in the base medium and aliquoted them into three transparent, flat-bottom 96-well plates (Corning). We then diluted each replicate culture at a 1:2 ratio into the wells of its corresponding plate, resulting in a final OD of 0.01 in 200 μL at time zero for the growth curve experiments. We grew the cells at 37 °C under shaking conditions (500 RPM) for 24 h in the Biotek LogPhase 600 plate reader (Agilent Technologies, Inc.), with measurements of OD at 600 nm every 10 min. We analyzed the growth curves by 1) performing a background correction of the data using media blanks with no cells added, 2) selecting a time interval of approximate stationary phase, 3) taking an average of the OD in that interval, and 4) quality control based on the coefficient of OD variation during the stationary interval and manual inspection of the fit (Dataset S2; *SI Appendix*, Figs. S10 and S11).

Analysis of Resource Scan Data. We fit growth rate and growth yield scans over resource concentrations to models (*SI Appendix*, Table S1 and section S2) using `scipy.optimize.curve_fit` for least-squares minimization. We supply initial guesses for each parameter: for the trait value at saturation, we guess the trait value measured at the maximum concentrations of both resources; for the affinities (growth rates) and stoichiometries (growth yields), we guess the maximum trait value divided by half the measured concentration range. We guess exponents of 1 for the Hill and generalized-additive models and zero minimum resource concentrations for models with $R_{\min}$ parameters. We bound all fitted parameters to be nonnegative. We calculated the Akaike information criterion (corrected for small sample size) for each model fit using

$$\mathrm{AIC} = 2n + n\log\left(\frac{\sum_{i=1}^{n}(f_i - y_i)^2}{n-k}\right) - 2k\left(\frac{k+1}{n-k-1}\right), \quad [7]$$

where n is the number of data points, y_i is the ith measured data point, f_i is the fitted value for that data point, and k is the number of parameters in the model (80). We calculate the relative Akaike weight for a model α as

$$w_\alpha = \frac{e^{-\mathrm{AIC}_\alpha/2}}{\sum_{\text{model }\beta} e^{-\mathrm{AIC}_\beta/2}}, \quad [8]$$

where the sum is over all fitted models. To generate the bootstrapped datasets, we randomly sample one of the three replicate measurements at each concentration condition and subject 100 datasets generated in this way to the same analysis.

Simulated Datasets. We simulate resource scan datasets by taking a model with parameters fit to the experimental data (either growth rate or growth yield) and generating trait values predicted by the model at the same resource concentrations used in the experiments. We add Gaussian noise to each measurement with mean zero and SD that is a linear function of the trait value at that point; this linear function is obtained by performing a linear regression of the SD of growth rates or yields across replicates to the mean growth rate or yield across replicates (see *SI Appendix*, Figs. S16 and S26, for parameter values).

Inferring Supplementations from Resource Scans. Let $\{R_{\mathrm{glu},i}\}$ and $\{R_{\mathrm{amm},j}\}$ be the sets of glucose and ammonium concentrations in our resource scan data. We calculate limitation coefficients for supplementations by iterating over each pair of background concentrations $R_{\mathrm{glu},i}$, $R_{\mathrm{amm},j}$ and each supplemented concentration $R_{\mathrm{glu},k} > R_{\mathrm{glu},i}$ and $R_{\mathrm{amm},\ell} > R_{\mathrm{amm},j}$. For each combination we calculate limitation coefficients as finite differences (Eq. **1**):

$$\begin{aligned} L^{\mathrm{rate}}_{\mathrm{glu},ijk} &= \frac{R_{\mathrm{glu},i}}{g(R_{\mathrm{glu},i}, R_{\mathrm{amm},j})} \times \frac{g(R_{\mathrm{glu},k}, R_{\mathrm{amm},j}) - g(R_{\mathrm{glu},i}, R_{\mathrm{amm},j})}{R_{\mathrm{glu},k} - R_{\mathrm{glu},i}}, \\ L^{\mathrm{rate}}_{\mathrm{amm},ij\ell} &= \frac{R_{\mathrm{amm},j}}{g(R_{\mathrm{glu},i}, R_{\mathrm{amm},j})} \times \frac{g(R_{\mathrm{glu},i}, R_{\mathrm{amm},\ell}) - g(R_{\mathrm{glu},i}, R_{\mathrm{amm},j})}{R_{\mathrm{amm},\ell} - R_{\mathrm{amm},j}}. \end{aligned} \quad [9]$$

We perform an analogous analysis for the growth yield data.

Collection and Analysis of Environmental Data. We collected 20 studies in which the parameters of the Monod growth model ($g_{\max}$ and K) for two resources were measured for the same species and strain. We extracted these data from a broader literature review of Monod parameters that we conducted earlier (39). Whenever possible, we estimated background environmental nutrient concentrations (i.e., the concentrations the organism is expected to experience in the environment from which it was isolated) from data provided in the original manuscript. When this was not provided, we estimated a range of environmental concentrations from the expected habitat of the organism. For instance, for *E. coli* sp. K12, we selected representative environmental concentrations of resources in the human gut (higher concentrations) and in soils (lower concentrations). For marine diatoms, we selected representative environmental concentrations of high-nutrient regions (coastal upwelling zones) and low-nutrient regions (surface open ocean). In some cases, the expected resource concentration range is large and spans at least an order of magnitude, in which case we took the midpoint of that range for calculations. Using the measured Monod parameters and estimated environmental concentrations, we calculated limitation coefficients using four common models (*SI Appendix*, Table S1 and section S2).

Data, Materials, and Software Availability. Code to reproduce the analyses have been deposited in GitHub (https://github.com/proteoceanLab/Heldetal2024_Nutrient_Colimitation_Theory) (81). All other data are included in the manuscript and/or supporting information.

ACKNOWLEDGMENTS. We thank Daniel Angst for help running automated growth curve measurements and Justus Fink for valuable feedback on the paper. N.A.H. was supported by the Principles of Microbial Ecosystems collaboration of the Simons Foundation (Grant ID 542379 to Martin Ackermann) and an Eidgenössische Technische Hochschule Zürich (ETH) Zurich Career Seed Grant (SEED-26 21-2 to N.A.H.). M.M. was supported by an Ambizione Grant from the Swiss NSF (PZ00P3_180147).

Author affiliations: [a]Department of Environmental Systems Science, Swiss Federal Institute of Technology (ETH) Zurich, Zurich 8006, Switzerland; [b]Department of Environmental Microbiology, Swiss Federal Institute of Aquatic Science and Technology (Eawag), Dübendorf 8600, Switzerland; [c]Department of Biological Sciences, Marine & Environmental Biology Section, University of Southern California, Los Angeles, CA 90089; [d]Department of Biology, Swiss Federal Institute of Technology (ETH) Zurich, Zurich 8006, Switzerland; [e]Center for Advanced Biotechnology and Medicine, Rutgers University, Piscataway, NJ 08854; and [f]Department of Biochemistry and Molecular Biology, Robert Wood Johnson Medical School, Rutgers University, Piscataway, NJ 08854

1. T. J. Browning, C. M. Moore, Global analysis of ocean phytoplankton nutrient limitation reveals high prevalence of co-limitation. *Nat. Commun.* **14**, 5014 (2023).
2. N. Wale *et al*., Resource limitation prevents the emergence of drug resistance by intensifying within-host competition. *Proc. Natl. Acad. Sci. U.S.A.* **114**, 13774–13779 (2017).
3. M. Zinn, B. Witholt, T. Egli, Dual nutrient limited growth: Models, experimental observations, and applications. *J. Biotechnol.* **113**, 263–279 (2004).
4. N. A. Held, M. Manhart, Are microbes colimited by multiple resources? *Curr. Opin. Microbiol.* **80**, 102509 (2024).
5. M. A. Saito, T. J. Goepfert, J. T. Ritt, Some thoughts on the concept of colimitation: Three definitions and the importance of bioavailability. *Limnol. Oceanogr.* **53**, 276–290 (2008).
6. C. M. Moore *et al*., Processes and patterns of oceanic nutrient limitation. *Nat. Geosci.* **6**, 701–710 (2013).
7. E. Du *et al*., Global patterns of terrestrial nitrogen and phosphorus limitation. *Nat. Geosci.* **13**, 221–226 (2020).
8. J. J. Elser *et al*., Global analysis of nitrogen and phosphorus limitation of primary producers in freshwater, marine and terrestrial ecosystems. *Ecol. Lett.* **10**, 1135–1142 (2007).
9. K. R. Arrigo, Marine microorganisms and global nutrient cycles. *Nature* **437**, 349–356 (2005).
10. D. Tilman, Tests of resource competition theory using four species of Lake Michigan algae. *Ecology* **62**, 802–815 (1981).
11. D. Tilman, The resource-ratio hypothesis of plant succession. *Am. Nat.* **125**, 827–852 (1985).
12. C. Bannon, I. Rapp, E. M. Bertrand, Community interaction co-limitation: Nutrient limitation in a marine microbial community context. *Front. Microbiol.* **13**, 846890 (2022).
13. M. Danger, T. Daufresne, F. Lucas, S. Pissard, G. Lacroix, Does Liebig's law of the minimum scale up from species to communities? *Oikos* **117**, 1741–1751 (2008).
14. T. J. Browning *et al*., Nutrient co-limitation at the boundary of an oceanic gyre. *Nature* **551**, 242–246 (2017).
15. T. J. Browning, E. P. Achterberg, A. Engel, E. Mawji, Manganese co-limitation of phytoplankton growth and major nutrient drawdown in the Southern Ocean. *Nat. Commun.* **12**, 884 (2021).
16. B. S. Twining *et al*., A nutrient limitation mosaic in the eastern tropical Indian Ocean. *Deep Sea Res. Part II* **166**, 125–140 (2019).
17. E. M. Bertrand *et al*., Vitamin B12 and iron colimitation of phytoplankton growth in the Ross Sea. *Limnol. Oceanogr.* **52**, 1079–1093 (2007).
18. J. K. Moore, S. C. Doney, Iron availability limits the ocean nitrogen inventory stabilizing feedbacks between marine denitrification and nitrogen fixation. *Global Biogeochem. Cycles* **21**, 1–12 (2007).
19. W. S. Harpole *et al*., Nutrient co-limitation of primary producer communities. *Ecol. Lett.* **14**, 852–862 (2011).
20. T. Egli, M. Zinn, The concept of multiple-nutrient-limited growth of microorganisms and its application in biotechnological processes. *Biotechnol. Adv.* **22**, 35–43 (2003).
21. J. von Liebig, *Organic Chemistry in Its Application to Agriculture and Physiology* (Taylor and Walton, London, UK, 1840).
22. D. Tilman, *Resource Competition and Community Structure* (Princeton University Press, Princeton, NJ, 1982).
23. E. Sperfeld, D. Raubenheimer, A. Wacker, Bridging factorial and gradient concepts of resource co-limitation: Towards a general framework applied to consumers. *Ecol. Lett.* **19**, 201–215 (2016).
24. J. Tang, W. J. Riley, Finding Liebig's law of the minimum. *Ecol. Appl.* **31**, e02458 (2021).
25. M. Danger, C. Oumarou, D. Benest, G. Lacroix, Bacteria can control stoichiometry and nutrient limitation of phytoplankton. *Funct. Ecol.* **21**, 202–210 (2007).
26. T. Egli, On multiple-nutrient-limited growth of microorganisms, with special reference to dual limitation by carbon and nitrogen substrates. *Antonie Van Leeuwenhoek* **60**, 225–234 (1991).
27. K. Kovárová-Kovar, T. Egli, Growth kinetics of suspended microbial cells: From single-substrate-controlled growth to mixed-substrate kinetics. *Microbiol. Mol. Biol. Rev.* **62**, 646–666 (1998).
28. M. E. Muscarella, J. P. O'Dwyer, Species dynamics and interactions via metabolically informed consumer–resource models. *Theor. Ecol.* **13**, 503–518 (2020).
29. E. Sperfeld, D. Martin-Creuzburg, A. Wacker, Multiple resource limitation theory applied to herbivorous consumers: Liebig's minimum rule vs. interactive co-limitation. *Ecol. Lett.* **15**, 142–150 (2012).
30. A. Redoglio, K. Radtke, E. Sperfeld, How nitrogen and phosphorus supply to nutrient-limited autotroph communities affects herbivore growth: Testing stoichiometric and co-limitation theory across trophic levels. *Oikos* **2022**, e09052 (2022).
31. D. R. O'Donnell, P. Wilburn, E. A. Silow, L. Y. Yampolsky, E. Litchman, Nitrogen and phosphorus colimitation of phytoplankton in Lake Baikal: Insights from a spatial survey and nutrient enrichment experiments. *Limnol. Oceanogr.* **62**, 1383–1392 (2017).
32. M. Rutgers, P. A. Balk, K. van Dam, Quantification of multiple-substrate controlled growth-simultaneous ammonium and glucose limitation in chemostat cultures of Klebsiella pneumoniae. *Arch. Microbiol.* **153**, 478–484 (1990).
33. R. Heinrich, S. Schuster, *The Regulation of Cellular Systems* (Chapman and Hall, New York, NY, 1996).
34. R. V. O'Neill, D. L. DeAngelis, J. J. Pastor, B. J. Jackson, W. M. Post, Multiple nutrient limitations in ecological models. *Ecol. Modell.* **46**, 147–163 (1989).
35. D. K. Button, Affinity of organisms for substrate. *Limnol. Oceanogr.* **31**, 435–456 (1986).
36. F. F. Blackman, Optima and limiting factors. *Ann. Bot.* **19**, 281–295 (1905).
37. J. R. Casey, M. J. Follows, A steady-state model of microbial acclimation to substrate limitation. *PLoS Comput. Biol.* **16**, e1008140 (2020).
38. J. Monod, The growth of bacterial cultures. *Annu. Rev. Microbiol.* **3**, 371–394 (1949).
39. J. W. Fink, N. A. Held, M. Manhart, Microbial population dynamics decouple growth response from environmental nutrient concentration. *Proc. Natl. Acad. Sci. U.S.A.* **120**, e2207295120 (2023).
40. K. W. Wirtz, O. Kerimoglu, Autotrophic stoichiometry emerging from optimality and variable co-limitation. *Front. Ecol. Evol.* **4**, 131 (2016).
41. F. Liu, L. Gaul, A. Giometto, M. Wu, A high throughput array microhabitat platform reveals how light and nitrogen colimit the growth of algal cells. *Sci. Rep.* **14**, 9860 (2024).
42. S. A. L. M. Kooijman, The synthesizing unit as model for the stoichiometric fusion and branching of metabolic fluxes. *Biophys. Chem.* **73**, 179–188 (1998).
43. D. Tilman, Resources: A graphical-mechanistic approach to competition and predation. *Am. Nat.* **116**, 362–393 (1980).
44. A. Bren, Y. Hart, E. Dekel, D. Koster, U. Alon, The last generation of bacterial growth in limiting nutrient. *BMC Syst. Biol.* **7**, 27 (2013).
45. R. E. Lenski, M. R. Rose, S. C. Simpson, S. C. Tadler, Long-term experimental evolution in *Escherichia coli*. I. Adaptation and divergence during 2,000 generations. *Am. Nat.* **138**, 1315–1341 (1991).
46. M. Kim *et al*., Need-based activation of ammonium uptake in *Escherichia coli*. *Mol. Syst. Biol.* **8**, 616 (2012).
47. J. P. Folsom, R. P. Carlson, Physiological, biomass elemental composition and proteomic analyses of *Escherichia coli* ammonium-limited chemostat growth, and comparison with iron- and glucose-limited chemostat growth. *Microbiology* **161**, 1659–1670 (2015).
48. N. Yang *et al*., Molecular mechanisms underlying iron and phosphorus co-limitation responses in the nitrogen-fixing cyanobacterium Crocosphaera. *ISME J.* **16**, 2702–2711 (2022).
49. M. Droop, Some thoughts on nutrient limitation in algae. *J. Phycol.* **9**, 264–272 (1974).
50. H. Veldkamp, H. W. Jannasch, Mixed culture studies with the chemostat. *J. Appl. Chem. Biotechnol.* **22**, 105–123 (1972).
51. N. G. Walworth *et al*., Nutrient-colimited *Trichodesmium* as a nitrogen source or sink in a future ocean. *Appl. Environ. Microbiol.* **84**, 1–14 (2018).
52. M. L. Larsen, S. W. Wilhelm, J. T. Lennon, Nutrient stoichiometry shapes microbial coevolution. *Ecol. Lett.* **22**, 1009–1018 (2019).
53. F. M. M. Morel, The co-evolution of phytoplankton and trace element cycles in the oceans. *Geobiology* **6**, 318–324 (2008).
54. J. C. Poggiale, M. Baklouti, B. Queguiner, S. A. L. M. Kooijman, How far details are important in ecosystem modelling: The case of multi-limiting nutrients in phytoplankton-zooplankton interactions. *Philos. Trans. R. Soc. B* **365**, 3495–3507 (2010).
55. S. Sharma, R. Steuer, Modelling microbial communities using biochemical resource allocation analysis. *J. R. Soc. Interface* **16**, 20190474 (2019).
56. F. Schreiber *et al*., Phenotypic heterogeneity driven by nutrient limitation promotes growth in fluctuating environments. *Nat. Microbiol.* **1**, 1–7 (2016).
57. M. E. S. Bracken *et al*., Signatures of nutrient limitation and co-limitation: Responses of autotroph internal nutrient concentrations to nitrogen and phosphorus additions. *Oikos* **124**, 113–121 (2015).
58. M. A. Saito *et al*., Multiple nutrient stresses at intersecting Pacific Ocean biomes detected by protein biomarkers. *Science* **345**, 1173–1177 (2014).
59. X. Zeng *et al*., Gut bacterial nutrient preferences quantified in vivo. *Cell* **185**, 3441–3456.e19 (2022).
60. N. R. Cohen *et al*., Dinoflagellates alter their carbon and nutrient metabolic strategies across environmental gradients in the central Pacific Ocean. *Nat. Microbiol.* **6**, 173–186 (2021).
61. H. Bachmann *et al*., Availability of public goods shapes the evolution of competing metabolic strategies. *Proc. Natl. Acad. Sci. U.S.A.* **110**, 14302–14307 (2013).
62. P. A. del Giorgio, J. J. Cole, Bacterial growth efficiency in natural aquatic systems. *Annu. Rev. Ecol. Syst.* **29**, 503–541 (1998).
63. C. M. Godwin, E. A. Whitaker, J. B. Cotner, Growth rate and resource imbalance interactively control biomass stoichiometry and elemental quotas of aquatic bacteria. *Ecology* **98**, 820–829 (2017).
64. D. A. Lipson, The complex relationship between microbial growth rate and yield and its implications for ecosystem processes. *Front. Microbiol.* **6**, 615 (2015).
65. M. Novak, T. Pfeiffer, R. E. Lenski, U. Sauer, S. Bonhoeffer, Experimental tests for an evolutionary trade-off between growth rate and yield in *E. coli*. *Am. Nat.* **168**, 242–251 (2006).
66. C. Cheng *et al*., Laboratory evolution reveals a two-dimensional rate-yield tradeoff in microbial metabolism. *PLoS Comput. Biol.* **15**, e1007066 (2019).
67. H. Venables, C. M. Moore, Phytoplankton and light limitation in the Southern Ocean: Learning from high-nutrient, high-chlorophyll areas. *J. Geophys. Res.: Oceans* **115**, C02015 (2010).
68. K. Z. Coyte, H. Tabuteau, E. A. Gaffney, K. R. Foster, W. M. Durham, Microbial competition in porous environments can select against rapid biofilm growth. *Proc. Natl. Acad. Sci. U.S.A.* **114**, E161–E170 (2017).
69. D. P. Lloyd, R. J. Allen, Competition for space during bacterial colonization of a surface. *J. R. Soc. Interface* **12**, 20150608 (2015).
70. Y. C. Yeh, J. A. Fuhrman, Effects of phytoplankton, viral communities, and warming on free-living and particle-associated marine prokaryotic community structure. *Nat. Commun.* **13**, 7905 (2022).
71. C. A. Suttle, Marine viruses–Major players in the global ecosystem. *Nat. Rev. Microbiol.* **5**, 801–812 (2007).
72. D. Zheng, T. Liwinski, E. Elinav, Interaction between microbiota and immunity in health and disease. *Cell Res.* **30**, 492–506 (2020).
73. Z. Cao *et al*., The gut virome: A new microbiome component in health and disease. *EBioMedicine* **81**, 104113 (2022).
74. E. T. Granato, T. A. Meiller-Legrand, K. R. Foster, The evolution and ecology of bacterial warfare. *Curr. Biol.* **29**, R521–R537 (2019).
75. S. T. Rutherford, B. L. Bassler, Bacterial quorum sensing: Its role in virulence and possibilities for its control. *Cold Spring Harb. Perspect. Med.* **2**, a012427 (2012).
76. C. R. Harris *et al*., Array programming with NumPy. *Nature* **585**, 357–362 (2020).
77. P. Virtanen *et al*., SciPy 1.0: Fundamental algorithms for scientific computing in Python. *Nat. Methods* **17**, 261–272 (2020).
78. J. D. Hunter, Matplotlib: A 2D graphics environment. *Comput. Sci. Eng.* **9**, 90–95 (2007).
79. R. Kishony, S. Leibler, Environmental stresses can alleviate the average deleterious effect of mutations. *J. Biol.* **2**, 14 (2003).
80. K. P. Burnham, D. R. Anderson, *Model Selection and Multimodal Inference: A Practical Information-Theoretic Approach* (Springer-Verlag, New York, NY, ed. 2, 2002).
81. N. Held *et al*., Nutrient colimitation is a quantitative, dynamic property of microbial populations. Github. https://github.com/proteoceanLab/Heldetal2024_Nutrient_Colimitation_Theory. Deposited 24 October 2024.

Supporting Information for

Nutrient colimitation is a quantitative, dynamic property of microbial populations

Noelle A. Held, Aswin Krishna, Donat Crippa, Rachana Rao Battaje, Alexander J. Devaux, Anastasia Dragan, Michael Manhart

Noelle A. Held: nheld@usc.edu
Michael Manhart: mmanhart@rutgers.edu

This PDF file includes:

Other supporting materials for this manuscript include the following:

Datasets S1 to S3

Supporting Information Text

Contents

S1. Mathematical properties of limitation coefficients and the effective number of limiting factors

A. Quantitative interpretation of the limitation coefficient. Here we provide a quantitative interpretation of the limitation coefficient; we explain this in terms of the growth rate limitation coefficient L^{rate} (main text Eq. 1), but these points apply similarly to the growth yield limitation coefficient L^{yield}. Consider a small change Δr in a limiting process rate r (e.g., a resource uptake rate proportional to its external concentration as in main text Eq. 4). The growth rate changes according to

$$\begin{aligned} g(r+\Delta r) &\approx g(r) + \Delta r \frac{\partial g}{\partial r} \\ &= g(r)\left(1 + \frac{\Delta r}{r}\frac{r}{g(r)}\frac{\partial g}{\partial r}\right) \\ &= g(r)\left(1 + \frac{\Delta r}{r} L^{\text{rate}}\right). \end{aligned} \tag{S1}$$

Hence we can think of L^{rate} as the approximate factor by which a small relative change in the rate r changes the relative magnitude of growth rate. For example, if $L^{\text{rate}} = 1$, then any relative change in r entails the same relative change in g: a 1% change in r means approximately a 1% change in g. If $L^{\text{rate}} = 0.5$, then any relative change in r entails only half that relative change in g: a 1% change in r means approximately a 0.5% change in g. Equivalently, we can think of L^{rate} as being the exponent of the power-law scaling of g with r, at a particular value of r:

$$g(r) \sim r^{L^{\text{rate}}}. \tag{S2}$$

B. Range of limitation coefficient values. For the growth rate limitation coefficient L_i^{rate}, we expect $L_i^{\text{rate}} = 0$ at high values of r_i, when process i is saturating and no longer limiting. At low values of r_i, $L_i^{\text{rate}} = 1$ usually, meaning that g is proportional to r_i. This range holds for most common models of growth rate dependence on resource concentrations (section S2), such as the Blackman (main text Eq. 5) and Monod (main text Eq. 6) models. However, negative values are possible if growth rate decreases with increasing r, as would occur if process i is uptake of an antibiotic; uptake of some resources may also be toxic at extremely high concentrations. Values greater than 1 are possible if the growth rate scales super-linearly with r_i, as occurs for the Hill model of growth rate (1) (also known as the Moser model (2) or Holling Type III model (3)). This may occur if the process in question involves cooperativity or sensing of a threshold before activation. These bounds generally hold for growth yield limitation coefficients L_i^{yield} as well, at least for the phenomenological models considered in this work (section S2).

C. Proof of normalization for limitation coefficients. Let the total growth rate g of biomass be a function of M individual processes with rates r_i:

$$g = g(r_1, r_2, \ldots, r_M). \tag{S3}$$

Since both g and the individual rates r_i must have units of per time, then g must depend on the rates according to the functional form

$$g(r_1, r_2, \ldots, r_M) = r_j f_j\left(\frac{r_1}{r_j}, \frac{r_2}{r_j}, \ldots, \frac{r_{j-1}}{r_j}, \frac{r_{j+1}}{r_j}, \ldots, \frac{r_M}{r_j}\right). \tag{S4}$$

We can argue this by dimensional analysis: we must be able to write g as the product of one rate r_j (to give g the same units) and a dimensionless function f_j of all other rates which must depend only on the $M-1$ dimensionless ratios of the rates. By symmetry this form holds for any rate r_j but with a different function f_j. In the case of the Monod model for a single resource, let $r_1 = aR$ be the rate of resource uptake and $r_2 = g_{\max}$ the rate of downstream metabolism. We can thus write the growth rate (main text Eq. 6) as

$$\begin{aligned} g(r_1, r_2) &= \frac{r_1 r_2}{r_1 + r_2} \\ &= r_1 f_1\left(\frac{r_2}{r_1}\right) \\ &= r_2 f_2\left(\frac{r_1}{r_2}\right). \end{aligned} \tag{S5}$$

where $f_1(r_2/r_1) = 1/(r_1/r_2 + 1)$ and $f_2(r_1/r_2) = 1/(r_2/r_1 + 1)$.

We can now calculate the sum of limitation coefficients according to this functional form. First, for $i \neq j$,

$$\begin{aligned} L_i^{\text{rate}} &= \frac{r_i}{g}\frac{\partial g}{\partial r_i} \\ &= \frac{r_i f_j^{(i)}\left(\frac{r_1}{r_j}, \frac{r_2}{r_j}, \ldots, \frac{r_{j-1}}{r_j}, \frac{r_{j+1}}{r_j}, \ldots, \frac{r_M}{r_j}\right)}{r_j f_j\left(\frac{r_1}{r_j}, \frac{r_2}{r_j}, \ldots, \frac{r_{j-1}}{r_j}, \frac{r_{j+1}}{r_j}, \ldots, \frac{r_M}{r_j}\right)}, \end{aligned} \tag{S6}$$

where the superscript (i) means that we take the derivative of f_j with respect to the argument in which r_i appears (the ith argument for $i < j$, and the $(i-1)$th argument for $i > j$). When $i = j$, the limitation coefficient is

$$\begin{aligned} L_j^{\text{rate}} &= \frac{r_j}{g}\frac{\partial g}{\partial r_j} \\ &= \frac{r_j}{g}\left[f_j\left(\frac{r_1}{r_j}, \frac{r_2}{r_j}, \ldots, \frac{r_{j-1}}{r_j}, \frac{r_{j+1}}{r_j}, \ldots, \frac{r_M}{r_j}\right) - r_j \sum_{i\neq j} \frac{r_i}{r_j^2} f_j^{(i)}\left(\frac{r_1}{r_j}, \frac{r_2}{r_j}, \ldots, \frac{r_{j-1}}{r_j}, \frac{r_{j+1}}{r_j}, \ldots, \frac{r_M}{r_j}\right)\right] \\ &= 1 - \sum_{i\neq j} \frac{r_i f_j^{(i)}\left(\frac{r_1}{r_j}, \frac{r_2}{r_j}, \ldots, \frac{r_{j-1}}{r_j}, \frac{r_{j+1}}{r_j}, \ldots, \frac{r_M}{r_j}\right)}{r_j f_j\left(\frac{r_1}{r_j}, \frac{r_2}{r_j}, \ldots, \frac{r_{j-1}}{r_j}, \frac{r_{j+1}}{r_j}, \ldots, \frac{r_M}{r_j}\right)}. \end{aligned} \tag{S7}$$

Thus $L_j^{\text{rate}} = 1 - \sum_{i\neq j} L_i^{\text{rate}}$, and hence $\sum_{i=1}^{M} L_i^{\text{rate}} = 1$ (main text Eq. 2).

Note that this normalization condition holds even if some limitation coefficients have values outside the range 0 to 1; this means that if one process has limitation coefficient greater than 1 (as occurs, for example, in the Hill model of growth rates (1)), there must be at least one process with negative limitation coefficient. We can apply a similar argument to show normalization of yield limitation coefficients if we assume biomass depends on all limiting factors via contributions that also have units of biomass; for example, biomass depends on a resource R times a stoichiometric factor with units of biomass per unit resource.

D. Colimitation among a subset of limiting factors. While the definition of the effective number of limiting factors M_{eff} in the main text (main text Eq. 3) is over all possible factors (e.g., the maximum in the denominator is over all limitation coefficients), sometimes we want to consider the effective number of limiting factors among just a subset of factors. We can do this by renormalizing each limitation coefficient by the sum of limitation coefficients in that subset. That is, among a subset of factors $\mathcal{S}$ we define the relative limitation coefficients as

$$L_{i,\mathcal{S}} = \frac{L_i}{\sum_{j\in\mathcal{S}} L_j} \tag{S8}$$

and calculate the effective number of limiting factors within just that subset:

$$\begin{aligned} M_{\text{eff},\mathcal{S}} &= \frac{1}{\max_{i\in\mathcal{S}} L_{i,\mathcal{S}}} \\ &= \frac{1}{\max_{i\in\mathcal{S}}\left(\frac{L_i}{\sum_{j\in\mathcal{S}} L_j}\right)} \\ &= \frac{\sum_{i\in\mathcal{S}} L_i}{\max_{i\in\mathcal{S}} L_i}. \end{aligned} \tag{S9}$$

For example, in our experiments with varying glucose and ammonium, we may wish to calculate colimitation between just glucose and ammonium, besides calculating the total amount of colimitation among glucose, ammonium, and implicit factors.

E. Range of the effective number of limiting factors. If all limitation coefficients are between 0 and 1, then the effective number of limiting factors M_{eff} (main text Eq. 3) always ranges from a minimum of 1 (when all limitation is for a single factor) to M, the total number of limiting factors under consideration. Note that when we coarse-grain multiple limiting factors (e.g., invariant resources or internal processes such as transcription and translation) into a single implicit factor, they count only as one limiting factor toward M_{eff}.

However, this range of M_{eff} can be different if some limitation coefficients are less than 0 or greater than 1. For example, assume we have three factors with limitation coefficients $L_1 = 1$, $L_2 = 0.5$, and $L_3 = -0.5$ ($L_1 + L_2 + L_3 = 1$). The effective number of limiting factors, among all three factors, is $M_{\text{eff}} = 1$: there is one maximally limiting factor, another factor that is half as limiting, and a third factor that is negatively limiting at half the magnitude of the most limiting factor, which cancels the second half-limiting factor, leaving effectively just one limiting factor. We can also look at colimitation between subsets of these factors (section S1D). The effective number of limiting factors among the first two factors is $M_{\text{eff},\{1,2\}} = 1.5$. However, the effective number of limiting factors among the first and third factor is $M_{\text{eff},\{1,3\}} = 0.5$, and the effective number of limiting factors among the second and third factor is $M_{\text{eff},\{2,3\}} = 0$.

F. Geometric interpretation of the effective number of limiting factors. When all limitation coefficients range between 0 and 1 (as is the case for most common models of growth rate and yield), the normalization condition Eq. 2 (main text) means that the limitation coefficients form an $(M-1)$-simplex for M total limiting factors (Fig. S2). (Despite the normalization condition, they will not form a simplex in scenarios where limitation coefficients can be negative or greater than 1, as occur in the Hill model or in the presence of antibiotics.) In this case, we can think of the effective number of limiting factors M_{eff} (main text Eq. 3) as a measure of distance (not Euclidean) to the center of the simplex, where there is maximum colimitation (all limitation coefficients have the same value $1/M$; Fig. S2). Geometrically, M_{eff} is equivalent to taking whichever limitation coefficient is maximum (corresponding to the vertex closest to the point in the simplex where the population is), measuring the value along that axis ($\max_i L_i$), and finally taking the reciprocal of that value, so that higher M_{eff} means smaller distance to the simplex center (greater colimitation).

G. Quantifying the additivity of colimitation. Besides the effective number of limiting factors, another quantitative aspect of colimitation is its additivity (not to be confused with the additive model of growth rate or yield dependence on resources; section S2). This has been a major focus of previous studies that use supplementation experiments (Fig. S1) to test for colimitation (4, 5). For the following we focus on growth rate g with two variable resources (R_1 and R_2), but this can be generalized to growth yield N and additional resources as well. Let ΔR_1 be the supplemented concentration of resource 1 on the background concentration R_1, and let ΔR_2 be the supplement for resource 2 on the background R_2. Define the additive effect of these two supplementations as (4, 5)

$$\mathrm{AE} = \Big[g(R_1+\Delta R_1, R_2+\Delta R_2) - g(R_1,R_2)\Big] - \Big[g(R_1+\Delta R_1, R_2) - g(R_1,R_2)\Big] - \Big[g(R_1, R_2+\Delta R_2) - g(R_1,R_2)\Big]. \quad \text{[S10]}$$

That is, AE is the change in growth rate from supplementing both resources simultaneously, minus the effects of supplementing each resource individually. This is analogous to the concept of epistasis in genetics, which quantifies the additive effect of combining two mutations (6). Using this quantity we can classify the response as sub-additive (AE < 0), additive (AE $= 0$), or super-additive (AE > 0) (Fig. S1). In general AE depends on the specific supplemented concentrations ΔR_1 and ΔR_2 as well as the background concentrations R_1 and R_2. To obtain a simpler property of a given growth rate model, we can calculate this property for infinitesimal supplementations on each background condition:

$$\begin{aligned}\alpha(R_1,R_2) &= \lim_{\Delta R_1,\Delta R_2\to 0} \frac{\mathrm{AE}}{\Delta R_1 \Delta R_2} \\ &= \lim_{\Delta R_1,\Delta R_2\to 0} \frac{[g(R_1+\Delta R_1, R_2+\Delta R_2) - g(R_1,R_2+\Delta R_2)] - [g(R_1+\Delta R_1,R_2) - g(R_1,R_2)]}{\Delta R_1 \Delta R_2} \\ &= \frac{\partial^2 g(R_1,R_2)}{\partial R_1 \partial R_2}.\end{aligned} \quad \text{[S11]}$$

Thus the first derivatives of growth rate with respect to resource concentration indicate whether there is colimitation at all (through the limitation coefficients and the effective number of limiting factors), while the second derivatives indicate the additivity of that colimitation.

H. Effect of implicit resources on empirical estimates of limitation and colimitation in natural environments. In Fig. 4B,C we estimate growth rate limitation coefficients and the effective number of limiting resources for several species in natural environments. One caveat of these estimates is that they are based on measurements of growth rate response and environmental concentration of only a few resources for each species. It is therefore important to address the possible effects of implicit, unmeasured resources on this analysis.

Let resource 1 be the focal, variable resource (one of those reported in Dataset S3 and plotted in Fig. 4), and let resource 2 be an implicit resource that was not measured or varied. The implicit resource 2 enters at two points in our analysis. First, it enters in the measurement condition for the growth rate response, where it could affect the measured half-saturation concentration K_1. In previous work we showed how the concentration of an implicit resource in that condition affects the apparent half-saturation concentration of a variable resource (7). Ideally, R_2 is sufficiently high in those measurement conditions so that K_1 does not depend on it; each model we consider for this analysis (Liebig Monod, PAT, additive, and multiplicative Monod) has the property that the model for M resources reduces to the same model for $M-1$ resources if one of the resource concentrations is taken to infinity (section S2). However, if R_2 is low enough (e.g., $R_2 \sim K_2$) in the measurement condition for growth rate response, it may bias measurements of K_1. For example, the measured value of K_1 will underestimate its true value under the Liebig Monod, PAT, and additive models, although for the multiplicative Monod model the measured K_1 does not depend on R_2 even at low concentrations (7).

The second point in our analysis at which implicit resources could affect the outcome is in the natural environment condition where we aim to estimate the limitation coefficients. In our analysis, we assume the growth rate response of the organism in the natural environment is the same as in the measurement conditions for K (e.g., in a laboratory experiment). However, this assumption could break down if the implicit resources have much lower concentrations in the natural environment compared to the measurement condition. We can use the plots of the growth rate models in Fig. S3 to deduce how an implicit resource would quantitatively affect our estimates of limitation for the variable resource. For example, the contours in the second row of Fig. S3 tell us how the limitation coefficient L_1^{rate} of a measured resource 1 is affected by the concentration R_2 of an implicit resource 2. If the implicit resource is at high concentration R_2 relative to its half-saturation concentration K_2, then it has little effect on the limitation coefficient of the variable resource (i.e., blue contours of L_1^{rate} depend only weakly on R_2 for high R_2) under the PAT and additive models, and for the Liebig Monod and multiplicative Monod models it has no effect at all since the blue contours are vertical. This is the ideal case where the natural condition matches the measurement condition (implicit resource is saturated in both cases). However, if the implicit resource is low relative to its half-saturation concentration, then the limitation coefficient estimated without the implicit resource will always be an overestimate of the true value (i.e., the variable resource is not as limiting as one would think because the implicit resource is also significantly limiting). For the Liebig Monod model, the true limitation coefficient for the variable resource may even be zero if the implicit resource is sufficiently scarce. For the multiplicative Monod model, the limitation coefficient for the variable resource remains independent of all other resource concentrations. Therefore, the limitation coefficients we calculate in Fig. 4B are at worst upper bounds on the true

limitation coefficients in the natural environments, all other aspects of the environments being equal. This bound holds for most other phenomenological growth rate models as well (section S2), with a few exceptions (e.g., the Mankad-Bungay model).

An alternative way to understand the effects of implicit resources is through the parameter $g_{\max}$, which is the maximum possible growth rate when limited only by implicit factors (the variable resources are saturated and not limiting at all). This parameter therefore depends on the concentrations of the implicit resources. An equivalent framing of the foregoing argument is whether $g_{\max}$ in the measurement condition for the growth rate response is the same as $g_{\max}$ in the natural environment; if it is, then the limitation coefficient estimates for the variable resources in the natural environment already include any contributions from implicit resources. However, if $g_{\max}$ is significantly different in the natural environment (e.g., much lower because implicit resources are at much lower concentrations), then those limitation estimates may be overestimates because they do not include sufficient limitation from the implicit factors.

Finally, we address the effect of implicit resources on colimitation, as quantified by the effective number of rate-limiting resources $M_{\text{eff}}^{\text{rate}}$ (Fig. 4C). Here we calculate colimitation only between the two variable resources (Eq. S9), rather than colimitation between them and implicit resources (which would require knowing $g_{\max}$ in the natural environment). For the Liebig Monod, additive, and multiplicative Monod models we use in the analysis, implicit resources in the natural environment condition do not affect colimitation between the variable resources. The effect of implicit resources on colimitation is trivial in the Liebig Monod model, since $M_{\text{eff}}^{\text{rate}} = 1$ always by construction. In the multiplicative Monod model, the limitation coefficients for the variable resources do not depend on the implicit resources in the natural environment, so their colimitation is also unaffected. In the additive model, implicit resources can reduce the limitation coefficients for the variable resources (as aforementioned), but they do so through the denominator in Eq. S42, which is the same for each variable resource. Since the effective number of limiting resources between the two variable resources depends only on the ratio of their limitation coefficients ($M_{\text{eff}}^{\text{rate}} = (L_1^{\text{rate}} + L_2^{\text{rate}})/\max(L_1^{\text{rate}}, L_2^{\text{rate}})$), the effect of the implicit resources cancels. For the PAT model, though, implicit resources do not rescale the limitation coefficients for the variable resources equally (i.e., see Eq. S38), and thus they could affect estimates of colimitation under that model. If the implicit resources in the natural environment are lower than in the growth rate response measurement condition, then the estimated degree of colimitation between the variable resources will be an overestimate.

S2. Phenomenological models of growth rate and growth yield colimitation

Many different mathematical models of how growth rate depends on resource concentrations have been studied in the literature. For the most part these models have been introduced and used phenomenologically, although recent work has proposed that some models may represent different approximations of the same underlying process (8–10). Here we summarize a variety of the most common models, discussing their mechanistic interpretations (if any) but with a particular focus on their limitation properties. These models have almost all been devised for growth rate, but we apply them phenomenologically to growth yield as well. Table S1 lists all models for a generic growth trait z (which represents either growth rate g or growth yield N) in the special case of two variable resources, which we use for fitting our scans of *E. coli* growth across glucose and ammonium concentrations (Figs. S14 and S24).

Each model has the form of either growth rate g or growth yield N as a function of $\mathbf{R} = (R_1, R_2, \ldots, R_M)$, the vector of the M variable resource concentrations. All growth rate models include the parameters $g_{\max}$, which is the maximum growth rate g when the variable resources R_i are unlimited and captures limitation by implicit factors (other resources that are not varied as well as internal processes such as a transcription and translation), and the specific affinity a_i for each resource i, which is the growth rate per unit resource i when resource i is rare. The mathematical equivalents of these parameters for growth yield N are the maximum yield $N_{\max}$ and the stoichiometry s_i, which is the amount of biomass produced per unit resource i when resource i is rare. For each model we express its mathematical form as well as calculate its limitation coefficients L_i (main text Eq. 1) for each variable resource i and the effective number of limiting factors M_{eff} (main text Eq. 3). The limitation coefficient for the implicit factors is determined by the normalization condition $L_{\text{imp}}^{\text{rate}} = 1 - \sum_{\text{resource } i} L_i^{\text{rate}}$ or equivalently by taking derivatives with respect to $g_{\max}$, since that is the rate of the implicit processes:

$$L_{\text{imp}}^{\text{rate}} = \frac{g_{\max}}{g} \frac{\partial g}{\partial g_{\max}}, \qquad \text{[S12]}$$

with an analogous expression in the case of growth yield limitation for $L_{\text{imp}}^{\text{yield}}$. An important property of each model is how resources coarse-grain into these implicit factors (9). For example, if we consider a model with explicit sources of carbon, nitrogen, and phosphorus, how does it coarse-grain into a model with only explicit sources of carbon and nitrogen (with phosphorus fixed)?

The growth rate models discussed in this section are alternatively parameterized using the half-saturation concentrations $K_i = g_{\max}/a_i$ instead of the specific affinities a_i (7). However, we favor parameterizing in terms of the specific affinities for two reasons. First, this parameterization better aligns with the mechanistic interpretations of these models (where a_i is the uptake rate of resource i per unit resource; main text Eq. 4). Second, this parameterization explicitly isolates the dependence on the implicit factors into the maximum growth rate $g_{\max}$, which is otherwise conflated with the affinities in the parameterization using K_i. In particular, that makes it more complicated to correctly calculate limitation by the implicit factors (Eq. S12) and verify the normalization condition (main text Eq. 2).

Model name	Parameters	Formula for trait z (growth rate g or growth yield N)	Colimitation between resources?	Colimitation with implicit factors?
Liebig Blackman	$z_{\max}$,c_1,c_2	$z_{\max} \min\left(\frac{c_1 R_2}{z_{\max}}, \frac{c_2 R_2}{z_{\max}}, 1\right)$	No	No
Liebig Monod	$z_{\max}$,c_1,c_2	$z_{\max} \min\left(\frac{c_1 R_1}{c_1 R_1 + z_{\max}}, \frac{c_2 R_2}{c_2 R_2 + z_{\max}}\right)$	No	Yes
Liebig Hill	$z_{\max}$,c_2,c_2, n_1,n_2	$z_{\max} \min\left(\frac{(c_1 R_1)^{n_1}}{(c_1 R_1)^{n_1} + z_{\max}^{n_1}}, \frac{(c_2 R_2)^{n_2}}{(c_2 R_2)^{n_2} + z_{\max}^{n_2}}\right)$	No	Yes
Liebig Bertalanffy	$z_{\max}$,c_1,c_2	$z_{\max} \min\left(1 - 2^{-c_1 R_1 / z_{\max}}, 1 - 2^{-c_2 R_2 / z_{\max}}\right)$	No	Yes
Multiplicative Blackman	$z_{\max}$,c_1,c_2	$z_{\max} \min\left(\frac{c_1 R_2}{z_{\max}}, 1\right) \cdot \min\left(\frac{c_2 R_2}{z_{\max}}, 1\right)$	Yes (super-additive)	No
Multiplicative Monod	$z_{\max}$,c_1,c_2	$z_{\max} \left(\frac{c_1 R_1}{c_1 R_1 + z_{\max}}\right) \left(\frac{c_2 R_2}{c_2 R_2 + z_{\max}}\right)$	Yes (super-additive)	Yes
Multiplicative Hill	$z_{\max}$,c_2,c_2, n_1,n_2	$z_{\max} \left(\frac{(c_1 R_1)^{n_1}}{(c_1 R_1)^{n_1} + z_{\max}^{n_1}}\right) \left(\frac{(c_2 R_2)^{n_2}}{(c_2 R_2)^{n_2} + z_{\max}^{n_2}}\right)$	Yes (super-additive)	Yes
Multiplicative Bertalanffy	$z_{\max}$,c_1,c_2	$z_{\max} \left(1 - 2^{-c_1 R_1 / z_{\max}}\right) \left(1 - 2^{-c_2 R_2 / z_{\max}}\right)$	Yes (super-additive)	Yes
Poisson arrival time (PAT) / synthesizing unit	$z_{\max}$,c_1,c_2	$z_{\max} \frac{c_1 R_1 c_2 R_2 (c_1 R_1 + c_2 R_2)}{c_1 R_1 c_2 R_2 (c_1 R_1 + c_2 R_2) + z_{\max}[(c_1 R_1)^2 + c_1 R_1 c_2 R_2 + (c_2 R_2)^2]}$	Yes (super-additive)	Yes
Additive	$z_{\max}$,c_1,c_2	$\frac{1}{(c_1 R_1)^{-1} + (c_2 R_2)^{-1} + z_{\max}^{-1}}$	Yes (super-additive)	Yes
Mankad-Bungay	$z_{\max}$,c_1,c_2	$z_{\max} \left(\frac{c_1 R_1 c_2 R_2}{c_1 R_1 + c_2 R_2}\right) \left(\frac{1}{c_1 R_1 + z_{\max}} + \frac{1}{c_2 R_2 + z_{\max}}\right)$	Yes (super- and sub-additive)	Yes
Generalized additive	$z_{\max}$,c_1,c_2, q	$\frac{1}{\left((c_1 R_1)^{-q} + (c_2 R_2)^{-q} + z_{\max}^{-q}\right)^{1/q}}$	Yes (super-additive $q > -1$, sub-additive $q < -1$)	Yes
Saito substitutable	$z_{\max}$,c_1,c_2	$z_{\max} \frac{c_1 R_1 + c_2 R_2}{c_1 R_1 + c_2 R_2 + z_{\max}}$	Yes (sub-additive)	Yes
Mean Monod	$z_{\max}$,c_1,c_2	$z_{\max} \left(\frac{1}{2} \frac{c_1 R_1}{c_1 R_1 + z_{\max}} + \frac{1}{2} \frac{c_2 R_2}{c_2 R_2 + z_{\max}}\right)$	Yes (additive)	Yes
Chemically-dependent	$z_{\max}$,c_1,c_2	$z_{\max} \frac{c_1 R_1 c_2 R_2}{c_1 R_1 c_2 R_2 + z_{\max}(c_2 R_2 + z_{\max})}$	Yes (super- and sub-additive)	Yes

Table S1. Summary of all trait models for fitting resource scans. Each model has a corresponding version (labeled with the suffix "Rmin") in which the resource concentrations R_1 and R_2 are shifted by additional free parameters $R_{1,\min}$ and $R_{2,\min}$. When the trait z is growth rate g, the maximum trait parameter is $z_{\max} = g_{\max}$ and the coefficients are $c_i = a_i$, the specific affinities. When the trait z is the growth yield N, the maximum trait parameter is $z_{\max} = N_{\max}$ and the coefficients are $c_i = s_i$, the biomass to resource stoichiometries. See Figs. S14 and S24 for fits of all these models to the growth rate and growth yield data.

A. Liebig models. This is arguably the most widely-used class of models of multiple-resource dependence (8, 10–13), likely due to its mathematical simplicity. It is inspired by the Law of the Minimum attributed to Justus von Liebig (14): that only a single resource determines growth rate under any given set of conditions. Heuristically, we can interpret this model for growth rate as meaning that total biomass growth consists of multiple processes in parallel (uptake of each variable resource along with all implicit limiting processes), such that the total rate of all processes is set by whichever process is the slowest (8, 10). Mathematically, this is expressed as a minimum over a set of functions for each resource. As a result, none of these models entail colimitation among variable resources, although some include colimitation between variable resources and implicit factors (Table S1). The asymmetric treatment of the variable resources and implicit factors means that many of these models are not robust under coarse-graining of the number of resources.

A.1. Liebig Blackman. The Blackman model for growth rate (main text Eq. 5) with one variable resource is a minimum function of the uptake rate for that resource and the rate of all implicit processes (15), so the Liebig Blackman model extends this to a minimum over all variable resources as well as the implicit factors:

$$\begin{aligned} g(\mathbf{R}) &= \min_{\text{resource } i} \left[\min\left(a_i R_i, g_{\max}\right) \right] \\ &= g_{\max} \min\left(1, \frac{a_1 R_1}{g_{\max}}, \frac{a_2 R_2}{g_{\max}}, \ldots, \frac{a_M R_M}{g_{\max}}\right). \end{aligned} \tag{S13}$$

Here we parameterize this model (rescaling each $a_i R_i$ by $g_{\max}$) differently than the Blackman model in the main text (Eq. 5) so that the minimum function is dimensionless and can thus be rescaled by $g_{\max}$ overall to get the total rate. This is convenient because it better matches the form of the other models (Table S1). Coarse-graining out a resource k depends on whether $a_k R_k < g_{\max}$ (i.e., resource k is more limiting than the implicit factors). If so, then we transform $g_{\max} \to a_k R_k$ to coarse-grain the model into a new model for the remaining $M-1$ resources, with resource k as the new dominant implicit factor. If $a_k R_k > g_{\max}$, then we simply drop $a_k R_k$ from the minimum function (since it is never the minimum) and the model with the same parameters holds for the remaining $M-1$ resources.

The limitation coefficient for each variable resource is

$$\begin{aligned} L_i^{\text{rate}}(\mathbf{R}) &= \frac{R_i}{g}\frac{\partial g}{\partial R_i} \\ &= \begin{cases} 1 & \text{if } \dfrac{a_i R_i}{z_{\max}} = \min\left(1, \dfrac{a_1 R_1}{g_{\max}}, \dfrac{a_2 R_2}{g_{\max}}, \ldots, \dfrac{a_M R_M}{g_{\max}}\right), \\ 0 & \text{otherwise.} \end{cases} \end{aligned} \tag{S14}$$

Therefore exactly one limitation coefficient (either for a resource L_i^{rate} or for the implicit factors $L_{\text{imp}}^{\text{rate}}$) is 1 while all others are 0, meaning there is no colimitation among variable resources or the implicit factors. Thus the number of limiting factors is always $M_{\text{eff}}^{\text{rate}} = 1$.

For yield colimitation, the Liebig Blackman model is arguably the simplest model since it holds if we assume fixed stoichiometry for all resources and that growth stops only once at least one resource is completely exhausted. For example, if we assume that each unit of biomass requires exactly s_i units of resource i, then the total biomass yield must be (see section S3A)

$$N(\mathbf{R}) = \min\left(N_{\max}, s_1 R_1, s_2 R_2, \ldots, s_M R_M\right). \tag{S15}$$

A.2. Liebig Monod. This is the most common form of Liebig model for growth rate (8, 10–13) although its empirical support is weak, generally favoring other models when compared head-to-head (10, 16, 17). Here the minimum taken over individual Monod models for each resource (Fig. S3, first row and first column):

$$g(\mathbf{R}) = g_{\max} \min_{\text{resource } i} \left(\frac{a_i R_i}{a_i R_i + g_{\max}} \right). \tag{S16}$$

One shortcoming of the Liebig Monod model is that it does not robustly transform under resource coarse-graining. If we are coarse-graining a resource k at infinite concentration, then we can simply drop it from the minimum function to obtain the model for the remaining $M-1$ resources with no other changes. For example, the Liebig Monod model reduces to a regular Monod model for a single resource if all other resources are unlimited. However, if R_k is finite, then the Liebig Monod model does not coarse-grain into another Liebig Monod model, but a hybrid of the Liebig Monod and Blackman models, since the Monod function for resource k will remain in the minimum function as a constant.

The limitation coefficient for each variable resource in the Liebig model is

$$\begin{aligned} L_i^{\text{rate}}(\mathbf{R}) &= \frac{R_i}{g}\frac{\partial g}{\partial R_i} \\ &= \begin{cases} \dfrac{g_{\max}}{a_i R_i + g_{\max}} & \text{if } i = \arg\min\limits_{\text{resource } j} \left(\dfrac{a_j R_j}{a_j R_j + g_{\max}} \right), \\ 0 & \text{otherwise.} \end{cases} \end{aligned} \tag{S17}$$

Unlike the Liebig Blackman model, where all limitation is completely concentrated in either one variable resource or the implicit factors, the Liebig Monod model always has nonzero limitation coefficient for one of the variable resources (with all other variable resources having zero limitation), but that limitation coefficient is less than 1. This means that the Liebig Monod model has colimitation between a variable resource and the implicit factors, but no colimitation between variable resources. (Mathematically it is possible to have colimitation between the resources when there is an exact balance of the two resources $a_i R_i = a_j R_j$, but we discount this possibility biologically since that fine-tuning is extremely unlikely.)

Figure S3 shows the limitation coefficients L_1^{rate}, L_2^{rate} (second row, first column) and effective number of limiting factors $M_{\text{eff}}^{\text{rate}}$ (third row, first column) for this model in the case of two variable resources. The lack of overlap between the contours of L_1^{rate} (blue) and L_2^{rate} (orange) represents the lack of colimitation between the resources, while the plot of $M_{\text{eff}}^{\text{rate}}$ shows that the only smooth regions of colimitation ($M_{\text{eff}}^{\text{rate}} > 1$) occur where either $R_1 \approx g_{\max}/a_1$ or $R_2 \approx g_{\max}/a_2$ (colimitation between one resource and the implicit factors, $M_{\text{eff}}^{\text{rate}} \approx 2$). Conceptually, this asymmetric treatment of the variable resources and implicit factors is why resources do not consistently coarse-grain into the implicit factors in this model.

A.3. Liebig Hill. The Liebig Hill model is similar to the Liebig Monod model but uses Hill models (1) (also known as the Moser model (2) or Holling Type III model (3)) for each resource in the minimizing function, rather than Monod models:

$$g(\mathbf{R}) = g_{\max} \min_{\text{resource } i} \left(\frac{(a_i R_i)^{n_i}}{(a_i R_i)^{n_i} + g_{\max}^{n_i}} \right), \tag{S18}$$

where n_i is a cooperativity coefficient for each resource. Hill dependence is uncommon in ecological and microbiology models, but one study observed it for yeast auxotrophs growing on lysine (1). When $n_i = 1$, the dependence is equivalent to Monod, but $n_i > 1$ creates cooperativity such that growth rate increases super-linearly with resource concentration at low concentrations. In particularly, this allows for switch-like dependence such that growth rate depends only weakly on a resource when it is low, but then rapidly jumps to a maximum concentration above a threshold concentration of that resource (1). The Liebig Hill model has coarse-graining properties similar to those of the Liebig Monod model — one can only coarse-grain resources at infinite concentrations to obtain reduced versions of the same model.

The limitation coefficient for each variable resource is

$$\begin{aligned} L_i^{\text{rate}}(\mathbf{R}) &= \frac{R_i}{g} \frac{\partial g}{\partial R_i} \\ &= \begin{cases} \dfrac{n_i g_{\max}^{n_i}}{(a_i R_i)^{n_i} + g_{\max}^{n_i}} & \text{if } i = \arg\min_{\text{resource } j} \left(\dfrac{(a_j R_j)^{n_j}}{(a_j R_j)^{n_j} + g_{\max}^{n_j}} \right), \\ 0 & \text{otherwise.} \end{cases} \end{aligned} \tag{S19}$$

Like the Liebig Monod model, there is no colimitation between variable resources, but there is colimitation between the most limiting variable resource and the implicit factors. Unlike the Liebig Monod and Liebig Blackman models, though, the super-linear dependence in the Hill model means that limitation coefficients can be greater than 1 for some resources (section S1B), which in turn means that other limitation coefficients must be negative so that the sum of limitation coefficients remains normalized (main text Eq. 2). For example, when R_i is extremely low, $L_i^{\text{rate}} \approx n_i$, which will be greater than 1 if there is cooperativity, while the limitation coefficient for the implicit factors must then be $L_{\text{imp}}^{\text{rate}} \approx 1 - n_i$, which will be negative if $n_i > 1$. This suggests that under a Hill model, increasing the implicit factors actually decreases growth rate when another resource is strongly limiting. This also means that the effective number of limiting factors $M_{\text{eff}}^{\text{rate}}$ can be less than 1 when counting these negatively-limiting factors (section S1E).

A.4. Liebig Bertalanffy. This model is similar to the Liebig Monod and Liebig Hill models but uses the Bertalanffy model (16) for each resource, which saturates more rapidly at high resource concentrations (exponentially) compared to the Monod and Hill models (power laws):

$$g(\mathbf{R}) = g_{\max} \min_{\text{resource } i} \left(1 - 2^{-a_i R_i / g_{\max}}\right). \tag{S20}$$

The applicability of the Bertalanffy model is unknown since it is rarely used in ecological and microbiology contexts, with one recent exception that found it did fit data better than other models (16). The Liebig Bertalanffy model has coarse-graining properties similar to those of the Liebig Monod model — one can only coarse-grain resources at infinite concentrations to obtain reduced versions of the same model.

The limitation coefficient for each variable resource is

$$\begin{aligned} L_i^{\text{rate}}(\mathbf{R}) &= \frac{R_i}{g} \frac{\partial g}{\partial R_i} \\ &= \begin{cases} \dfrac{a_i R_i}{g_{\max}} \dfrac{\log 2}{2^{a_i R_i / g_{\max}} - 1} & \text{if } i = \arg\min_{\text{resource } j} \left(1 - 2^{-a_j R_j / g_{\max}}\right), \\ 0 & \text{otherwise.} \end{cases} \end{aligned} \tag{S21}$$

Its limitation coefficients and colimitation are qualitatively similar to those of the Liebig Monod model: just one variable resource has limitation coefficient between 0 and 1, with all other variable resources having zero limitation. There is colimitation between the one limiting variable resource and the implicit factors, but no colimitation between variable resources.

B. Multiplicative models. Multiplicative models are also a common form of growth rate dependence on multiple resources (12, 13, 16). Heuristically, these models for growth rate are based on the law of mass action, in which a reaction rate is a product of rates for input reactions. Muscarella and O'Dwyer (8) showed that a multiplicative dependence of growth rate emerges when implicit processes are slow compared to uptake of the variable resources, which is the opposite limit of the Liebig dependence (when uptake is slow compared to downstream implicit factors).

In contrast to the Liebig models (no colimitation between resources, but sometimes colimitation with implicit factors), all multiplicative models entail colimitation between variable resources, which is always super-additive (section S1G; Table S1). The models vary, though in terms of whether there is colimitation with implicit factors. One salient feature of all multiplicative models is that the limitation coefficient for each resource is independent of all other resource concentrations. As a result these models robustly transform under coarse-graining of resources. Another consequence of this property is that when multiple resources are colimiting (large limitation coefficients that sum to greater than 1), limitation of the implicit factors must be negative to maintain normalization of total limitation. This means that increasing the implicit factors (e.g., $g_{\max}$) would actually decrease growth rate in that regime. It is unclear whether this is a biologically meaningful property, though, or an indication that coarse-graining in these models is invalid (9).

B.1. Multiplicative Blackman. This model is analogous to the Liebig Blackman model, but multiplying individual Blackman models for each resource:

$$g(\mathbf{R}) = g_{\max} \prod_{\text{resource } i} \min\left(\frac{a_i R_i}{g_{\max}}, 1\right). \qquad \text{[S22]}$$

To coarse-grain a resource k less limiting than the implicit factors ($a_k R_k > g_{\max}$), we drop the factor for k from the product to obtain the coarse-grained model for the remaining $M-1$ resources (with no other changes to parameters). If resource k is more limiting than the implicit factors ($a_k R_k < g_{\max}$), then we must transform $g_{\max} \to a_k R_k$ (this resource becomes the dominant implicit factor) as well as transform the affinities $a_i \to a_i a_k R_k / g_{\max}$ (i.e., the effective affinities decrease by the factor $a_k R_k / g_{\max}$ to account for the new most limiting implicit factor). For all multiplicative Models, the half-saturation concentration $K_i = g_{\max}/a_i$ is arguably more convenient because these parameters remain invariant under coarse-graining.

The limitation coefficient for each variable resource is

$$\begin{aligned} L_i^{\text{rate}}(\mathbf{R}) &= \frac{R_i}{g}\frac{\partial g}{\partial R_i} \\ &= \begin{cases} 1 & \text{if } \dfrac{a_i R_i}{g_{\max}} < 1, \\ 0 & \text{otherwise.} \end{cases} \end{aligned} \qquad \text{[S23]}$$

Therefore there is perfect colimitation among each variable resource with $a_i R_i / g_{\max} < 1$. If there is more than one such variable resource, then the limitation coefficient for the implicit factors becomes negative to compensate. As a result, the effective number of limiting factors, including all variable resources and the implicit factors, is always $M_{\text{eff}}^{\text{rate}} = 1$, but it can take on other values for subsets of factors. For example, if there are two variable resources with $a_i R_i / g_{\max} < 1$, then the effective number of limiting resources is $M_{\text{eff},\{1,2\}} = 2$, but the effective number of limiting factors between one of those resources and the implicit factors is $M_{\text{eff},\{1,\text{imp}\}} = 0$ (section S1E).

B.2. Multiplicative Monod. This model is a product of Monod models for each resource (12, 16, 17), and besides the Liebig Monod model, is probably the most commonly-used model for growth rate (Fig. S3, first row and second column):

$$g(\mathbf{R}) = g_{\max} \prod_{\text{resource } i} \frac{a_i R_i}{a_i R_i + g_{\max}}. \qquad \text{[S24]}$$

Coarse-graining a resource k entails absorbing its Monod function into $g_{\max}$ ($g_{\max} \to g_{\max} a_k R_k / (a_k R_k + g_{\max})$) as well as transforming the affinities $a_i \to a_i a_k R_k / (a_k R_k + g_{\max})$. Again we see that the half-saturation concentrations $K_i = g_{\max}/a_i$ are invariant under these transformations. Some empirical tests have favored this model (17), especially over the Liebig Monod model, although theoretical work has criticized it on the basis of its coarse-graining properties (10).

Since the growth rate exactly factorizes into separate contributions from each resource, the limitation coefficients for the multiple-resource case are the same as for the single-resource Monod model:

$$\begin{aligned} L_i^{\text{rate}}(\mathbf{R}) &= \frac{R_i}{g}\frac{\partial g}{\partial R_i} \\ &= \frac{g_{\max}}{a_i R_i + g_{\max}}. \end{aligned} \qquad \text{[S25]}$$

This is the first model we have discussed so far with colimitation between all variable resources and the implicit factors. The limitation coefficient for each variable resource ranges between 0 and 1, but like the multiplicative Blackman model, it is possible for the implicit factors to be negatively limiting if multiple variable resources are sufficiently limiting.

Figure S3 shows the limitation coefficients L_1^{rate}, L_2^{rate} (second row, second column) and effective number of limiting factors $M_{\text{eff}}^{\text{rate}}$ (third row, second column) for this model in the case of two variable resources. The overlap between the contours of

L_1^{rate} (blue) and L_2^{rate} (orange) represents colimitation between the resources, while the plot of $M_{\text{eff}}^{\text{rate}}$ shows extensive regions of colimitation ($M_{\text{eff}}^{\text{rate}} > 1$) between the two resources and the implicit factors (compare to the schematic in Fig. 1B). Colimitation is maximized in this case at $M_{\text{eff}}^{\text{rate}} = 3$ when $a_1 R_1 = a_2 R_2 = 2g_{\max}$ (where $L_1 = L_2 = 1/3$).

B.3. Multiplicative Hill. This model is similar to the multiplicative Monod model but using Hill models for each resource (1):

$$g(\mathbf{R}) = g_{\max} \prod_{\text{resource } i} \frac{(a_i R_i)^{n_i}}{(a_i R_i)^{n_i} + g_{\max}^{n_i}}. \tag{S26}$$

Like the Liebig Hill model, it has been rarely applied in ecology or microbiology. The coarse-graining properties of this model are analogous to those of the multiplicative Monod model. The limitation coefficient for each resource is the same as for the single-resource Hill model:

$$\begin{aligned} L_i^{\text{rate}}(\mathbf{R}) &= \frac{R_i}{g}\frac{\partial g}{\partial R_i} \\ &= \frac{n_i g_{\max}^{n_i}}{(a_i R_i)^{n_i} + g_{\max}^{n_i}}. \end{aligned} \tag{S27}$$

Like the Liebig Hill model, it allows for limitation coefficients greater than 1 and negative limitation for implicit factors in some regimes. Like the multiplicative Monod model, there is generally colimitation between all variable resources and the implicit factors.

B.4. Multiplicative Bertalanffy. This model is similar to the multiplicative Monod and Hill models but using Bertalanffy models for each resource (16):

$$g(\mathbf{R}) = g_{\max} \prod_{\text{resource } i} \left(1 + 2^{-a_i R_i / g_{\max}}\right). \tag{S28}$$

Like the Liebig Bertalanffy model, it has been rarely applied in ecology or microbiology. The coarse-graining properties of this model are analogous to those of the multiplicative Monod model. The limitation coefficient for each variable resource is the same as for a single-resource Bertalanffy model:

$$\begin{aligned} L_i^{\text{rate}}(\mathbf{R}) &= \frac{R_i}{g}\frac{\partial g}{\partial R_i} \\ &= \frac{a_i R_i}{g_{\max}} \frac{\log 2}{2^{a_i R_i / g_{\max}} - 1} \end{aligned} \tag{S29}$$

The limitation coefficients and colimitation are qualitatively similar to those of the multiplicative Monod model.

C. Poisson arrival time (PAT)/synthesizing-unit model. Besides the Liebig and multiplicative classes of models, there are several other distinct models for how growth rate may depend on resource concentrations (which can also be applied phenomenologically to growth yield). The Poisson arrival time (PAT) model, also sometimes called the synthesizing-unit (SU) model, has been favored theoretically by some researchers due to its derivation from a semi-mechanistic view of biomass growth (10, 11, 16, 18). Tang and Riley (10) argued that the PAT model represents the most general approximation of a more detailed chemical kinetic model of biomass growth, with other models (Liebig Monod and additive) being further approximations; however, they did not find that the PAT model provided a significantly superior fit to data.

The idea of the PAT model is that the time t_{biomass} to make a new unit of biomass is the sum of the time $t_{\text{uptake,total}}$ to uptake units of all resources and the time $t_{\text{metabolism}}$ to metabolize those resources into new biomass:

$$t_{\text{biomass}} = t_{\text{uptake,total}} + t_{\text{metabolism}}. \tag{S30}$$

In general, these times for uptake and metabolism are stochastic, described by some probability distributions. We approximate the overall growth rate of biomass as the reciprocal of the mean time:

$$\begin{aligned} g &= \frac{1}{\langle t_{\text{biomass}} \rangle} \\ &= \frac{1}{\langle t_{\text{uptake,total}} \rangle + \langle t_{\text{metabolism}} \rangle}. \end{aligned} \tag{S31}$$

We assume the mean time of metabolism $\langle t_{\text{metabolism}} \rangle$ does not depend on the environmental resource concentrations $\mathbf{R}$, since metabolism relies on resources already recruited into cells in sufficient quantities. Without loss of generality, we therefore parameterize the mean time of metabolism as $\langle t_{\text{metabolism}} \rangle = 1/g_{\max}$, since this will be the maximum growth rate if uptake time is 0.

The PAT model assumes that uptake of each resource unit occurs as an independent Poisson process, where the uptake time $t_{\text{uptake},i}$ of the ith resource has an exponential probability distribution

$$p_{\text{uptake},i}(t_{\text{uptake},i}) = a_i R_i e^{-a_i R_i t_{\text{uptake},i}}. \tag{S32}$$

We therefore assume the rate of each resource unit's uptake is proportional to the concentration R_i of the resource in the environment, with a constant of proportionality a_i (this is the stochastic equivalent to the law of mass action in main text Eq. 4 that also defines the specific affinity a_i). Since uptake of each resource unit occurs independently, the total uptake time for all resource units is the maximum of their individual uptake times:

$$t_{\text{uptake,total}} = \max_{\text{resource } i} t_{\text{uptake},i}. \tag{S33}$$

We want to calculate the average total uptake time so we can calculate the growth rate using Eq. S31. The cumulative probability that the total uptake time $t_{\text{uptake,total}}$ is less than t equals the probability that all individual resource uptake times are less than t:

$$\begin{aligned} p\left(t_{\text{uptake,total}} < t\right) &= \prod_{\text{resource } i} p_i(t_{\text{uptake},i} < t) \\ &= \prod_{\text{resource } i} \left(1 - e^{-a_i R_i t}\right), \end{aligned} \tag{S34}$$

where we have used the exponential distribution for the individual resource uptake times (Eq. S32) and the fact these times are independent of each other. The probability distribution of the total uptake time $t_{\text{uptake,total}}$ is the derivative of this cumulative distribution:

$$\begin{aligned} p(t_{\text{uptake,total}}) &= \frac{d}{dt}\, p\left(t_{\text{uptake,total}} < t\right) \\ &= \sum_{\text{resource } i} a_i R_i e^{-a_i R_i t_{\text{uptake,total}}} \prod_{\text{resource } j \neq i} \left(1 - e^{-a_j R_j t_{\text{uptake,total}}}\right). \end{aligned} \tag{S35}$$

We can now calculate the average total uptake time:

$$\begin{aligned} \langle t_{\text{uptake,total}} \rangle &= \int_0^\infty dt_{\text{uptake,total}}\; p(t_{\text{uptake,total}})\; t_{\text{uptake,total}} \\ &= \sum_{\text{resource } i} a_i R_i \int_0^\infty dt_{\text{uptake,total}}\; t_{\text{uptake,total}} e^{-a_i R_i t_{\text{uptake,total}}} \prod_{\text{resource } j \neq i} \left(1 - e^{-a_j R_j t_{\text{uptake,total}}}\right) \\ &= \sum_{\text{resource } i} \frac{1}{a_i R_i} - \sum_{\text{resource pairs } i,j} \frac{1}{a_i R_i + a_j R_j} + \sum_{\text{resource triplets } i,j,k} \frac{1}{a_i R_i + a_j R_j + a_k R_k} - \cdots, \end{aligned} \tag{S36}$$

where the sums are over individual, pair, triplet, etc. combinations of distinct resources (e.g., pairs of resource indices i and j such that $i \neq j$). Note the alternating signs across these sums.

Thus the overall growth rate from Eq. S31 for the PAT model is (Fig. S3, first row and third column)

$$\begin{aligned} g(\mathbf{R}) &= \frac{g_{\max}}{1 + g_{\max}\langle t_{\text{uptake,total}} \rangle} \\ &= g_{\max} \left(1 + g_{\max} \left[\sum_{\text{resource } i} \frac{1}{a_i R_i} - \sum_{\text{resource pairs } i,j} \frac{1}{a_i R_i + a_j R_j} + \sum_{\text{resource triplets } i,j,k} \frac{1}{a_i R_i + a_j R_j + a_k R_k} - \cdots \right] \right)^{-1}. \end{aligned} \tag{S37}$$

Taking the maximum uptake time across all resources generally causes the PAT model to not transform robustly while coarse-graining resources. If a resource to be coarse-grained is unlimited, then the PAT model does reduce to a model for the remaining $M-1$ resources with unchanged parameters. For example, if all resources but one are unlimited, then the PAT model is equivalent to a Monod model for the single limiting resource. However, if resource k has finite concentration, then it cannot be coarse-grained to transform the model into another PAT model for $M-1$ resources.

The limitation coefficient for each resource in the PAT model is

$$\begin{aligned} L_i^{\text{rate}}(\mathbf{R}) &= \frac{R_i}{g} \frac{\partial g}{\partial R_i} \\ &= -\frac{g}{g_{\max}} R_i \frac{\partial}{\partial R_i} \left(g_{\max} \langle t_{\text{uptake,total}} \rangle\right) \\ &= g a_i R_i \left(\frac{1}{(a_i R_i)^2} - \sum_{\text{resource } j \neq i} \frac{1}{(a_i R_i + a_j R_j)^2} + \sum_{\text{resources } j \neq i, k \neq i, k \neq j} \frac{1}{(a_i R_i + a_j R_j + a_k R_k)^2} - \cdots \right). \end{aligned} \tag{S38}$$

These limitation coefficients range between 0 and 1; there is super-additive colimitation between all variable resources and colimitation with implicit factors. In the special case of two variable resources, the limitation coefficients are

$$\begin{aligned} L_1^{\text{rate}} &= \frac{g_{\max}(a_2R_2)^2(2a_1R_1 + a_2R_2)}{(a_1R_1 + a_2R_2)\left[a_1R_1a_2R_2(a_1R_1 + a_2R_2) + g_{\max}((a_1R_1)^2 + a_1R_1a_2R_2 + (a_2R_2)^2)\right]}, \\ L_2^{\text{rate}} &= \frac{g_{\max}(a_1R_1)^2(a_1R_1 + 2a_2R_2)}{(a_1R_1 + a_2R_2)\left[a_1R_1a_2R_2(a_1R_1 + a_2R_2) + g_{\max}((a_1R_1)^2 + a_1R_1a_2R_2 + (a_2R_2)^2)\right]}. \end{aligned} \quad \text{[S39]}$$

Figure S3 shows the limitation coefficients L_1^{rate}, L_2^{rate} (second row, third column) and effective number of limiting factors $M_{\text{eff}}^{\text{rate}}$ (third row, third column) for the PAT model in this case. The overlap between the contours of L_1^{rate} (blue) and L_2^{rate} (orange) represents colimitation between the resources, while the plot of $M_{\text{eff}}^{\text{rate}}$ shows extensive regions of colimitation ($M_{\text{eff}}^{\text{rate}} > 1$) between the two resources and the implicit factors (compare to the schematic in Fig. 1B). Note that these regions for the PAT model are smaller than those of the multiplicative Monod model with the same parameter values (compare second and third columns in the third row of Fig. S3), which suggests that the PAT model has less colimitation in some sense. Colimitation is also maximized at a different combination of parameters compared to the multiplicative Monod model ($a_1R_1 = a_2R_2 = 3g_{\max}/4$).

D. Additive model. This model (unrelated to the additivity property of resource supplementation, section S1G) has a similar motivation to that of the PAT model, in terms of decomposing biomass growth into uptake of individual units of resources followed by metabolism. However, instead of assuming uptake processes of all resource units occur in parallel, such that the total uptake time is the maximum of these individual uptake times (Eq. S33), we assume that the uptake processes occur sequentially, such that the individual uptake times add up to the total uptake time (11, 16):

$$t_{\text{uptake,total}} = \sum_{\text{resource } i} t_{\text{uptake},i}. \quad \text{[S40]}$$

We otherwise make the same assumptions, i.e., that uptake of each resource unit is a Poisson process with rate a_iR_i. Therefore the growth rate is (Fig. S3, first row and fourth column)

$$\begin{aligned} g(\mathbf{R}) &= \frac{1}{\langle t_{\text{metabolism}}\rangle + \langle t_{\text{uptake,total}}\rangle} \\ &= \frac{1}{\langle t_{\text{metabolism}}\rangle + \sum_{\text{resource } i}\langle t_{\text{uptake},i}\rangle} \\ &= \frac{1}{g_{\max}^{-1} + \sum_{\text{resource } i}(a_iR_i)^{-1}}. \end{aligned} \quad \text{[S41]}$$

Additive model dependence has also emerged in more complex physiological models of biomass growth (19, 20). Tang and Riley (10) argued that the additive model is an approximation of the PAT model but found that it fit data at least as well as the PAT model did. Otherwise, there are few other empirical tests of this model.

Unlike the PAT model, the additive model is robust to coarse-graining resources. To coarse-grain a resource k, we simply absorb its contribution in the denominator of Eq. S41 into $g_{\max}^{-1}$, i.e., $g_{\max} \to (g_{\max}^{-1} + (a_kR_k)^{-1})^{-1}$. Note that in the additive model, the specific affinities a_i are invariant under coarse-graining while the half-saturation concentrations $K_i = g_{\max}/a_i$ are not; in the multiplicative models, it is the opposite. Thus the question of which of these two parameterizations (using specific affinities a_i or half-saturation concentrations K_i) is more fundamental may depend on which of these growth rate models (multiplicative or additive) is correct.

The limitation coefficient for each resource in the additive model is (Fig. S3, second row and fourth column)

$$\begin{aligned} L_i^{\text{rate}}(\mathbf{R}) &= \frac{R_i}{g}\frac{\partial g}{\partial R_i} \\ &= \frac{(a_iR_i)^{-1}}{g_{\max}^{-1} + \sum_{\text{resource } j}(a_jR_j)^{-1}}. \end{aligned} \quad \text{[S42]}$$

Limitation in the additive model is qualitatively identical to that of the PAT model: the limitation coefficients range between 0 and 1, and there is super-additive colimitation between all variable resources and colimitation with implicit factors. Figure S3 shows the limitation coefficients L_1^{rate}, L_2^{rate} (second row, fourth column) and effective number of limiting factors $M_{\text{eff}}^{\text{rate}}$ (third row, fourth column) for this model with two variable resources. The overlap between the contours of L_1^{rate} (blue) and L_2^{rate} (orange) represents colimitation between the resources, while the plot of $M_{\text{eff}}^{\text{rate}}$ shows regions of colimitation ($M_{\text{eff}}^{\text{rate}} > 1$) between the two resources and the implicit factors (compare to the schematic in Fig. 1B). Note that these regions for the additive model are smaller than those of the multiplicative Monod and but larger than colimitation regions of the PAT models with the same parameter values (compare fourth column in the third row of Fig. S3 to the second and third columns in the third row), which suggests that the additive model has an intermediate extent of colimitation compared to the multiplicative Monod and PAT models. Colimitation is also maximized at a different combination of parameters compared to the multiplicative Monod and PAT models ($a_1R_1 = a_2R_2 = g_{\max}$).

E. Mankad-Bungay model. The Mankad-Bungay model is a phenomenological model proposed by Mankad and Bungay (21, 22) in the form of a weighted sum of Monod functions for each resource (originally for two resources only, but generalized here to an arbitrary number):

$$\begin{aligned} g(\mathbf{R}) &= g_{\max} \sum_{\text{resource } i} \left(\frac{(a_i R_i)^{-1}}{\sum_{\text{resource } j} (a_j R_j)^{-1}} \right) \left(\frac{a_i R_i}{a_i R_i + g_{\max}} \right) \\ &= g_{\max} \frac{\sum_{\text{resource } i} (a_i R_i + g_{\max})^{-1}}{\sum_{\text{resource } i} (a_i R_i)^{-1}}. \end{aligned} \tag{S43}$$

This model is very rarely used and thus has little empirical or theoretical support; one study claimed it fit data better than the multiplicative Monod model did, but this was based on very few data points (21). Like the Liebig models and the PAT model, the Mankad-Bungay model is only robust to coarse-graining resources if those resources are at infinite concentrations.

The limitation coefficient for each resource is

$$\begin{aligned} L_i^{\text{rate}}(\mathbf{R}) &= \frac{R_i}{g} \frac{\partial g}{\partial R_i} \\ &= -\frac{a_i R_i}{(a_i R_i + g_{\max})^2 \sum_{\text{resource } j} (a_j R_j + g_{\max})^{-1}} + \frac{1}{a_i R_i \sum_{\text{resource } j} (a_j R_j)^{-1}}. \end{aligned} \tag{S44}$$

Note that the Mankad-Bungay model has non-monotonic dependence on resource concentrations in some regimes, unlike all other models considered here, so there can be negative limitation for a resource in those conditions. Specifically, the growth rate decreases as a function of R_1 when

$$R_1 > \frac{1}{a_1} \left(a_2 R_2 + \sqrt{2 a_2 R_2 (g_{\max} + a_2 R_2)} \right). \tag{S45}$$

In general, this model has colimitation between the variable resources and implicit factors. Colimitation between resources is mostly super-additive except in regimes of strong single limitation, where it can be sub-additive. These unusual properties compared to more common models may be artifacts of this model's particular formulation, and may indicate that it does not have a sound mechanistic basis.

F. Generalized-additive model of essential and substitutable resources. The aforementioned additive model (section S2D) is based on the idea that the total time to uptake all resources is the sum of uptake times for each one. This means the growth rate is the harmonic sum (reciprocal sum of reciprocals) of the rates for each step in the process. A phenomenological way to generalize this is to use a generalized sum, based on the idea of the generalized (or power) mean (23); this is a family of ways to average over a set of numbers, encompassing several more common means such as the arithmetic, harmonic, and geometric means. The generalized-additive model of growth rate is

$$g(\mathbf{R}) = \left(g_{\max}^{-q} + \sum_{\text{resource } i} (a_i R_i)^{-q} \right)^{-1/q}. \tag{S46}$$

Coarse-graining a resource k in this model is similar to that in the regular additive model: $g_{\max} \to (g_{\max}^{-q} + (a_k R_k)^{-q})^{-1/q}$.

This definition has several convenient properties, mostly mediated by the key parameter q. First we consider the regime where $q > 0$. Since the growth rate $g(\mathbf{R})$ will then always be 0 if any one resource i has zero concentration R_i, this regime describes essential, non-substitutable resources, all of which are required for nonzero growth. It also has linear proportionality to R_i in the limit where $R_i \ll g_{\max}/a_i$ and $R_i \ll a_j R_j / a_i$ for all other resources $j \neq i$. One of the most important properties of the generalized-additive model is that in the limit of $q \to \infty$, the model recovers Liebig Blackman dependence on resources (Eq. S13):

$$\lim_{q \to \infty} g(\mathbf{R}) = \min\left(g_{\max}, a_1 R_1, a_2 R_2, \ldots, a_M R_M\right). \tag{S47}$$

Finite values of q thus represent deviations from this Liebig limit. Another interesting limit is $q = 1$, where the growth rate is equivalent to the additive model (Eq. S41):

$$\lim_{q \to 1} g(\mathbf{R}) = \left(g_{\max}^{-1} + \sum_{\text{resource } i} (a_i R_i)^{-1} \right)^{-1}. \tag{S48}$$

Note that with positive values of q, the smallest values of $a_i R_i$ always dominate the sum, and the magnitude of q determines by how much — infinite q represents complete dominance of the minimum (Liebig case), while finite q allows for a soft dependence on the other non-minimum resources. We also point out that the growth rate $g(\mathbf{R})$ is a monotonically increasing function of the parameter q, so that the Liebig case ($q \to \infty$) always represents the greatest growth rate that can be produced for a given set of resources. Finite values of q therefore represent less efficient growth. Altogether this suggests that we can think of the magnitude of the parameter q as measuring the interaction between resources in determining the total growth rate.

So far we have considered only models for resources that are essential and non-substitutable, like a carbon source and a nitrogen source, such that growth rate is nonzero only if all resources are present at nonzero concentrations. However, some resources are substitutable, such as a two different carbon sources, so it is valuable to consider growth rate limitation on these resources as well. If substitutable resources are consumed sequentially (diauxie), then their growth rate limitation is the same as for single resources, since by definition only a single resource affects growth rate at any instant in time. Therefore the important case to consider here is when the resources are consumed (and therefore affect growth rate) simultaneously. This is described by the generalized-additive model with $q < 0$: the total growth rate is a sum over the rates themselves (raised to a power), instead of the reciprocal of the sum of reciprocal rates, and as a result growth rate is only zero if all resources have zero concentration. However, for $q \neq -1$, this includes nonlinear dependences on those resource concentrations, which makes it unusual compared to more common models of growth dependence on substitutable resources (sections S2G,H).

The limitation coefficient for each resource in the generalized-additive model is

$$\begin{aligned} L_i^{\text{rate}}(\mathbf{R}) &= \frac{R_i}{g}\frac{\partial g}{\partial R_i} \\ &= \frac{(a_i R_i)^{-q}}{g_{\max}^{-q} + \sum_{\text{resource } j} (a_j R_j)^{-q}}. \end{aligned} \tag{S49}$$

These limitation coefficients range from 0 (if resource i is unlimited, so $R_i \to \infty$) to 1 (if resource i is the only finite resource). Like the additive model, there is colimitation between all variable resources as well as colimitation with implicit factors. Colimitation between resources is super-additive if $q > -1$ (which includes all cases with non-substitutable resources) and sub-additive if $q < -1$; it is exactly additive when $q = -1$ since then the growth rate is a linear sum of contributions from each resource.

G. Saito substitutable model. Besides the generalized-additive model with $q < 0$, a more common model of growth rate dependence on substitutable resources is attributable to Saito (13) (Fig. S4, first column and first row):

$$g(\mathbf{R}) = g_{\max}\frac{\sum_{\text{resource } i} a_i R_i}{g_{\max} + \sum_{\text{resource } i} a_i R_i}. \tag{S50}$$

This model is not robust to coarse-graining resources under any case. In particular, if any one resource is unlimited, then the growth rate is constant in this model, regardless of the concentrations of the other resources.

The limitation coefficients are

$$\begin{aligned} L_i^{\text{rate}}(\mathbf{R}) &= \frac{R_i}{g}\frac{\partial g}{\partial R_i} \\ &= \frac{g_{\max} a_i R_i}{\left(\sum_{\text{resource } j} a_j R_j\right)\left(g_{\max} + \sum_{\text{resource } j} a_j R_j\right)}. \end{aligned} \tag{S51}$$

The limitation coefficients range between 0 and 1, with colimitation between variable resources and with the implicit factors. Unlike most of the other models here, colimitation between the variable resources is sub-additive in the Saito substitutable model.

Figure S4 shows the limitation coefficients L_1^{rate}, L_2^{rate} (second row, first column) and effective number of limiting factors $M_{\text{eff}}^{\text{rate}}$ (third row, first column) for this model with two variable resources. The overlap between the contours of L_1^{rate} (blue) and L_2^{rate} (orange) represents colimitation between the resources, while the plot of $M_{\text{eff}}^{\text{rate}}$ shows regions of colimitation ($M_{\text{eff}}^{\text{rate}} > 1$) between the two resources and the implicit factors. Note that the geometry of the limitation coefficients in this model is flipped from that of the previously-described models for non-substitutable resources (compare to Fig. S3, second row): in those models the limitation coefficients for a resource mostly depend on the concentration of that resource (e.g., the blue contours L_1^{rate} for resource 1 are mostly vertical), but for the Saito substitutable model, the limitation coefficient of a resource mostly depends on the other resource (e.g., the blue contours L_1^{rate} for resource 1 are more horizontal). That is, the population is only strongly limiting for a resource if the other substitutable resource is scarce.

H. Mean Monod model of substitutable resources. A second model of substitutable resources assumes that growth rate is a weighted average of Monod models over all resources (Fig. S4, second column and first row) (24):

$$g(\mathbf{R}) = g_{\max}\sum_{\text{resource } i} w_i \frac{a_i R_i}{a_i R_i + g_{\max}}, \tag{S52}$$

where the weights w_i are normalized: $\sum_{\text{resource } i} w_i = 1$. The growth rate saturates at $g_{\max}$ if all resources are unlimited, but note that if one resource is unlimited, the growth rate still responds to changes in concentration of the other resources (in contrast to the Saito model Eq. S50). However, it still does not transform robustly under coarse-graining, similar to the Saito model.

The limitation coefficients are

$$L_i^{\text{rate}}(\mathbf{R}) = \frac{R_i}{g}\frac{\partial g}{\partial R_i} = \frac{w_i a_i R_i g_{\max}/(a_i R_i + g_{\max})^2}{\sum_{\text{resource } j} w_j a_j R_j/(a_j R_j + g_{\max})}. \quad [S53]$$

There is colimitation between variable resources and implicit factors; colimitation between resources is perfectly additive due to the additive nature of the model (in contrast to sub-additive colimitation in the Saito model, Eq. S50).

Figure S4 shows the limitation coefficients L_1^{rate}, L_2^{rate} (second row, second column) and effective number of limiting factors $M_{\text{eff}}^{\text{rate}}$ (third row, second column) for this model with two variable resources. The overlap between the contours of L_1^{rate} (blue) and L_2^{rate} (orange) represents colimitation between the resources, while the plot of $M_{\text{eff}}^{\text{rate}}$ shows regions of colimitation ($M_{\text{eff}}^{\text{rate}} > 1$) between the two resources and the implicit factors. Note that the geometry of the limitation coefficients in this model is flipped relative to those in the Saito substitutable model (compare first and second columns in the second row of Fig. S4) and is actually more similar to the limitation coefficients of models for non-substitutable resources (Fig. S3, second row), meaning that the limitation coefficient for a resource mostly depends on that resource's own concentration rather than the concentration of the other resource. This behavior, along with the other distinct properties, suggests that the mean Monod and Saito models of substitutable resources are biologically quite different.

I. Chemically-dependent resource model. Another possible relationship between non-substitutable resources is where one resource may be chemically-dependent on the other for uptake or usage (13). This is true especially for pairs of resources involving a metal serving as an enzyme cofactor; for example, the growth rate dependence on bicarbonate in marine diatoms depends on the availability of zinc (13). In this case, growth rate will depend asymmetrically on the concentrations of both resources, since the dependent resource will have a weaker effect. In the case where resource 1 depends on resource 2, one such model for growth rate is (Fig. S4, third column and first row) (13)

$$g(R_1, R_2) = g_{\max}\frac{a_1 R_1 a_2 R_2}{a_1 R_1 a_2 R_2 + g_{\max}(a_2 R_2 + g_{\max})}. \quad [S54]$$

We can interpret this model as meaning that the effective half-saturation concentration for resource 1 ($(g_{\max}/a_1)\cdot(a_2R_2 + g_{\max})/(a_2R_2)$) depends on the concentration of resource 2: at low concentrations of resource 2, the effective half-saturation concentration for resource 1 becomes very large, while at high concentrations of resource 2, the half-saturation concentration for resource 1 decreases down to approximately an intrinsic lower limit of $K_1 = g_{\max}/a_1$.

The limitation coefficient for the dependent resource is

$$L_1^{\text{rate}}(R_1, R_2) = \frac{R_1}{g}\frac{\partial g}{\partial R_1} = \frac{g_{\max}(a_2 R_2 + g_{\max})}{a_1 R_1 a_2 R_2 + g_{\max}(a_2 R_2 + g_{\max})}. \quad [S55]$$

Again, this is equivalent to the limitation coefficient for resource 1 by itself but with an effective half-saturation concentration that depends on R_2. The limitation coefficient for the independent resource is

$$L_2^{\text{rate}}(R_1, R_2) = \frac{R_2}{g}\frac{\partial g}{\partial R_2} = \frac{g_{\max}^2}{a_1 R_1 a_2 R_2 + g_{\max}(a_2 R_2 + g_{\max})}. \quad [S56]$$

Both limitation coefficients range between 0 and 1. Colimitation between the variable resources is mostly super-additive except when the independent resource R_2 is limiting and the dependent resource R_1 is abundant.

Figure S4 shows the limitation coefficients L_1^{rate}, L_2^{rate} (second row, third column) and effective number of limiting factors $M_{\text{eff}}^{\text{rate}}$ (third row, third column) for this model. The overlap between the contours of L_1^{rate} (blue) and L_2^{rate} (orange) represents colimitation between the resources, while the plot of $M_{\text{eff}}^{\text{rate}}$ shows regions of colimitation ($M_{\text{eff}}^{\text{rate}} > 1$) between the two resources and the implicit factors. The main difference between this model and the other models of non-substitutable but independent resources is the asymmetry of limitation regimes between the two resources (compare third column of Fig. S4 with analogous plots in Fig. S3), where the independent resource (resource 2) has a stronger effect on limitation for both resources.

S3. Mechanistic models of growth yield colimitation from population dynamics

In this section we show how different models of population dynamics give rise to mechanisms of colimitation for growth yield, in contrast to the phenomenological models of section S2.

A. General batch dynamics. These dynamics entail an initial biomass concentration $N(0)$ being given a set of initial concentrations of M resources $\mathbf{R}(0) = (R_1(0), R_2(0), \ldots, R_M(0))$ and allowing the biomass to consume the resources until growth stops. We assume these resources are essential and non-substitutable, so that growth stops only when at least one resource concentration reaches zero. The dynamics of the biomass $N(t)$ and resource concentrations $\mathbf{R}(t)$ over time are determined by

$$\begin{aligned} \frac{d}{dt}N(t) &= g(\mathbf{R}(t))N(t), \\ \frac{d}{dt}R_i(t) &= -\frac{1}{s_i(\mathbf{R})}\frac{d}{dt}N(t), \end{aligned} \tag{S57}$$

where $g(\mathbf{R})$ is the per-capita biomass growth rate that depends on the instantaneous environmental resource concentrations (e.g., one of the models from section S2) and s_i is the biomass stoichiometry of resource i (amount of new biomass produced per unit resource i). Note that we allow for the possibility that the stoichiometries can change depending on the resource concentrations. Equation S57 assumes that resources are consumed only by growth of new biomass (hence the proportionality of dR_i/dt with dN/dt), but in section S3B we address the case where resources are also consumed by existing biomass for maintenance. For the figures (Figs. 1C,E and S6) we solve these equations numerically using `scipy.integrate.solve_ivp` (25).

If we are concerned only with the relative dynamics of the resources, then we can simplify Eq. S57 to describe dynamics in the space of resource concentrations. For example, in the case of two resources, we obtain

$$\frac{dR_2}{dR_1} = \frac{s_1(R_1, R_2)}{s_2(R_1, R_2)}. \tag{S58}$$

We obtain this mathematically by taking the ratio of dR_2/dt and dR_1/dt and then changing variables from t to R_1, which is possible because both resource concentrations R_1 and R_2 must depend monotonically on time t since the resources are only consumed and not produced in this model. The right-hand side of Eq. S58 is the ratio of biomass stoichiometries for the two resources, which is the stoichiometry between those two resources in the biomass. For example, if every unit of biomass requires 3 units of resource 1 and 4 units of resource 2, then the stoichiometric ratio in Eq. S58 is 4/3.

This ratio thus defines the slope of depletion trajectories in the space of resource concentrations, as in Fig. 1E. Therefore depletion trajectories will be straight lines if the stoichiometry is constant over resource concentrations (Fig. S5A). However, if the stoichiometry is variable over concentrations, then the trajectories can curve (Fig. S5B). Let

$$R_2 = f(R_1) \tag{S59}$$

be any solution to Eq. S58. The solution for a specific set of initial concentrations $R_1(0)$ and $R_2(0)$ is therefore

$$R_2 = R_2(0) + f(R_1) - f(R_1(0)). \tag{S60}$$

For example, in the case where stoichiometry is constant, then $f(R_1)$ is a linear function of R_1 and so

$$R_2 = R_2(0) - \frac{s_1}{s_2}\left(R_1(0) - R_1\right). \tag{S61}$$

The growth yield of the population is the amount of new biomass produced in the infinite time limit:

$$\begin{aligned} \lim_{t\to\infty} N(t) - N(0) &= \Delta N \\ &= \int_0^\infty dt\ \frac{d}{dt}N(t) \\ &= -\int_{R_1(0)}^{\lim_{t\to\infty} R_1(t)} dR_1\ s_1(R_1, R_2(R_1)) \\ &= -\int_{R_2(0)}^{\lim_{t\to\infty} R_2(t)} dR_2\ s_2(R_1(R_2), R_2), \end{aligned} \tag{S62}$$

where the latter two equations are obtained from the first by changing variables from time t to either resource concentration R_1 or R_2 using Eq. S57 (which, as aforementioned, is valid since these quantities all depend monotonically with each other). To calculate the growth yield, we therefore need to know the limit of either R_1 or R_2 in the infinite time limit. In batch models, growth stops only when one or both resources reach zero concentration (Figs. 1E and S5A); this is the case for all the growth rate models for non-substitutable resources discussed in section S2, where $g(R_1, R_2) = 0$ if and only if $R_1 = 0$ or $R_2 = 0$. In this case, either $\lim_{t\to\infty} R_1(t) = 0$ or $\lim_{t\to\infty} R_2(t) = 0$, but not necessarily both. Which limit is realized depends on the initial conditions $R_1(0)$ and $R_2(0)$. If we imagine the phase portrait of Eq. S58 (Fig. S5A,B), this problem is geometrically realized as determining which trajectories terminate at the vertical $R_1 = 0$ axis (the population runs out of resource 1 first) or at the horizontal $R_2 = 0$ axis (the population runs out of resource 2 first).

There is only one trajectory that hits the origin $(R_1, R_2) = (0, 0)$ (runs out of both resources simultaneously). The initial conditions that follow this trajectory are defined by $R_2(0) = f(R_1(0)) - f(0)$ (using Eq. S60). Because trajectories cannot

cross each other, all trajectories above this one will end at the $R_1 = 0$ axis, while all trajectories below will end at the $R_2 = 0$ axis. Define the former region as Ω_1 and the latter region as Ω_2, or more precisely,

$$\begin{aligned}\Omega_1 &= \{(R_1(0), R_2(0)) \text{ such that } R_2(0) > f(R_1(0)) - f(0)\},\\ \Omega_2 &= \{(R_1(0), R_2(0)) \text{ such that } R_2(0) < f(R_1(0)) - f(0)\}.\end{aligned} \tag{S63}$$

For example, in the case of constant stoichiometry, the set of initial conditions that follow the trajectory ending at the origin is given by the straight line $R_2(0) = (s_1/s_2)R_1(0)$ (Fig. S5A). So all initial conditions above this line ($R_2(0) > (s_1/s_2)R_1(0)$, region Ω_1) will follow trajectories terminating at $R_1 = 0$, while all trajectories below ($R_2(0) < (s_1/s_2)R_1(0)$, region Ω_2) will terminate at $R_2 = 0$ (Fig. S5A). Equation S63 holds for curved resource depletion trajectories from variable stoichiometry as well, but with a more complex boundary between Ω_1 and Ω_2 (Fig. S5B).

We can now formally express the resource concentration limits $\lim_{t\to\infty} R_1(t)$ and $\lim_{t\to\infty} R_2(t)$, and in turn the growth yield of the biomass, in terms of the initial conditions $R_1(0)$, $R_2(0)$:

$$\Delta N = \begin{cases} \displaystyle\int_0^{R_1(0)} dR_1 \; s_1\left(R_1, R_2(0) + f(R_1) - f(R_1(0))\right) & \text{if } (R_1(0), R_2(0)) \in \Omega_1,\\ \displaystyle\int_0^{R_2(0)} dR_2 \; s_2\left(R_1(0) + f^{-1}(R_2) - f^{-1}(R_2(0)), R_2\right) & \text{if } (R_1(0), R_2(0)) \in \Omega_2, \end{cases} \tag{S64}$$

where f^{-1} is the inverse function of f as defined by a solution to Eq. S58. That is, we choose the resource integral from Eq. S62 based on which resource goes to zero (since that simplifies the limits of the integral) and use the solution to the resource dynamics ODE (Eq. S58) to express the integral fully in terms of that one resource (using Eq. S60). In the special case of constant stoichiometry, Eq. S64 simplifies to

$$\begin{aligned}\Delta N &= \begin{cases} s_1 R_1(0) & \text{if } R_2(0) > (s_1/s_2)R_1(0),\\ s_2 R_2(0) & \text{if } R_2(0) < (s_1/s_2)R_1(0),\end{cases}\\ &= \min\left(s_1 R_1(0), s_2 R_2(0)\right).\end{aligned} \tag{S65}$$

That is, the growth yield equals the biomass produced by whichever resource is initially less, according to its stoichiometry. This is a derivation of the Liebig Blackman model for growth yield (section S2A.1). For constant stoichiometry, there is no yield colimitation between the resources.

Equation S64 also says that for initial conditions in Ω_1, the growth yield always depends on $R_1(0)$ (as expected since resource 1 runs out at the end), but it can also depend on the initial resource 2 $R_2(0)$ if the biomass stoichiometry s_1 for resource 1 depends on the concentration R_2 of resource 2. The reverse is true for initial conditions in Ω_2. Thus, for the growth yield to depend on both resources simultaneously (yield colimitation), the biomass stoichiometry for one resource must depend on the concentration of the other resource. We can interpret that property as a form of interaction between the resources: usage of one resource depends on the availability of the other. Note that this is a more specific requirement of the stoichiometries than just variable stoichiometry leading to curved resource depletion trajectories (Fig. S5B), which could occur without causing yield colimitation (e.g., s_1 depends on R_1 but not on R_2).

B. Batch dynamics with variable stoichiometry from maintenance resource consumption. In this section we consider the possibility of resources being consumed by existing biomass for maintenance, as well as to grow new biomass. This provides a specific mechanism for generating variable stoichiometry and yield colimitation.

B.1. One resource. We first consider the case of a single resource; there is no colimitation with only a single resource, but it provides a simpler foundation for the model. Modifying Eq. S57, the dynamics of biomass growth and resource consumption are given by

$$\begin{aligned}\frac{d}{dt}N(t) &= g(R(t))N(t),\\ \frac{d}{dt}R(t) &= \left(-\frac{1}{s_{\text{growth}}}\frac{d}{dt}N(t) - \frac{1}{s_{\text{main}}}N(t)\right)\Theta\left(R(t)\right),\end{aligned} \tag{S66}$$

where s_{growth} is the growth stoichiometry (amount of new biomass produced per unit resource consumed, same as the biomass stoichiometry in the original model of Eq. S57) and s_{main} is the maintenance stoichiometry (amount of existing biomass maintained per unit resource consumed per unit time). For simplicity, we assume these are constant parameters and do not also depend on the resource concentrations as in the previous section. The Heaviside step function Θ is necessary so that once resources reach zero, there is no additional consumption due to maintenance (otherwise resource concentrations will become negative). Presumably the existing biomass will start to decay at some point after that, but we do not model it here.

We can express the second line of Eq. S66 in terms of an effective growth stoichiometry

$$\frac{d}{dt}R(t) = -\frac{1}{\tilde{s}_{\text{growth}}(R(t))}\frac{d}{dt}N(t) \tag{S67}$$

where

$$\tilde{s}_{\text{growth}}(R) = \left(\frac{1}{s_{\text{growth}}} + \frac{1}{s_{\text{main}}g(R)}\right)^{-1}. \tag{S68}$$

This predicts a positive but nonlinear correlation between growth rate and stoichiometry, across varying resource concentrations R (26, 27). In particular, when the growth rate is zero, the effective growth stoichiometry is also zero, because all resource consumption goes to maintenance. When the growth rate is infinite, then the effective growth stoichiometry converges to the regular growth stoichiometry s_{growth}, since maintenance consumption becomes negligible. If the growth rate is described by a Monod model $g(R) = g_{\max}aR/(aR + g_{\max})$, then the effective growth stoichiometry becomes

$$\tilde{s}_{\text{growth}}(R) = \tilde{s}_{\text{growth}}(\infty)\frac{R}{R + \frac{\tilde{s}_{\text{growth}}(\infty)}{as_{\text{main}}}}, \tag{S69}$$

where the effective growth stoichiometry at infinite resource is

$$\tilde{s}_{\text{growth}}(\infty) = \left(\frac{1}{s_{\text{growth}}} + \frac{1}{s_{\text{main}}g_{\max}}\right)^{-1}. \tag{S70}$$

Thus the effective growth stoichiometry depends as a Monod function on the resource concentration R, with a saturating yield at $\tilde{s}_{\text{growth}}(\infty)$ (the growth stoichiometry at maximum growth rate) and a half-saturation concentration of $\tilde{s}_{\text{growth}}(\infty)/(as_{\text{main}})$. This therefore constitutes a model of variable stoichiometry: the resource consumption changes dynamically over a growth cycle.

To determine the growth yield, we can integrate Eq. S67 to get the total change in biomass:

$$\begin{aligned}\Delta N &= \int_0^{R(0)} dR\ \tilde{s}_{\text{growth}}(R) \\ &= \tilde{s}_{\text{growth}}(\infty)\left(R(0) + \frac{\tilde{s}_{\text{growth}}(\infty)}{as_{\text{main}}}\log\left[\frac{\frac{\tilde{s}_{\text{growth}}(\infty)}{as_{\text{main}}}}{\frac{\tilde{s}_{\text{growth}}(\infty)}{as_{\text{main}}} + R(0)}\right]\right).\end{aligned} \tag{S71}$$

For very large initial resource concentrations $R(0)$ this is approximately the regular growth yield $\tilde{s}_{\text{growth}}(\infty)R(0)$, since growth consumption dominates over maintenance in that case. The logarithm term is a correction at low initial resource concentrations $R(0)$ due to maintenance.

B.2. Two resources. We now consider two resources to see how variable stoichiometry from maintenance resource consumption leads to yield colimitation. The effective growth stoichiometries are

$$\begin{aligned}\tilde{s}_{1,\text{growth}}(R_1, R_2) &= \left(\frac{1}{s_{1,\text{growth}}} + \frac{1}{s_{1,\text{main}}g(R_1, R_2)}\right)^{-1}, \\ \tilde{s}_{2,\text{growth}}(R_1, R_2) &= \left(\frac{1}{s_{2,\text{growth}}} + \frac{1}{s_{2,\text{main}}g(R_1, R_2)}\right)^{-1}.\end{aligned} \tag{S72}$$

If we take the ratio to get the stoichiometry between resources, we can then express the depletion trajectory of both resources as

$$\begin{aligned}\frac{dR_2}{dR_1} &= \frac{\tilde{s}_{1,\text{growth}}(R_1, R_2)}{\tilde{s}_{2,\text{growth}}(R_1, R_2)} \\ &= \frac{\left(\frac{1}{s_{2,\text{growth}}} + \frac{1}{s_{2,\text{main}}g(R_1,R_2)}\right)}{\left(\frac{1}{s_{1,\text{growth}}} + \frac{1}{s_{1,\text{main}}g(R_1,R_2)}\right)}.\end{aligned} \tag{S73}$$

Since the stoichiometry varies with the resource concentrations, this will lead to curved trajectories of resource depletion (Fig. S6A). Since the stoichiometry only depends on the resources through the growth rate, we can characterize its behavior as a function of growth rate. That is, the stoichiometry interpolates between two values at different extremes of growth rate:

$$\frac{s_1}{s_2} \approx \begin{cases} \frac{s_{1,\text{main}}}{s_{2,\text{main}}} & \text{for slow growth (low resource concentrations),} \\ \frac{\left(\frac{1}{s_{1,\text{growth}}} + \frac{1}{s_{1,\text{main}}g_{\max}}\right)}{\left(\frac{1}{s_{2,\text{growth}}} + \frac{1}{s_{2,\text{main}}g_{\max}}\right)} & \text{for fast growth (high resource concentrations).} \end{cases} \tag{S74}$$

We plot an example phase portrait of this using the additive model of growth rate (Eq. S41) in Fig. S6A. Moreover, since the yield for each resource depends on the other resource's concentration (e.g., s_1 depends on R_2 via the growth rate in Eq. S72), this will also produce biomass growth yield ΔN that depends on both resource concentrations (Fig. S6B). Thus resource consumption for maintenance is a mechanism for producing yield colimitation of two resources.

C. Batch dynamics with variable stoichiometry from dynamic proteome allocation. The basic mechanism by which maintenance causes variable stoichiometry is that it causes stoichiometry to depend on growth rate. However, another phenomenon besides maintenance that could cause stoichiometry to depend on growth rate is dynamic proteome allocation. We know that the allocation of protein biomass between different sectors of the proteome changes significantly across growth rates (28, 29). Suppose that cells consist of two biomass components, A and B. Let the biomass stoichiometries of component A on resources 1 and 2 be s_1^{A} and s_2^{A}, while the biomass stoichiometries of component B are s_1^{B} and s_2^{B}. Thus the resource stoichiometry of component A is $s_1^{\mathrm{A}}/s_2^{\mathrm{A}}$ and the resource stoichiometry of B is $s_1^{\mathrm{B}}/s_2^{\mathrm{B}}$. We assume these stoichiometries are unequal, since otherwise the two biomass components are equivalent in their resource usage.

Let the physiological state variable θ parameterize the fraction of biomass in component A (so the fraction in component B is $1-\theta$). The biomass stoichiometries of both resources depend on this biomass state according to

$$\begin{aligned} s_1 &= \left(\frac{\theta}{s_1^{\mathrm{A}}} + \frac{1-\theta}{s_1^{\mathrm{B}}}\right)^{-1}, \\ s_2 &= \left(\frac{\theta}{s_2^{\mathrm{A}}} + \frac{1-\theta}{s_2^{\mathrm{B}}}\right)^{-1}. \end{aligned} \qquad \text{[S75]}$$

We assume the physiological state is regulated by growth rate, such that the two are linearly proportional:

$$\theta(g) = \left(\frac{\theta_{\max} - \theta_{\min}}{g_{\max}}\right) g + \theta_{\min}, \qquad \text{[S76]}$$

so that at zero growth, $\theta_{\min}$ is the fraction of component A in the biomass, while at maximum growth rate $g_{\max}$, $\theta_{\max}$ is the fraction of A. This is motivated by the linear relationship between growth rate and fraction of a proteome sector (28). Without loss of generality, we assume the shift is in favor of component A at high growth rates.

Since the growth rate depends on the resource concentrations $g(R_1, R_2)$ (e.g., according to a model from section S2), we arrive at a model of resource depletion with variable stoichiometry:

$$\begin{aligned} \frac{s_1}{s_2} &= \frac{\frac{1}{s_2^{\mathrm{A}}}\theta(g(R_1,R_2)) + \frac{1}{s_2^{\mathrm{B}}}\left[1-\theta(g(R_1,R_2))\right]}{\frac{1}{s_1^{\mathrm{A}}}\theta(g(R_1,R_2)) + \frac{1}{s_1^{\mathrm{B}}}\left[1-\theta(g(R_1,R_2))\right]} \\ &= \frac{\frac{1}{s_2^{\mathrm{A}}}\left[\left(\frac{\theta_{\max}-\theta_{\min}}{g_{\max}}\right) g(R_1,R_2) + \theta_{\min}\right] + \frac{1}{s_2^{\mathrm{B}}}\left[1 - \left(\frac{\theta_{\max}-\theta_{\min}}{g_{\max}}\right) g(R_1,R_2) - \theta_{\min}\right]}{\frac{1}{s_1^{\mathrm{A}}}\left[\left(\frac{\theta_{\max}-\theta_{\min}}{g_{\max}}\right) g(R_1,R_2) + \theta_{\min}\right] + \frac{1}{s_1^{\mathrm{B}}}\left[1 - \left(\frac{\theta_{\max}-\theta_{\min}}{g_{\max}}\right) g(R_1,R_2) - \theta_{\min}\right]}. \end{aligned} \qquad \text{[S77]}$$

In Fig. S6C we plot an example phase portrait for this model. As with variable stoichiometry arising from maintenance, resource stoichiometry in this model interpolates between two values depending on the growth rate: at slow growth rates, the biomass is made mostly of component B, and so the resource stoichiometry is approximately that of component B ($s_1^{\mathrm{B}}/s_2^{\mathrm{B}}$), while at fast growth rates, the biomass is made mostly of A and therefore reflects that component's resource stoichiometry ($s_1^{\mathrm{A}}/s_2^{\mathrm{A}}$). Figure S6D shows how the growth yield depends on both initial resource concentrations simultaneously, demonstrating the existence of yield colimitation.

D. Chemostat dynamics. The batch models of sections S3A–C assume that growth stops only when at least one resource reaches zero concentration. However, it is possible that growth could stop before that point, i.e., when resources reach some nonzero concentrations $R_i^* > 0$ (Fig. S5C) (30). While this is possible under batch dynamics (e.g., if cells sense resources getting too low), a more typical scenario in which this occurs is chemostat dynamics, where cell birth must balance a nonzero death rate. We define chemostat dynamics using a model analogous to the batch case (Eq. S57):

$$\begin{aligned} \frac{d}{dt}N(t) &= \left(g(\mathbf{R}) - d\right) N(t), \\ \frac{d}{dt}R_i(t) &= -\frac{1}{s_i} g(\mathbf{R}) N(t) + d\left(R_i^{\mathrm{source}} - R_i(t)\right), \end{aligned} \qquad \text{[S78]}$$

where R_i^{source} is the concentration of resource i in the source media flowing into the chemostat and d is the dilution factor ($d = \omega/V$, where ω is volume flowing in and out per unit time and V is the total volume). Here we assume constant biomass stoichiometry s_i, but we can generalize our results to the case of variable stoichiometry as we do in the batch case (section S3A). Note that we express the resource consumption by biomass (first term on the right-hand side of dR_i/dt) as being proportional to $g(\mathbf{R})N(t)$ rather than dN/dt as in the batch model (Eq. S57). This is because dN/dt includes a death process as well as the growth of new biomass, while we assume resource consumption is only associated with growth of new biomass.

For chemostats we primarily care about their steady states, so let N^* and $\mathbf{R}^*$ be the steady-state concentrations of biomass and resources. To calculate these concentrations, we first set $dN/dt = 0$, which gives us the condition that the growth rate must equal the dilution rate:

$$g(\mathbf{R}^*) = d. \tag{S79}$$

Assuming there are M total resources, this defines an $(M-1)$-dimensional manifold in the space of resource concentrations $\mathbf{R}^*$. Next we must also set $dR_i/dt = 0$, which gives us

$$N^* = (R_i^{\text{source}} - R_i^*)s_i. \tag{S80}$$

Note this requires that $R_i^{\text{source}} > R_i^*$ for a steady state to exist. Since this must hold for each resource i, we have

$$(R_1^{\text{source}} - R_1^*)s_1 = (R_2^{\text{source}} - R_2^*)s_2 = \cdots = (R_M^{\text{source}} - R_M^*)s_M. \tag{S81}$$

These equations are also apparent from the assumption of constant stoichiometry of resources and biomass: the difference in resource concentrations between the source and the vessel corresponds to what the population is consuming, and that consumed quantity must exactly match the stoichiometry of the biomass (s_i/s_j) for it to be in steady state. To solve the steady state, we must solve for solutions of Eqs. S79 and S81 (M equations) to get the resource concentrations $\mathbf{R}^*$ (M unknowns), and then plug those into Eq. S80 to get the biomass concentration N^*. In Fig. 1D,F we plot the dynamics to steady state for an example chemostat model (solving numerically using `scipy.integrate.solve_ivp` (25)).

D.1. One resource. To define growth rate and growth yield limitation under chemostat dynamics, we first consider the case of a single resource. We define growth rate limitation as the response of the instantaneous growth rate to a small perturbation in resource concentration at steady state. Note that the response to this perturbation represents a transient departure from steady state itself. For a single resource, the steady-state resource concentration is determined by $g(R^*) = d$ (Eq. S79). Assuming a Monod model of growth rate $g(R) = g_{\max}aR/(aR + g_{\max})$, the resource concentration is (assuming $R^* < R^{\text{source}}$ such that a steady state exists)

$$R^* = \frac{g_{\max}d}{a(g_{\max} - d)}. \tag{S82}$$

Since the growth rate limitation coefficient for a single resource in the Monod model is $L^{\text{rate}} = g_{\max}/(aR + g_{\max})$ (main text Eq. 1), the limitation coefficient for a steady-state chemostat is

$$\begin{aligned} L^{\text{rate}} &= \frac{g_{\max}}{aR^* + g_{\max}} \\ &= 1 - \frac{d}{g_{\max}}. \end{aligned} \tag{S83}$$

Therefore if the dilution rate is far below the maximum growth rate of the population ($d \ll g_{\max}$), then limitation is very close to its maximum value of $L^{\text{rate}} = 1$. This makes sense as limitation is highest when growth rates are slow, which corresponds to low resources. In contrast, if the dilution rate d is very close to the maximum growth rate $g_{\max}$ (fast growth), then limitation becomes close to its minimum value of $L^{\text{rate}} = 0$, which corresponds to a high steady-state resource concentration R^*.

We similarly define yield limitation of a population growing under chemostat dynamics as the response of its steady-state biomass to changes in the source concentrations of resources being supplied. For a single resource, the biomass at steady state is (Eq. S80)

$$\begin{aligned} N^* &= (R^{\text{source}} - R^*)s \\ &= \left(R^{\text{source}} - \frac{g_{\max}d}{a(g_{\max} - d)}\right)s, \end{aligned} \tag{S84}$$

where we have used the solution for R^* in Eq. S82. Therefore the yield limitation coefficient is

$$\begin{aligned} L^{\text{yield}} &= \frac{R^{\text{source}}}{N^*}\frac{\partial N^*}{\partial R^{\text{source}}} \\ &= \frac{R^{\text{source}}}{R^{\text{source}} - \frac{g_{\max}d}{a(g_{\max}-d)}}. \end{aligned} \tag{S85}$$

When R^{source} is high, then the limitation coefficient takes approximately its minimum value of $L^{\text{yield}} = 1$: growth yield responds approximately linearly to changes in R^{source}. When R^{source} is low (i.e., close to its lower bound set by the dilution rate d and intrinsic growth traits $g_{\max}$ and a such that a steady state is feasible), then L^{yield} is much greater than 1. Note that while the biomass is always a linear function of R^{source} (Eq. S80), there is an apparent super-linearity here due to the shift in R^{source} by R^*. So on a log-log scale, N^* will increase with R^{source} faster than linear near that minimum value.

D.2. Two resources. For multiple resources, we repeat this procedure, although solving Eqs. S79 and S81 to obtain the steady-state concentrations $\mathbf{R}^*$ is more complicated and may only be possible numerically for complex growth rate models or many resources. As an example with two resources, let us consider the additive model of growth rate (Eq. S41):

$$g(R_1, R_2) = \frac{1}{g_{\max}^{-1} + (a_1 R_1)^{-1} + (a_2 R_2)^{-1}}. \tag{S86}$$

Therefore the steady-state resource concentrations R_1^* and R_2^* are determined by the following equations:

$$\begin{aligned} \frac{1}{g_{\max}^{-1} + (a_1 R_1^*)^{-1} + (a_2 R_2^*)^{-1}} &= d, \\ (R_1^{\text{source}} - R_1^*)s_1 &= (R_2^{\text{source}} - R_2^*)s_2. \end{aligned} \tag{S87}$$

Figure S6E shows the phase portrait of resource depletion trajectories. In this case we can still solve these equations analytically to obtain the steady-state resource concentrations:

$$\begin{aligned} R_1^* &= \frac{y_1 + y_2 + (\gamma - 1)(y_1 r_1 - y_2 r_2) + \sqrt{D}}{2y_1(\gamma - 1)} \frac{g_{\max}}{a_1}, \\ R_2^* &= \frac{y_1 + y_2 + (\gamma - 1)(y_2 r_2 - y_1 r_1) + \sqrt{D}}{2y_2(\gamma - 1)} \frac{g_{\max}}{a_2}, \end{aligned} \tag{S88}$$

where

$$\begin{aligned} \gamma &= g_{\max}/d, \\ r_1 &= \frac{a_1 R_1^{\text{source}}}{g_{\max}}, \\ r_2 &= \frac{a_2 R_2^{\text{source}}}{g_{\max}}, \\ y_1 &= \frac{g_{\max}}{a_1} s_1, \\ y_2 &= \frac{g_{\max}}{a_2} s_2, \\ D &= y_1^2(1 + r_1[r_1(\gamma - 1) - 2][\gamma - 1]) + y_2^2(1 + r_2[r_2(\gamma - 1) - 2][\gamma - 1]) \\ &\quad + 2y_1 y_2(1 - r_1 - r_2 - r_1 r_2 + [r_1 + r_2 + 2r_1 r_2]\gamma - r_1 r_2 \gamma^2). \end{aligned} \tag{S89}$$

The total biomass in steady state is therefore

$$\begin{aligned} N^* &= (R_1^{\text{source}} - R_1^*)s_1, \\ &= (R_2^{\text{source}} - R_2^*)s_2. \end{aligned} \tag{S90}$$

Figure S6F shows how the growth yield (biomass in steady state) depends on the source concentrations R_1^{source} and R_2^{source}, which indicates that even with constant stoichiometry, this yield depends on both resources simultaneously. This is also evident mathematically from the fact that N^* depends on R_1^* or R_2^*, which each depend on both R_1^{source} and R_2^{source} according to Eqs. S88 and S89. Therefore the yield of a population growing in a chemostat will be colimited by both resources.

References

1. SFM Hart, D Skelding, AJ Waite, JC Burton, W Shou, High-throughput quantification of microbial birth and death dynamics using fluorescence microscopy. *Quant Biol* **7**, 69–81 (2019).
2. H Moser, *The Dynamics of Bacterial Populations Maintained in the Chemostat.* (Carnegie Institution of Washington), (1958).
3. CS Holling, Some Characteristics of Simple Types of Predation and Parasitism I. *The Can. Entomol.* **91**, 358–369 (1959).
4. WS Harpole, et al., Nutrient co-limitation of primary producer communities. *Ecol Lett* **14**, 852–862 (2011).
5. E Sperfeld, D Raubenheimer, A Wacker, Bridging factorial and gradient concepts of resource co-limitation: towards a general framework applied to consumers. *Ecol Lett* **19**, 201–215 (2016).
6. J Domingo, BC Pablo, B Lehner, The causes and consequences of genetic interactions (epistasis). *Annu. Rev Genom Hum Genet.* **20**, 433–460 (2019).
7. JW Fink, NA Held, M Manhart, Microbial population dynamics decouple growth response from environmental nutrient concentration. *Proc Natl Acad Sci USA* **120**, e2207295120 (2023).
8. ME Muscarella, JP O'Dwyer, Species dynamics and interactions via metabolically informed consumer-resource models. *Theor Ecol* **13**, 503–518 (2020).
9. JY Tang, WJ Riley, SUPECA kinetics for scaling redox reactions in networks of mixed substrates and consumers and an example application to aerobic soil respiration. *Geosci Model. Dev* **10**, 3277–3295 (2017).
10. J Tang, WJ Riley, Finding Liebig's law of the minimum. *Ecol Appl* **31**, e02458 (2021).

11. RV O'Neill, DL DeAngelis, JJ Pastor, BJ Jackson, WM Post, Multiple nutrient limitations in ecological models. *Ecol Model.* **46**, 147–163 (1989).
12. M Zinn, B Witholt, T Egli, Dual nutrient limited growth: Models, experimental observations, and applications. *J Biotechnol* **113**, 263–279 (2004).
13. MA Saito, TJ Goepfert, JT Ritt, Some thoughts on the concept of colimitation: Three definitions and the importance of bioavailability. *Limnol Ocean.* **53**, 276–290 (2008).
14. J von Liebig, *Organic chemistry in its application to agriculture and physiology.* (Taylor and Walton, London), (1840).
15. JR Casey, MJ Follows, A steady-state model of microbial acclimation to substrate limitation. *PLoS Comput. Biol* **16**, e1008140 (2020).
16. E Sperfeld, D Martin-Creuzburg, A Wacker, Multiple resource limitation theory applied to herbivorous consumers: Liebig's minimum rule vs. interactive co-limitation. *Ecol Lett* **15**, 142–150 (2012).
17. F Liu, L Gaul, A Giometto, M Wu, A high throughput array microhabitat platform reveals how light and nitrogen colimit the growth of algal cells. *Sci Rep* **14**, 9860 (2024).
18. SALM Kooijman, The synthesizing unit as model for the stoichiometric fusion and branching of metabolic fluxes. *Biophys Chem* **73**, 179–188 (1998).
19. S Sharma, R Steuer, Modelling microbial communities using biochemical resource allocation analysis. *J R Soc Interface* **16**, 20190474 (2019).
20. MT Wortel, E Noor, M Ferris, FJ Bruggeman, W Liebermeister, Metabolic enzyme cost explains variable trade-offs between microbial growth rate and yield. *PLoS Comput. Biol* **14**, e1006010 (2018).
21. T Mankad, HR Bungay, Model for microbial growth with more than one limiting nutrient. *J Biotechnol* **7**, 161–166 (1988).
22. L Xie, AE Yuan, W Shou, Simulations reveal challenges to artificial community selection and possible strategies for success. *PLoS Biol* **17**, e3000295 (2019).
23. DW Cantrell, EW Weisstein, Power mean. From MathWorld–A Wolfram Web Resource (URL: https://mathworld.wolfram.com/PowerMean.html) (2023) Accessed: 2023-05-21.
24. D Gupta, S Garlaschi, S Suweis, S Azaele, A Maritan, Effective resource competition model for species coexistence. *Phys Rev Lett* **127**, 208101 (2021).
25. P Virtanen, et al., SciPy 1.0: Fundamental Algorithms for Scientific Computing in Python. *Nat. Methods* **17**, 261–272 (2020).
26. SJ Pirt, The maintenance energy of bacteria in growing cultures. *Proc R Soc B* **163**, 224–231 (1965).
27. DA Lipson, The complex relationship between microbial growth rate and yield and its implications for ecosystem processes. *Front Microbiol* **6**, 615 (2015).
28. M Scott, CW Gunderson, EM Mateescu, Z Zhang, T Hwa, Interdependence of cell growth and gene expression: Origins and consequences. *Science* **330**, 1099–1102 (2010).
29. M Mori, et al., From coarse to fine: the absolute Escherichia coli proteome under diverse growth conditions. *Mol Syst Biol* **17**, e9536 (2021).
30. D Tilman, *Resource competition and community structure.* (Princeton University Press, Princeton, NJ), (1982).
31. R Kishony, S Leibler, Environmental Stresses Can Alleviate the Average Deleterious Effect of Mutations. *J Biol* **2**, 14 (2003).

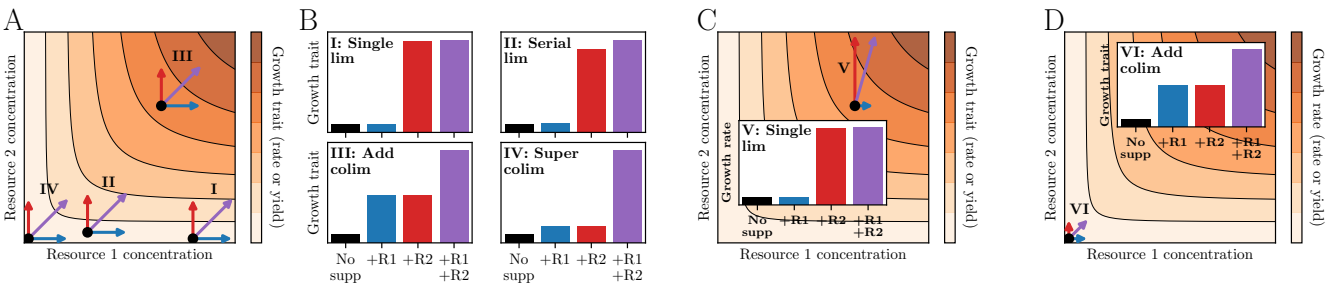

Fig. S1. Factorial supplementation experiments are incomplete tests of colimitation. (A) Schematic of four factorial supplementation experiments overlaid on the global dependence of a growth trait (e.g., growth rate or growth yield) on two resource concentrations. (B) Outcomes of the same four factorial supplementation experiments from (A), classified according to their apparent limitation state (single limitation, serial limitation, additive colimitation, super-additive colimitation; section S1G). (C) Factorial supplementation experiment on the same background concentrations as experiment III from (A) and (B), but with different supplemented concentrations of both resources leading to a qualitatively different outcome (apparent single limitation instead of additive colimitation). (D) Factorial supplementation experiment on the same background concentrations as experiment IV from (A) and (B), but with different supplemented concentrations of both resources leading to a qualitatively different outcome (apparent additive colimitation instead of super-additive colimitation).

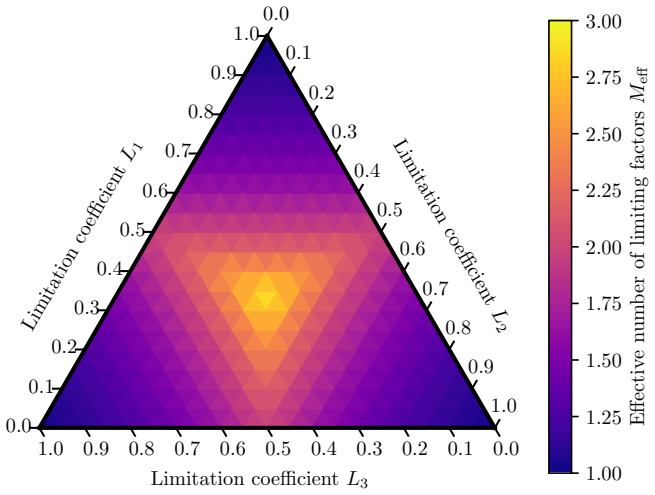

Fig. S2. Effective number of limiting factors over the limitation coefficient simplex. Example of three limiting factors whose limitation coefficients range from 0 to 1 and thus form a simplex, with the number of limiting factors M_{eff} (main text Eq. 3) plotted as color.

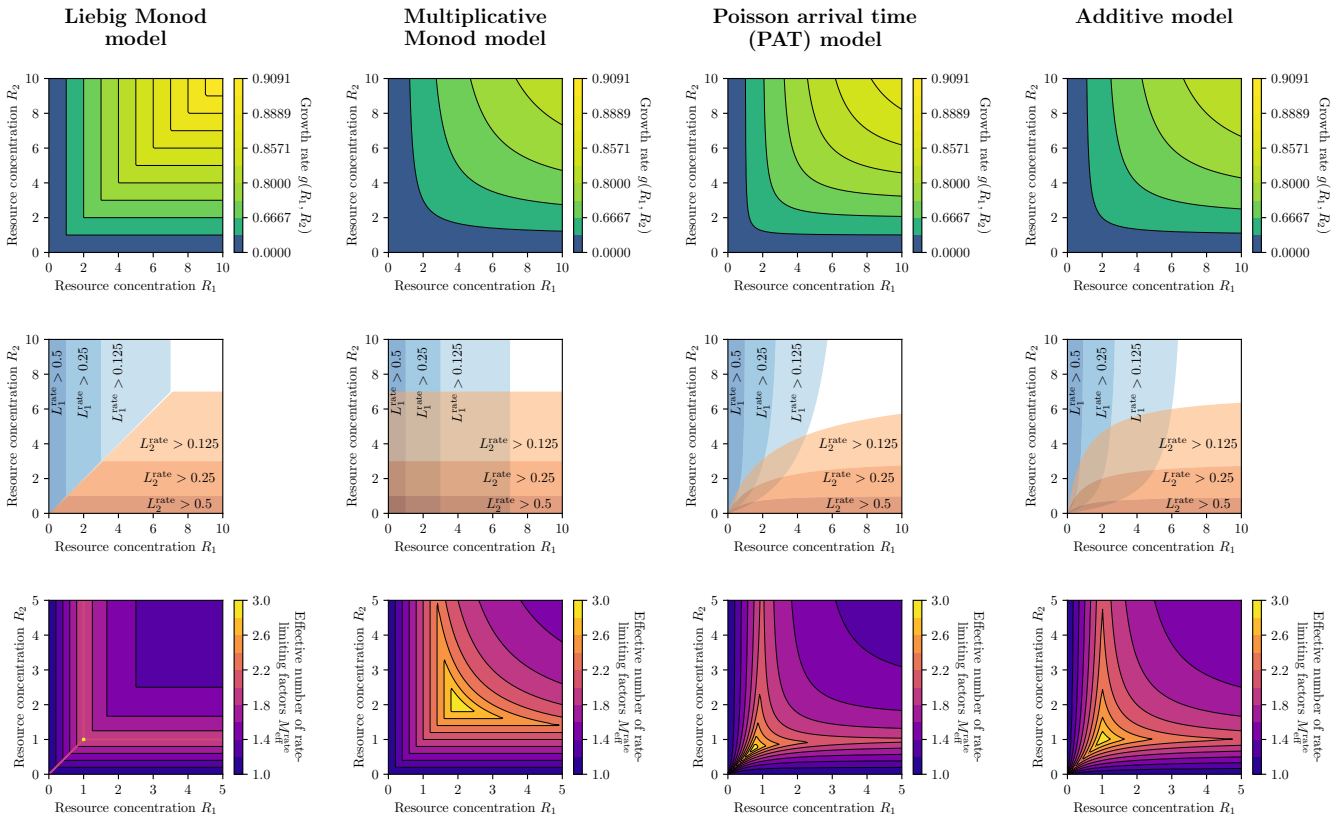

Fig. S3. Summary of common growth rate models and their limitation properties. Each column corresponds to a different common model of how growth rate depends on resource concentrations (section S2). These models can be equivalently applied to growth yield. First row: For each growth rate model in a different column, we show the growth rates $g(R_1, R_2)$ as functions of resource concentrations R_1 and R_2. Second row: Rate limitation coefficients for resource 1 (L_1^{rate}, blue contours) and for resource 2 (L_2^{rate}, orange contours) as functions of resource concentrations (compare to schematic in Fig. 1B). Third row: Effective number of rate-limiting factors $M_{\text{eff}}^{\text{rate}}$ (main text Eq. 3) as functions of resource concentrations (compare to schematic in Fig. 1B). Parameters in all models are $g_{\max} = a_1 = a_2 = 1$.

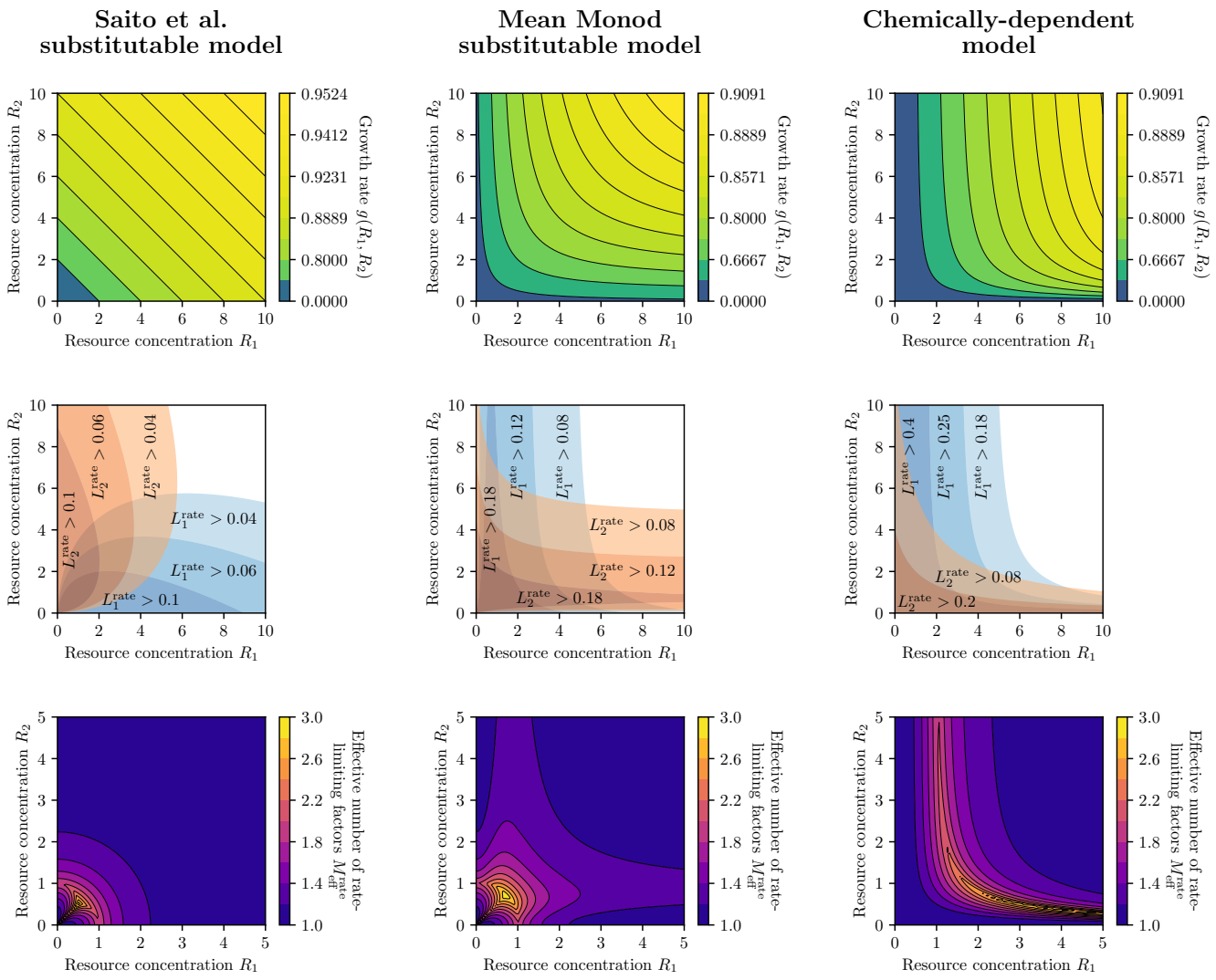

Fig. S4. Summary of growth rate models and their limitation properties for substitutable and chemically-dependent resources. Same as Fig. S3 but for the Saito et al. model (13) of substitutable resources (first column), the mean Monod model of substitutable resources (second column), and the model of chemically-dependent resources (13) (third column); see section S2 for definitions. These models can be equivalently applied to growth yield. Parameters in all models are $g_{\max} = a_1 = a_2 = 1$; the weights in the Mean Monod model are equal ($w_1 = w_2 = 1/2$).

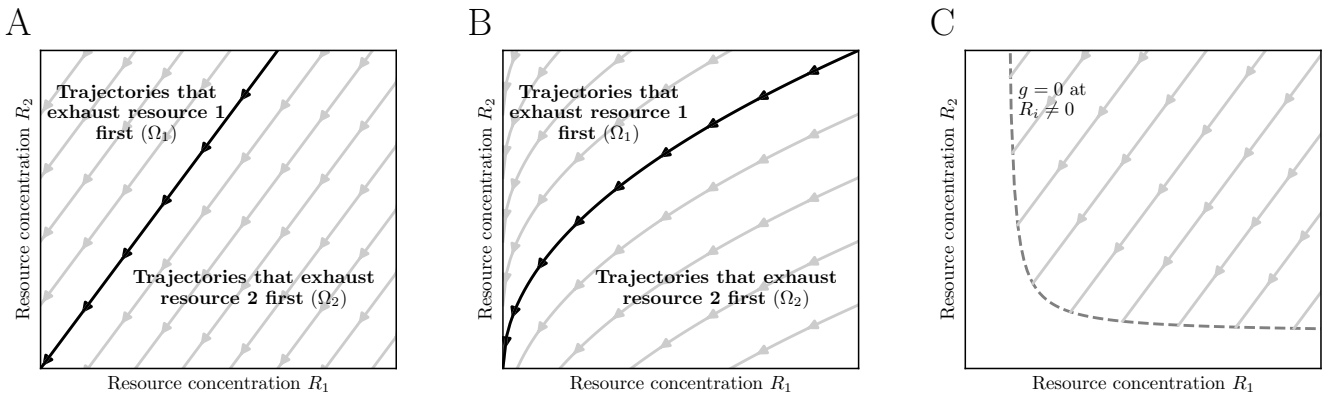

Fig. S5. Different qualitative regimes of resource depletion trajectories. (A) If resources are consumed with constant stoichiometry, then their concentrations deplete along straight lines (section S3A). The regions in which the first depleted resource is resource 1 or resource 2 are labeled as Ω_1 and Ω_2. (B) Same as (A) but for resources consumed with variable stoichiometry, which causes their depletion trajectories to curve (section S3). (C) Same as (A) for where resource depletion stops at some nonzero combination of concentrations (dashed gray line), e.g., when net growth rate reaches zero in a chemostat (section S3D).

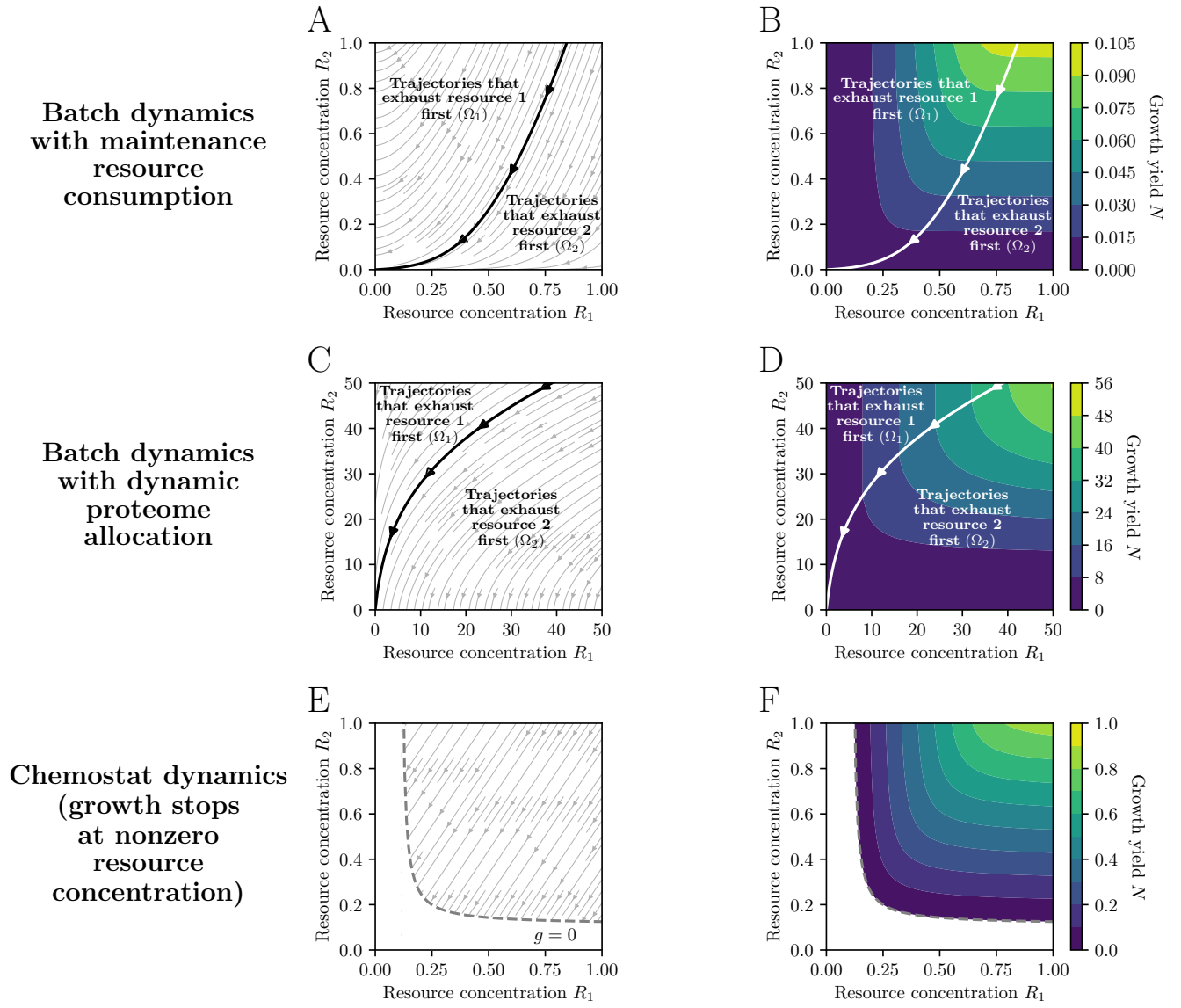

Fig. S6. Yield limitation in different mechanistic models. (A) Model of batch dynamics in which the population consumes resources for maintenance as well as for growth (section S3B). This causes stoichiometry to vary with resource concentration, and so depletion trajectories (gray stream lines) are curved. The black line shows the trajectory separating the regions where the first depleted resource is resource 1 (Ω_1) or resource 2 (Ω_2). We use the additive model of growth rate (Table S1, section S2) with parameter values $g_{\max} = 2$, $a_1 = a_2 = 2$, $s_{1,\text{main}} = 0.5$, $s_{2,\text{main}} = 10$, $s_{1,\text{growth}} = 2$, and $s_{2,\text{growth}} = 0.1$. (B) For the model in (A), we calculate the growth yield N after one batch growth cycle for all possible initial resource concentrations. (C) Same as (A) but for a model of batch dynamics in which stoichiometry varies with growth rate according to changes in proteome allocation (section S3C). We use the additive model of growth rate (Table S1, section S2) with parameter values $g_{\max} = 1$, $a_1 = a_2 = 1$, $\theta_{\min} = 0$, $\theta_{\max} = 1$, $s_1^{\text{A}} = s_1^{\text{B}} = 1$, $s_2^{\text{A}} = 10$, and $s_2^{\text{B}} = 0.1$. (D) Same as (B) but for the proteome allocation model in (C). (E) Model of resource consumption in which growth stops at nonzero concentrations of resources, as in a chemostat (section S3D). These concentrations (zero net-growth isocline, ZNGI) are shown as the dashed gray line in the space of concentrations for resources 1 and 2. Gray stream lines show trajectories of resource depletion with constant stoichiometry. We use the additive model of growth rate (Table S1, section S2) and parameter values $g_{\max} = 1$, $d = 0.1$, $a_1 = a_2 = 1$, $s_1 = 1.5$, and $s_2 = 1$. (F) Same as (B) but for the chemostat model in (E).

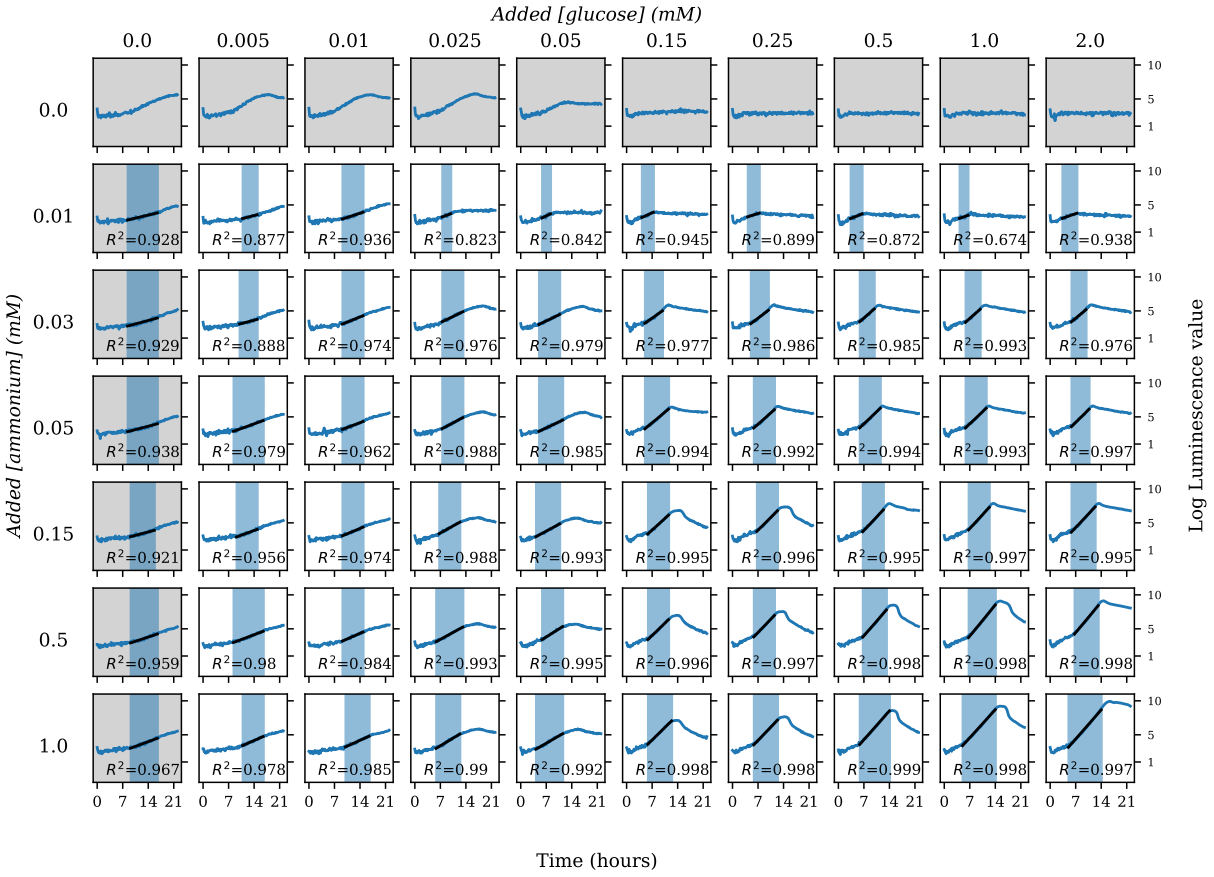

Fig. S7. Luminescence growth curves across glucose and ammonium concentrations for biological replicate 1. Growth curves of luminescent *E. coli* K-12 MG1655 pCS-λ (31) with each well having a different starting concentration of glucose and ammonium (Dataset S1, Materials and Methods). Data shown here is for replicate 1. The observed maximum growth rates, fitted from the data, are overlayed in black lines with the R^2 value. The fitting interval (exponential growth phase) is shown in colored shading. Gray shading indicates wells where the added concentration of either glucose or ammonium was zero. We skipped fits for some wells due to low quality.

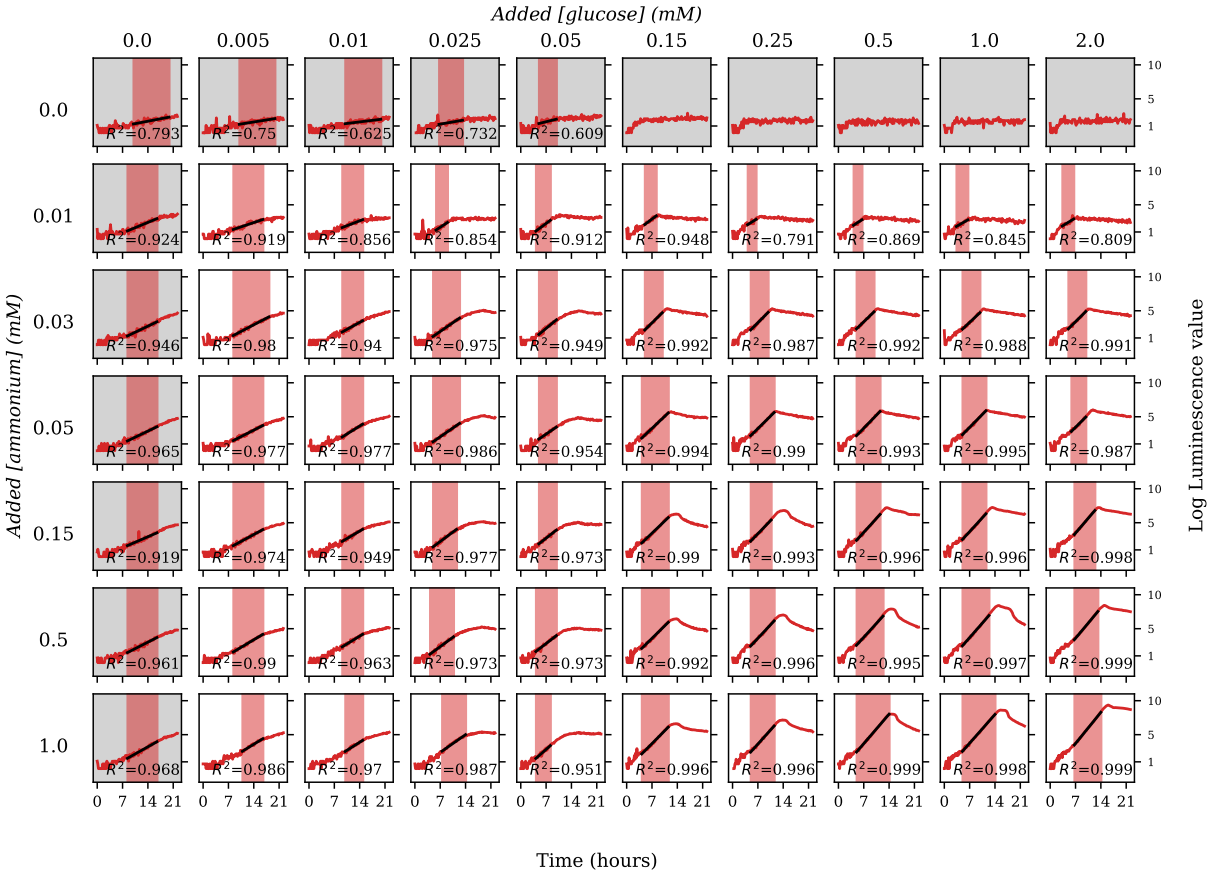

Fig. S8. Luminescence growth curves across glucose and ammonium concentrations for biological replicate 2. Same as Fig. S7 but for replicate 2.

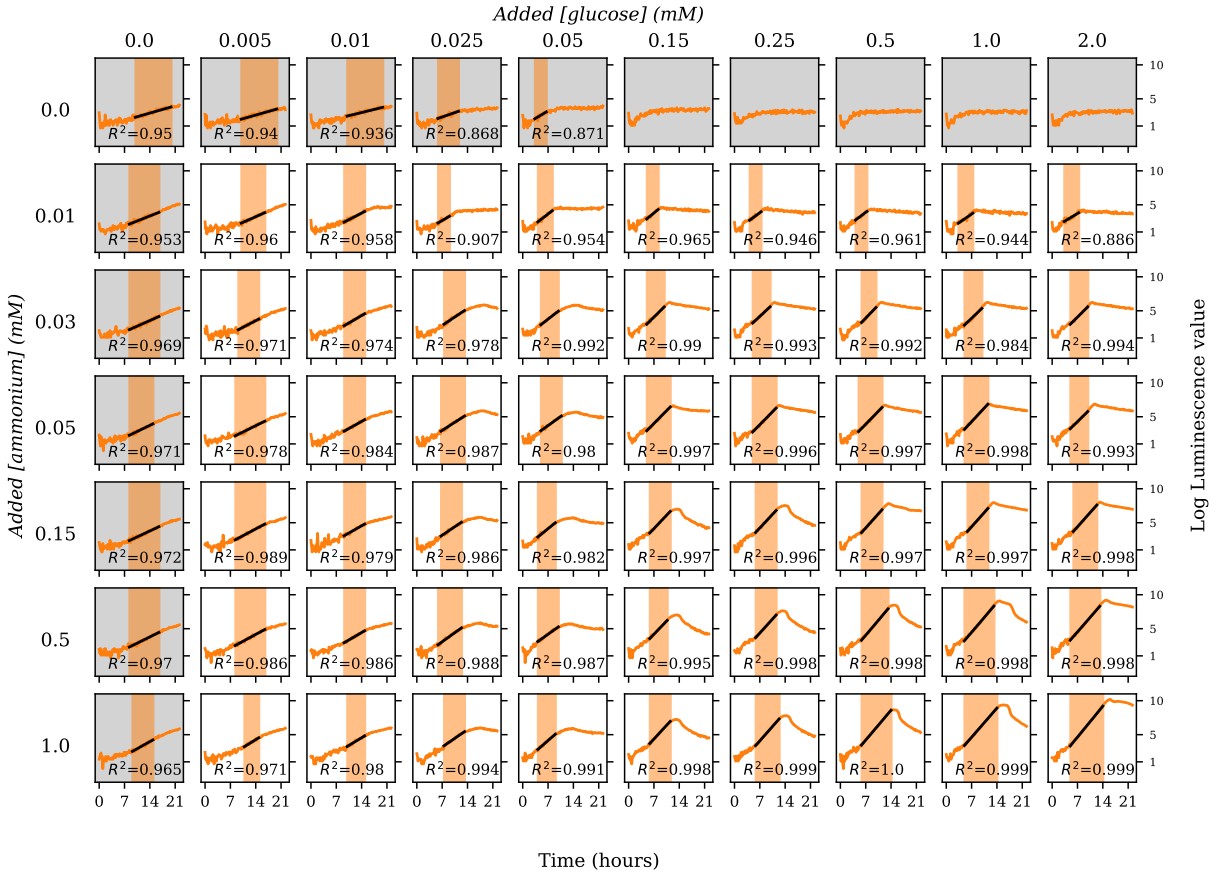

Fig. S9. Luminescence growth curves across glucose and ammonium concentrations for biological replicate 3. Same as Fig. S7 but for replicate 3.

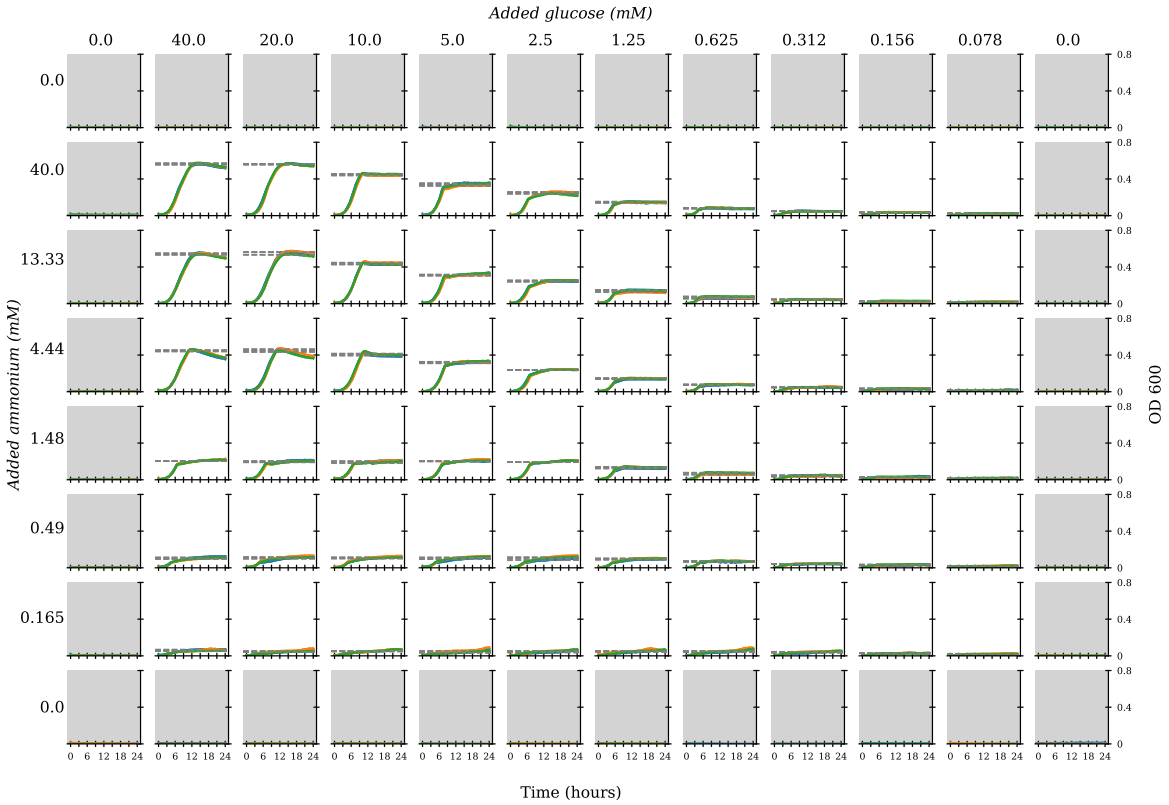

Fig. S10. Optical density growth curves across glucose and ammonium concentrations. Growth curves of OD at 600 nm for *E. coli* MG1655 with each well having a different starting concentration of glucose and ammonium (Dataset S2, Materials and Methods). Triplicate growth curves are shown as colored lines; the observed growth yields, fitted from the data (as averaged OD from 12 to 16 hours), are overlayed in gray dotted lines. Gray shading indicates wells were the concentration of either glucose or ammonium was zero. See Fig. S11 for the same data plotted on a log scale.

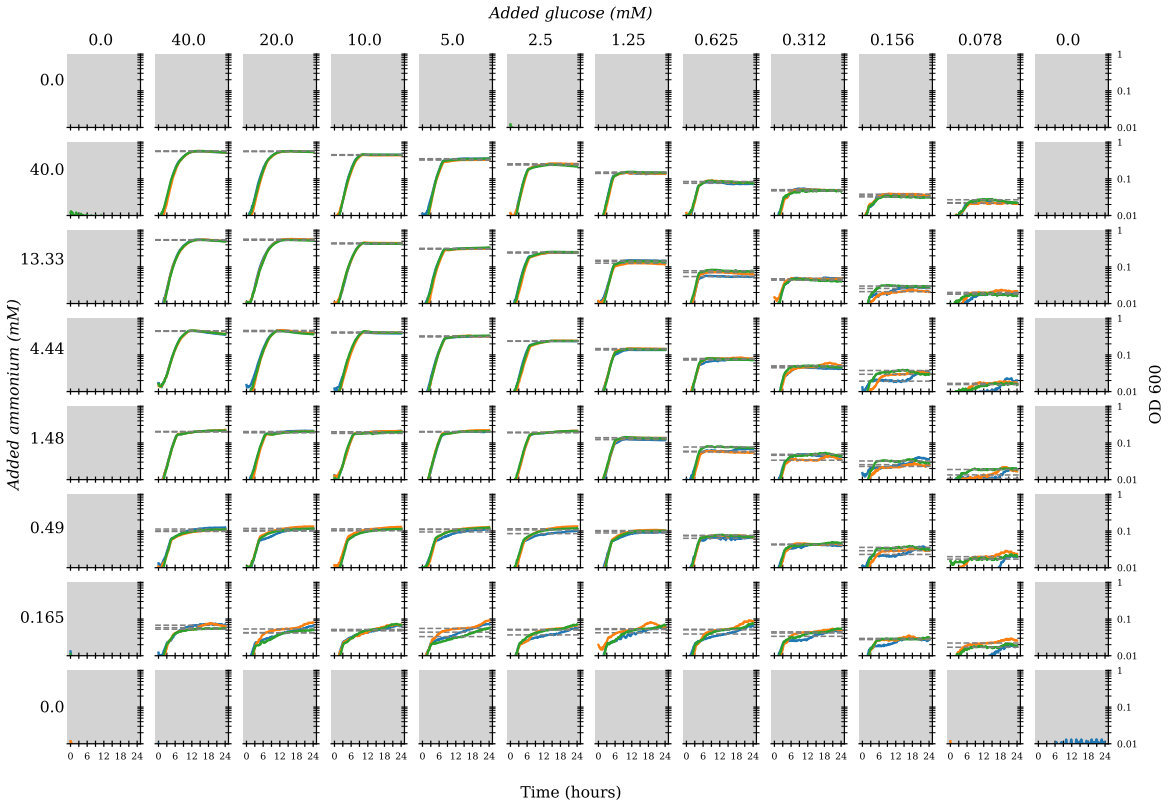

Fig. S11. Log optical density growth curves across glucose and ammonium concentrations. Same as Fig. S10 but with OD plotted on a logarithmic scale.

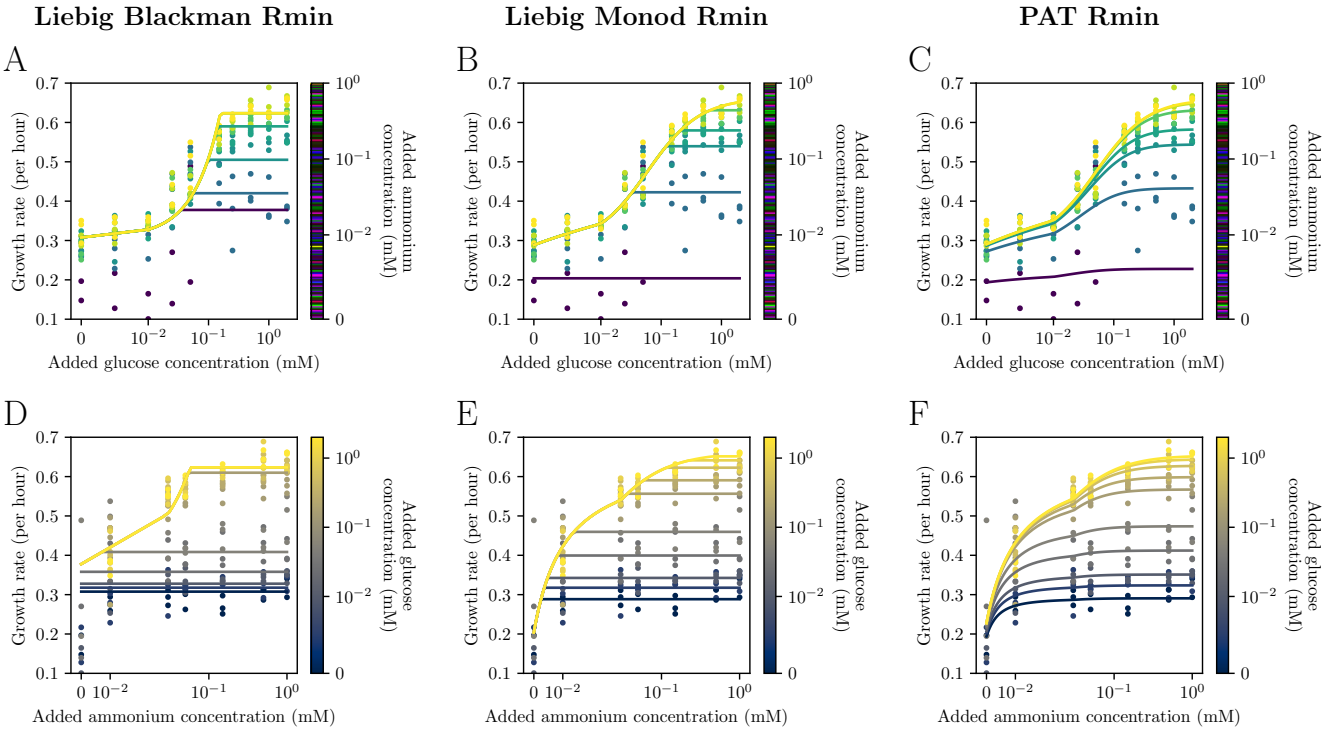

Fig. S12. Example fits of growth rate scans to models. Same as Fig. 2B but showing fits to the Liebig Blackman (A), Liebig Monod (B), and Poisson arrival time (C) models, all with nonzero minimum resource concentration parameters (Table S1, section S2). Panels (D)–(F) are the same but projected onto the axis of ammonium concentrations, with colors showing glucose concentrations.

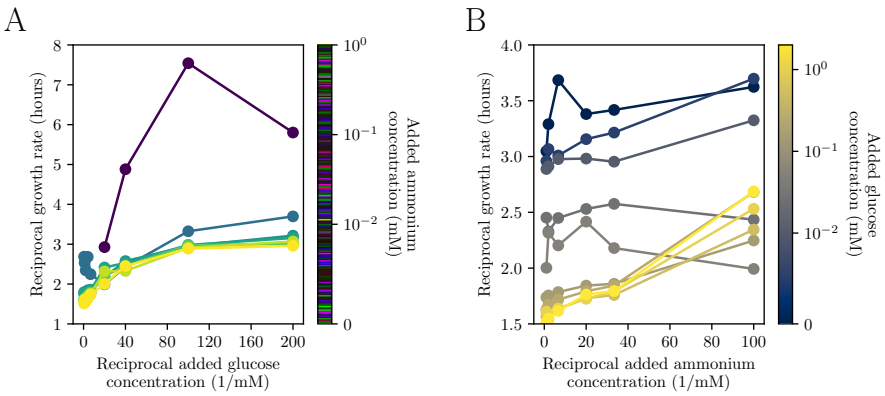

Fig. S13. Lineweaver-Burke plots of growth rate vs. resource concentration. Plot of reciprocal growth rate vs. reciprocal resource concentration, projected onto glucose concentrations (A) and ammonium concentrations (B), with colors in each panel representing the other resource concentration not plotted along the horizontal axis. Monod dependence appears as a straight line plotted this way. Points are averages over three experimental replicates.

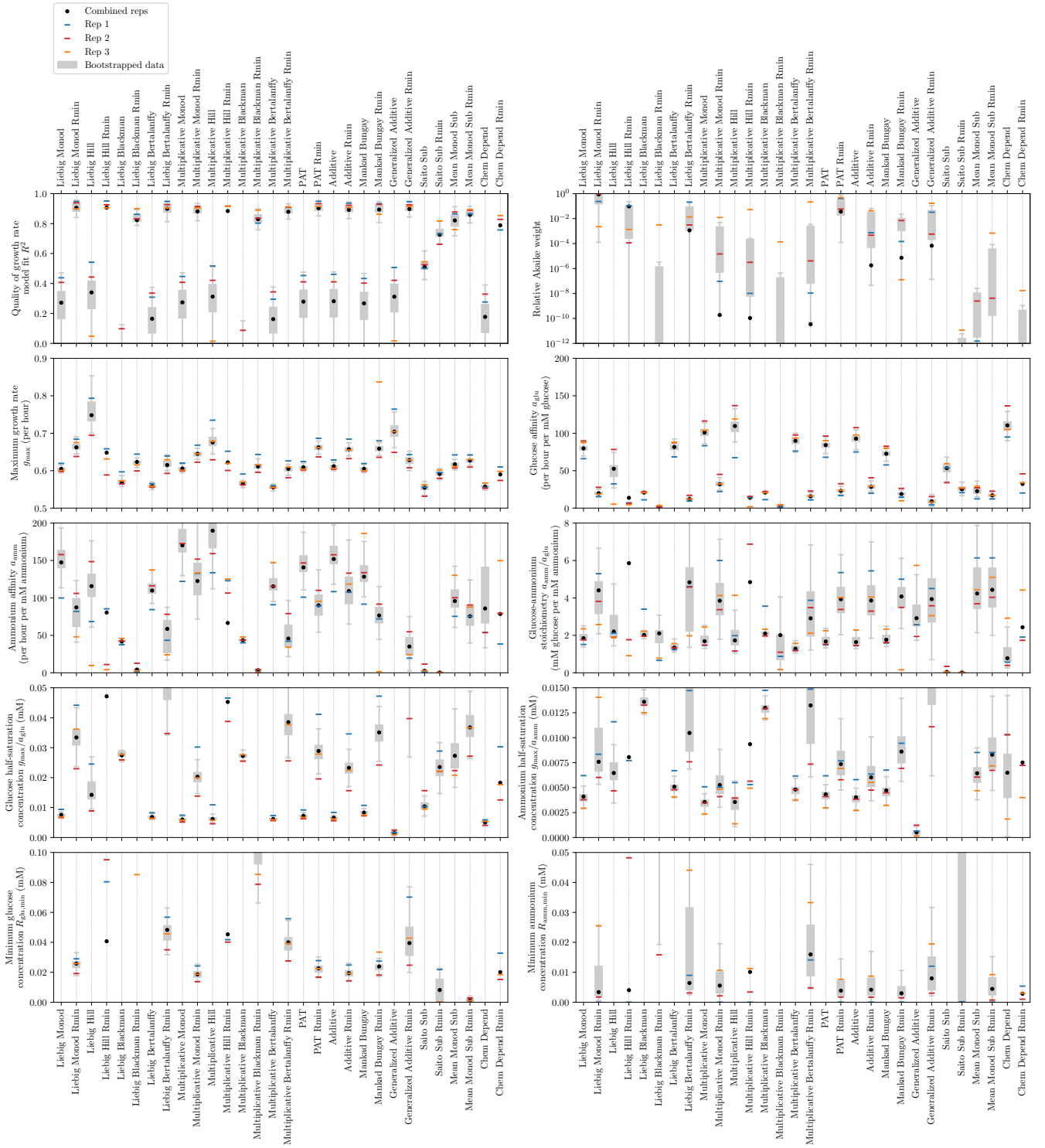

Fig. S14. Fits of growth rate scans to models. Each panel shows a different statistic from fitting the growth rate scan data to all models (across horizontal axes). The black dots mark statistics for fits to all three replicates together; the three colored bars show the statistics from the three replicates fitted separately. The gray boxes (first to third quartiles, with the whiskers extending to 1.5 times the interquartile range above and below) show the distributions of these statistics across 100 data sets bootstrapped from the three replicates (Materials and Methods). The thin vertical lines are to guide the eye to the model names on the bottom and top horizontal axes.

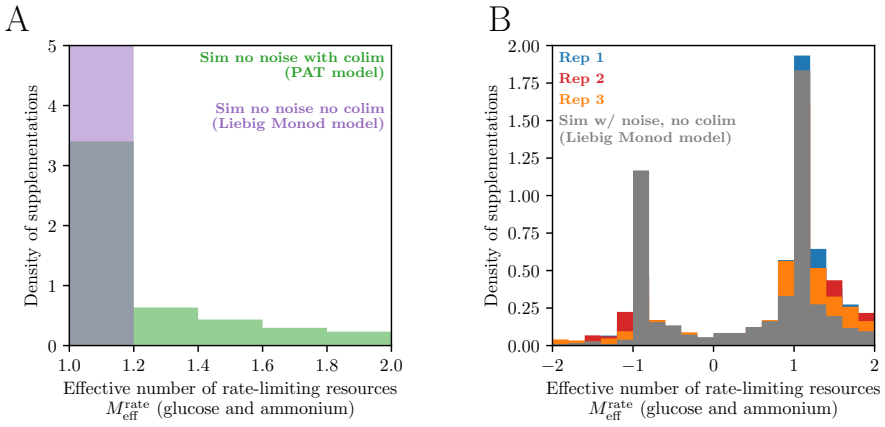

Fig. S15. Growth rate colimitation across supplementations. (A) Distribution of $M_{\text{eff}}^{\text{rate}}$ for glucose and ammonium (not counting implicit factors; section S1D) across supplementations for simulated growth rate models without resource colimitation (purple, Liebig Monod model; Table S1, section S2) and with resource colimitation (green, Poisson arrival time model; Table S1, section S2), in the absence of measurement noise. (B) Same as (A) but for experimental replicates (blue, red, and orange) of growth rate measurements and for one simulated data set with noise (gray, Liebig Monod model; Table S1, section S2).

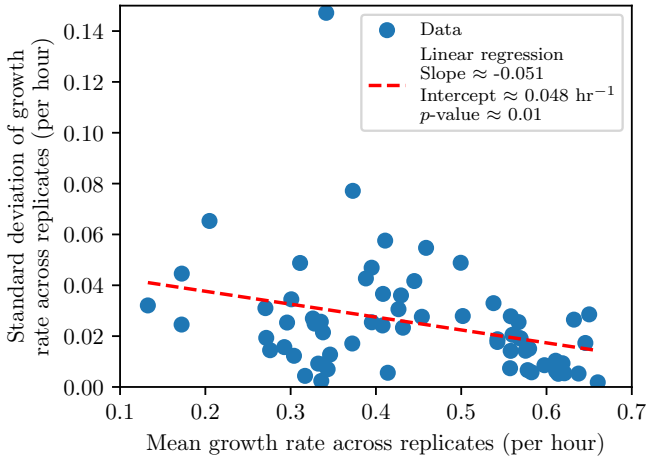

Fig. S16. Variation of growth rate measurements across replicates. Scaling of mean rate vs. standard deviation of rate across three experimental replicates (blue points). The red dashed line is the linear regression with parameters shown in the legend.

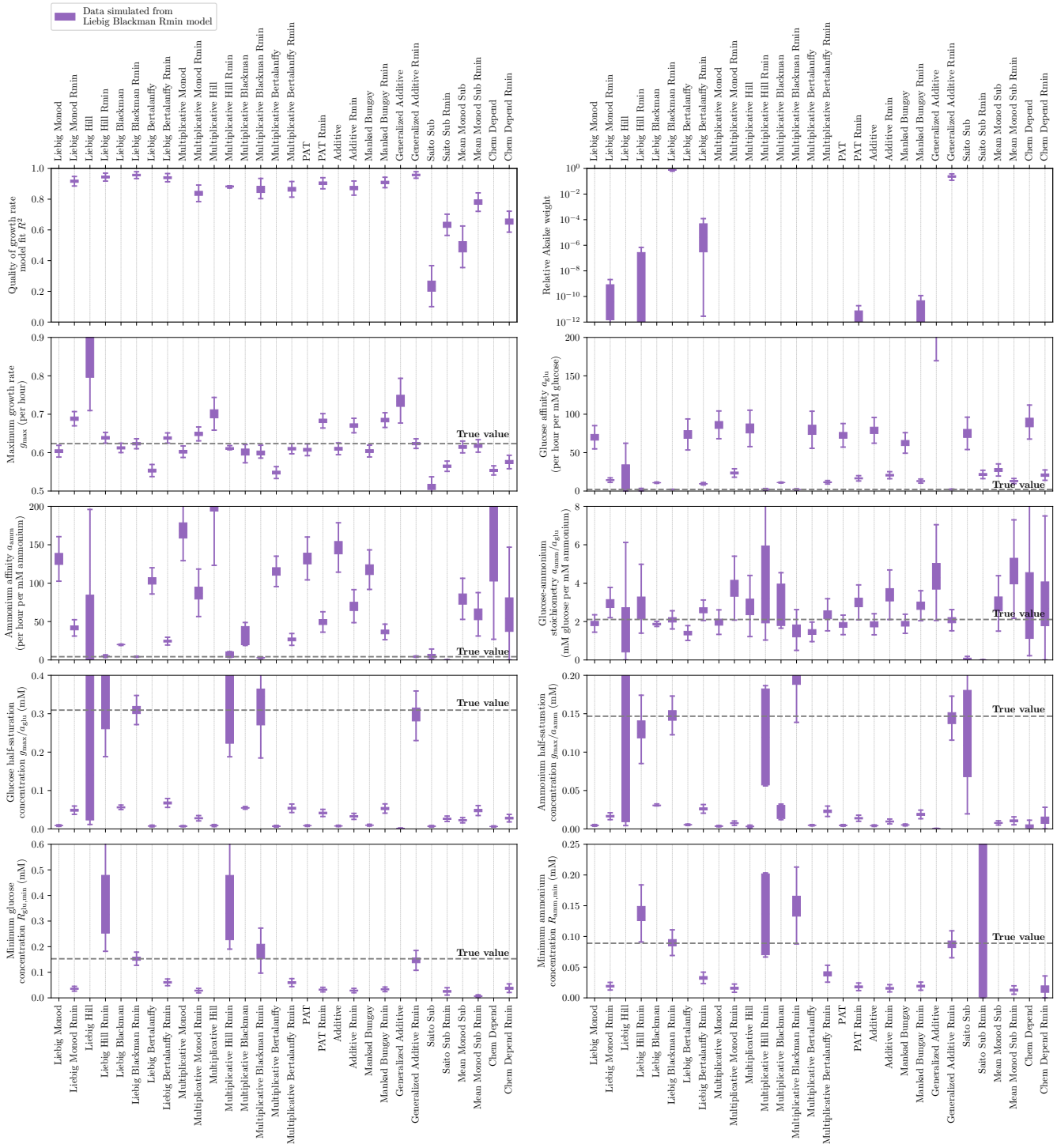

Fig. S17. Fits of simulated (Liebig Blackman model) growth rate scans to models. Similar to Fig. S14 but for fits to data simulated from the Liebig Blackman model (Materials and Methods; Table S1, section S2) with parameters from that model's fit to the experimental growth rate data ($g_{\max} \approx 0.62$ per hour, $a_{\mathrm{glu}} \approx 2.01$ per hour per mM glucose, $a_{\mathrm{amm}} \approx 4.2$ per hour per mM ammonium, $R_{\mathrm{glu,min}} \approx 0.15$ mM, $R_{\mathrm{amm,min}} \approx 0.089$ mM; Dataset S1). We incorporated experimental noise to the simulations by adding a Gaussian-distributed random number to each measurement with mean zero and standard deviation that is a linear function of the mean according to the linear regression in Fig. S16. The purple boxes (first to third quartiles, with the whiskers extending to 1.5 times the interquartile range above and below) show the distributions of these statistics across 10^4 simulated data sets. The true values of the parameters used in the simulations are marked by horizontal dashed lines.

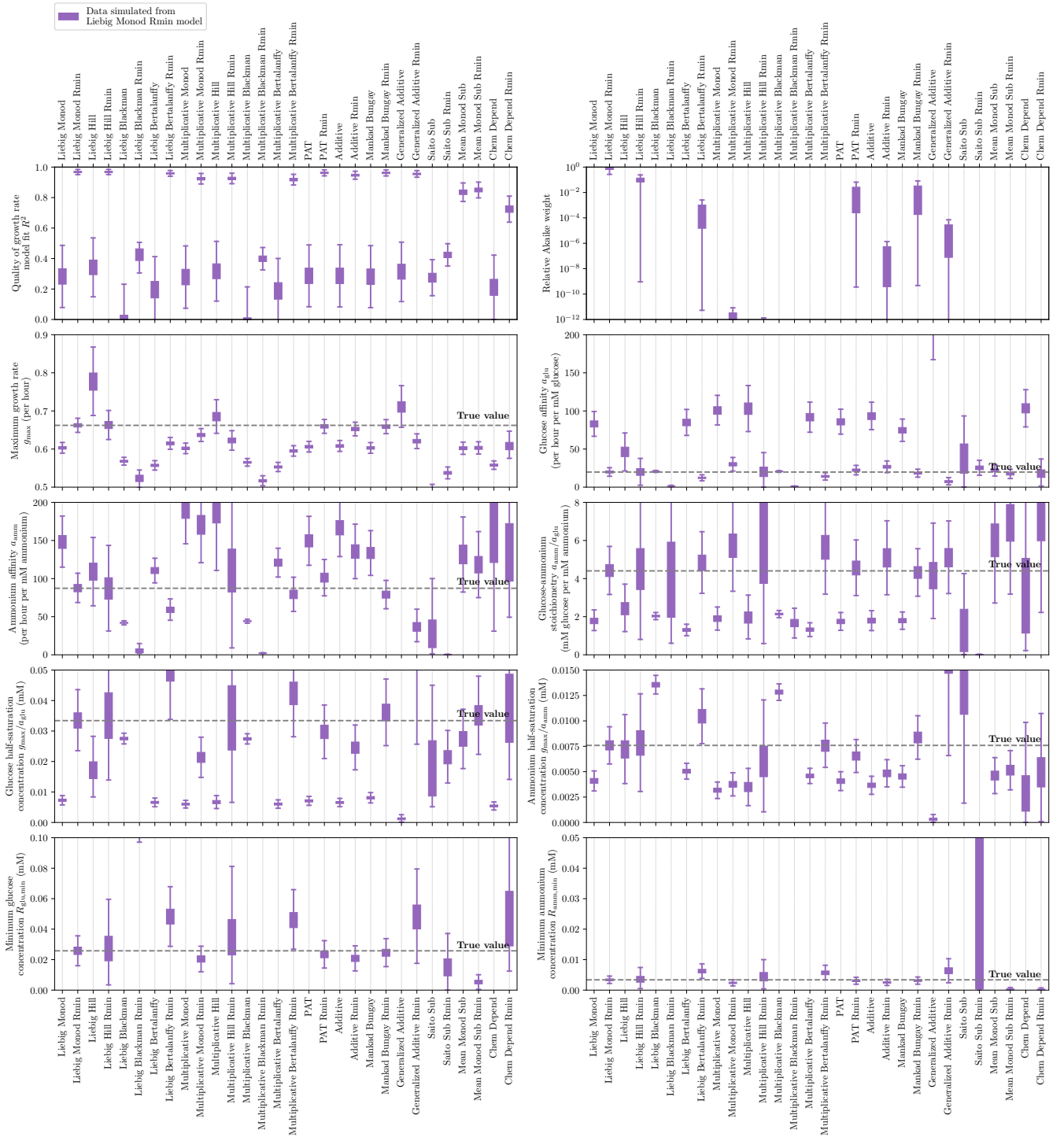

Fig. S18. Fits of simulated (Liebig Monod model) growth rate scans to models. Same as Fig. S17 but for 10^4 simulations of the Liebig Monod model (Materials and Methods; Table S1, section S2) with parameters from that model's fit to the experimental growth rate data ($g_{\max} \approx 0.66$ per hour, $a_{\mathrm{glu}} \approx 20$ per hour per mM glucose, $a_{\mathrm{amm}} \approx 87$ per hour per mM ammonium, $R_{\mathrm{glu,min}} \approx 0.026$ mM, $R_{\mathrm{amm,min}} \approx 0.0034$ mM; Dataset S1).

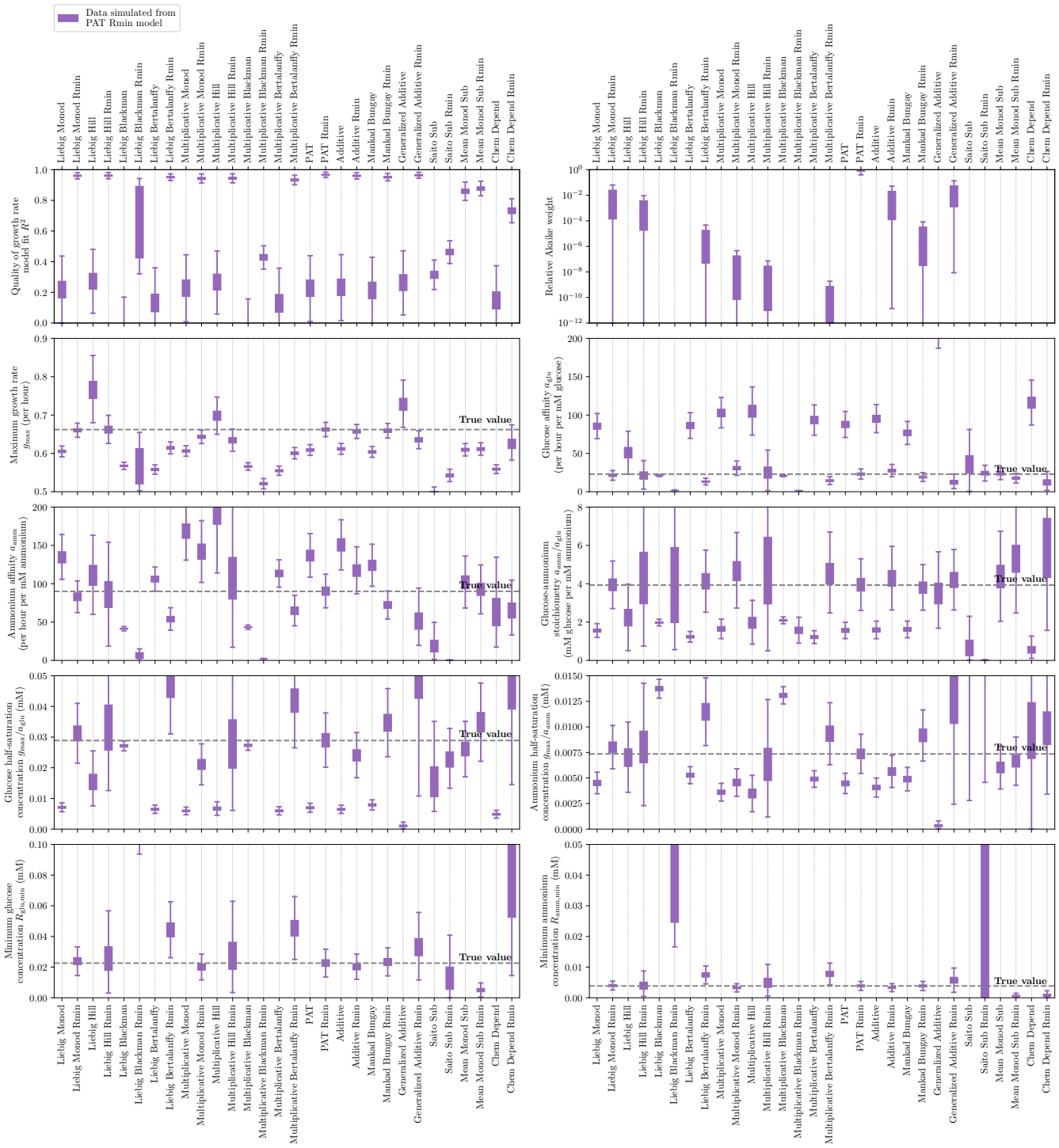

Fig. S19. Fits of simulated (PAT model) growth rate scans to models. Same as Fig. S17 but for 10^4 simulations of the Poisson arrival time model (Materials and Methods; Table S1, section S2) with parameters from that model's fit to the experimental growth rate data ($g_{\max} \approx 0.66$ per hour, $a_{\mathrm{glu}} \approx 23$ per hour per mM glucose, $a_{\mathrm{amm}} \approx 90$ per hour per mM ammonium, $R_{\mathrm{glu,min}} \approx 0.023$ mM, $R_{\mathrm{amm,min}} \approx 0.0039$ mM; Dataset S1).

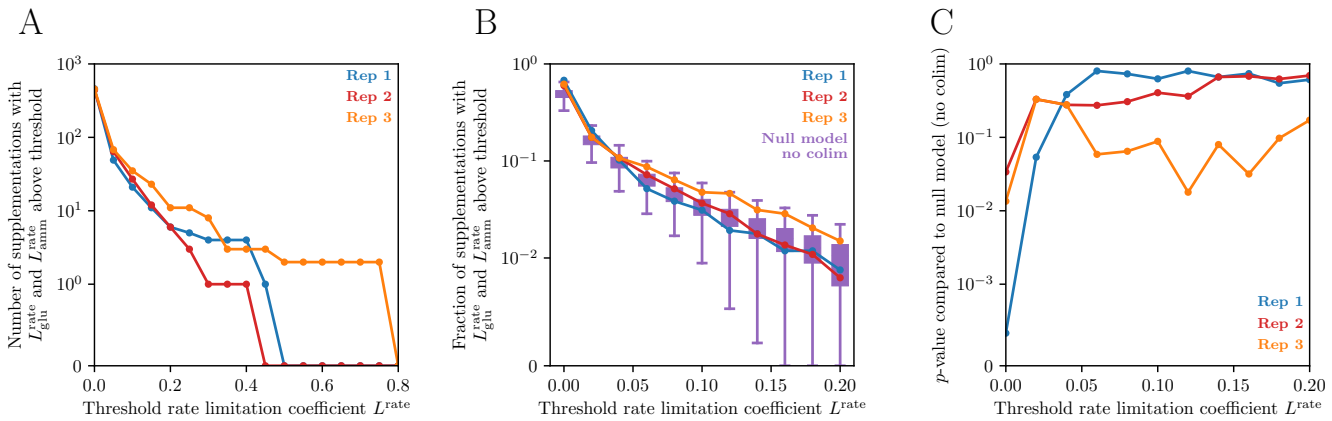

Fig. S20. Testing significance of growth rate colimitation at different thresholds. (A) Number of supplementations (Materials and Methods) with growth rate limitation coefficients for both glucose $L^{\text{rate}}_{\text{glu}}$ and ammonium $L^{\text{rate}}_{\text{amm}}$ above a given threshold, as a function of that threshold. (B) Fraction of supplementations with growth rate limitation coefficients for both glucose $L^{\text{rate}}_{\text{glu}}$ and ammonium $L^{\text{rate}}_{\text{amm}}$ above a given threshold, as a function of that threshold. Colored dots represent each of the three experimental replicates, and the purple boxes show distributions across 10^4 data sets simulated from a model with no colimitation between glucose and ammonium (Liebig Monod model, Table S1, section S2; Materials and Methods). (C) p-values of the observed fractions of supplementations with growth rate colimitation between glucose and ammonium as functions of the limitation threshold.

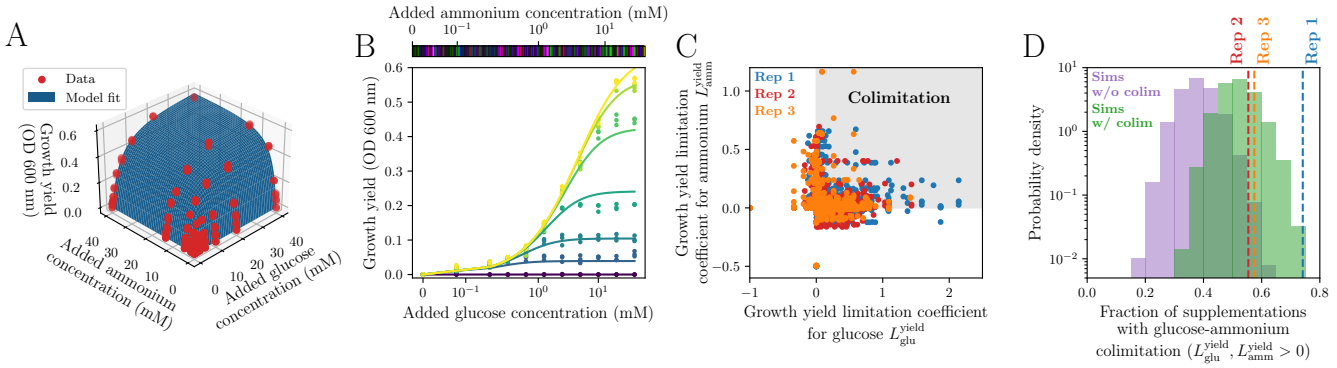

Fig. S21. Measuring growth yield colimitation in laboratory conditions. Same as Fig. 2 but for growth yield data (Dataset S2; see Figs. S10 and S11 for growth curves). In (A) the blue surface is a model fit to all replicate measurements (Poisson arrival time model with $N_{\max} \approx 0.68$ OD, $a_{\mathrm{glu}} \approx 0.15$ OD/mM glucose, and $a_{\mathrm{amm}} \approx 0.25$ OD/mM ammonium; Materials and Methods; Dataset S2). The p-values in (D) are $p = 0$ for replicate 1, $p = 0.0032$ for replicate 2, and $p = 0.0012$ for replicate 3.

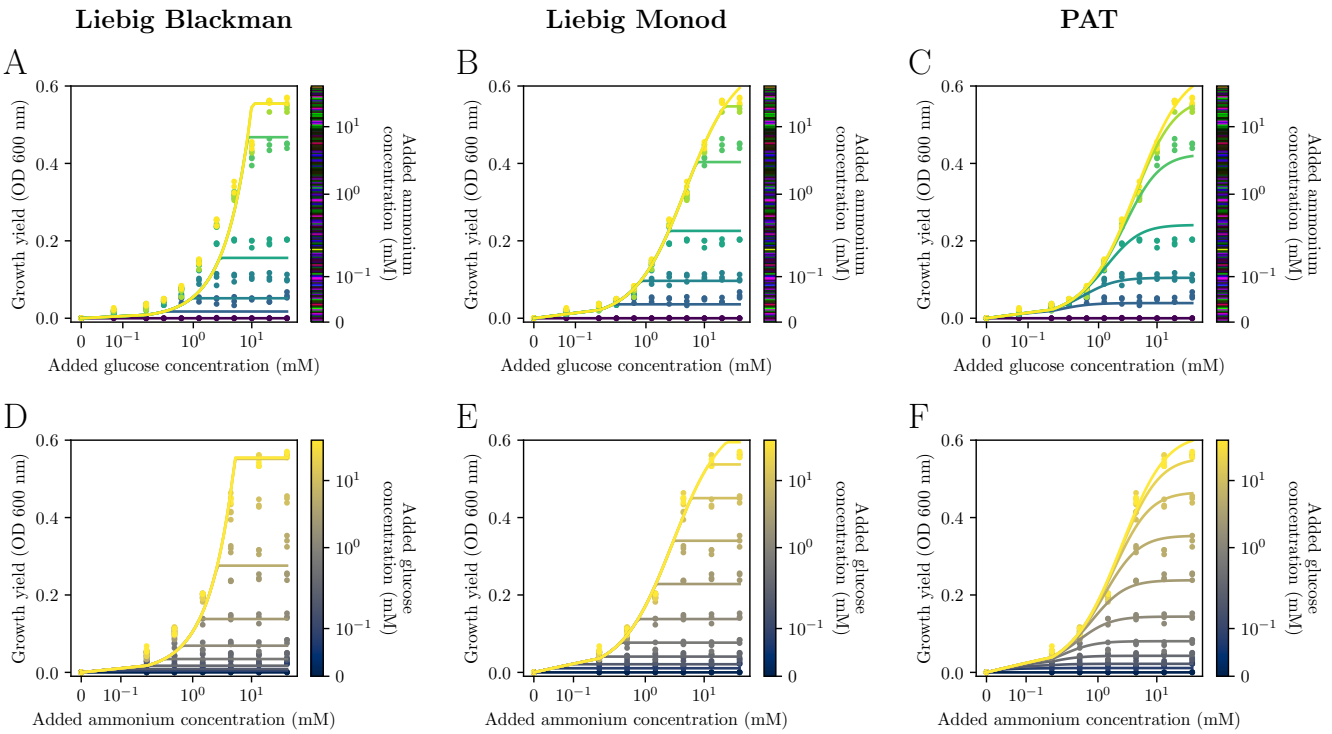

Fig. S22. Example fits of growth yield scans to models. Same as Fig. S12 but for growth yield data.

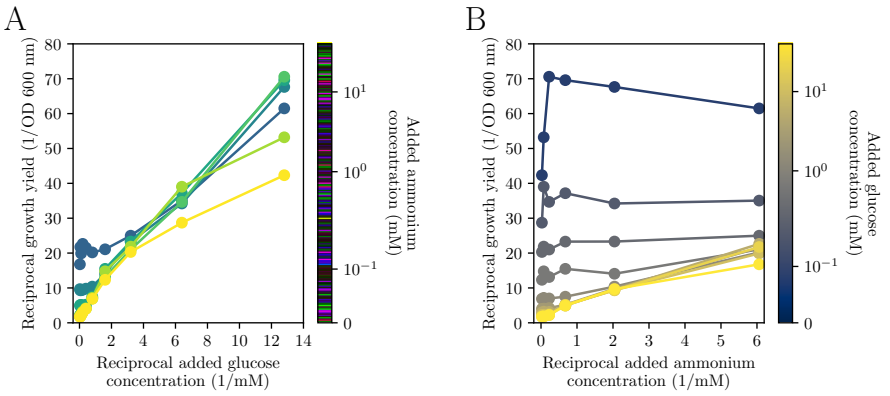

Fig. S23. Lineweaver-Burke plots of growth yield vs. resource concentration. Same as Fig. S13 but for growth yield.

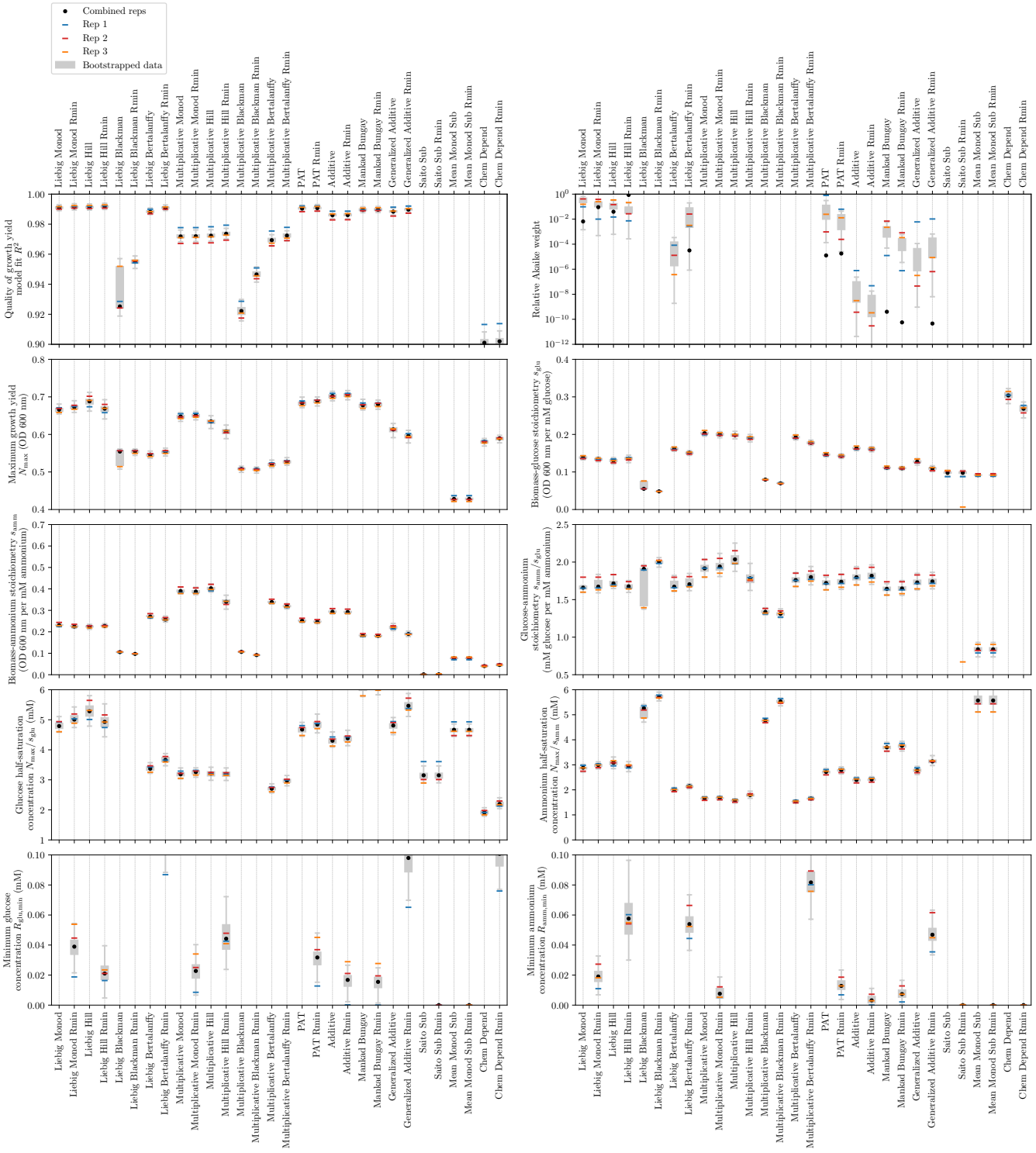

Fig. S24. Fits of growth yield scans to models. Same as Fig. S14 but for fits to growth yield data.

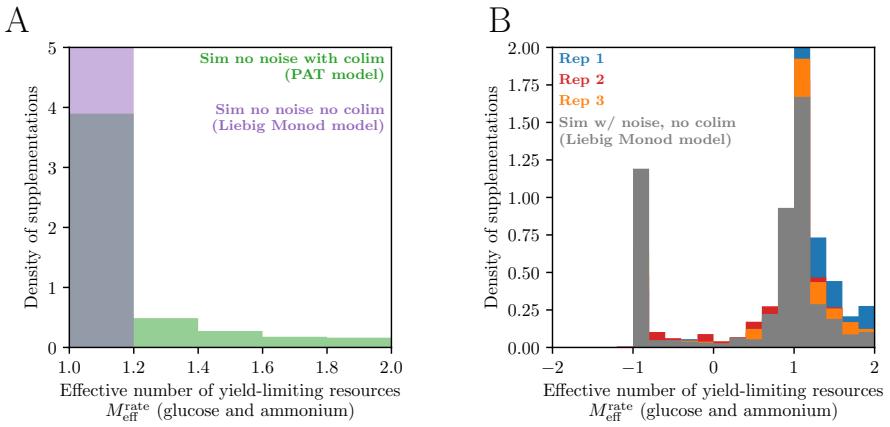

Fig. S25. Growth yield colimitation across supplementations. Same as Fig. S15 but for growth yield.

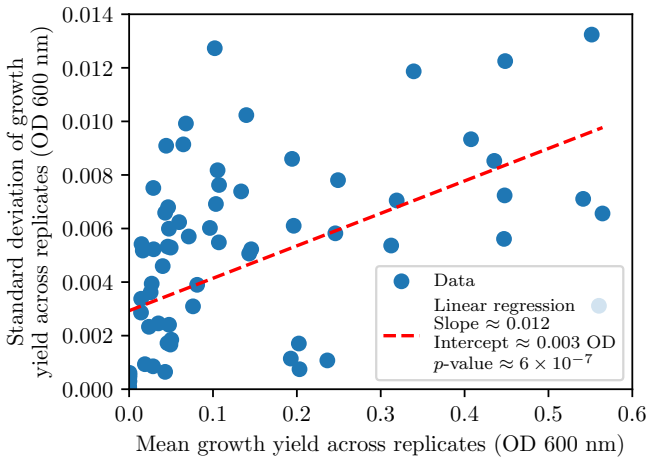

Fig. S26. Variation of growth yield measurements across replicates. Same as Fig. S16 but for growth yield data.

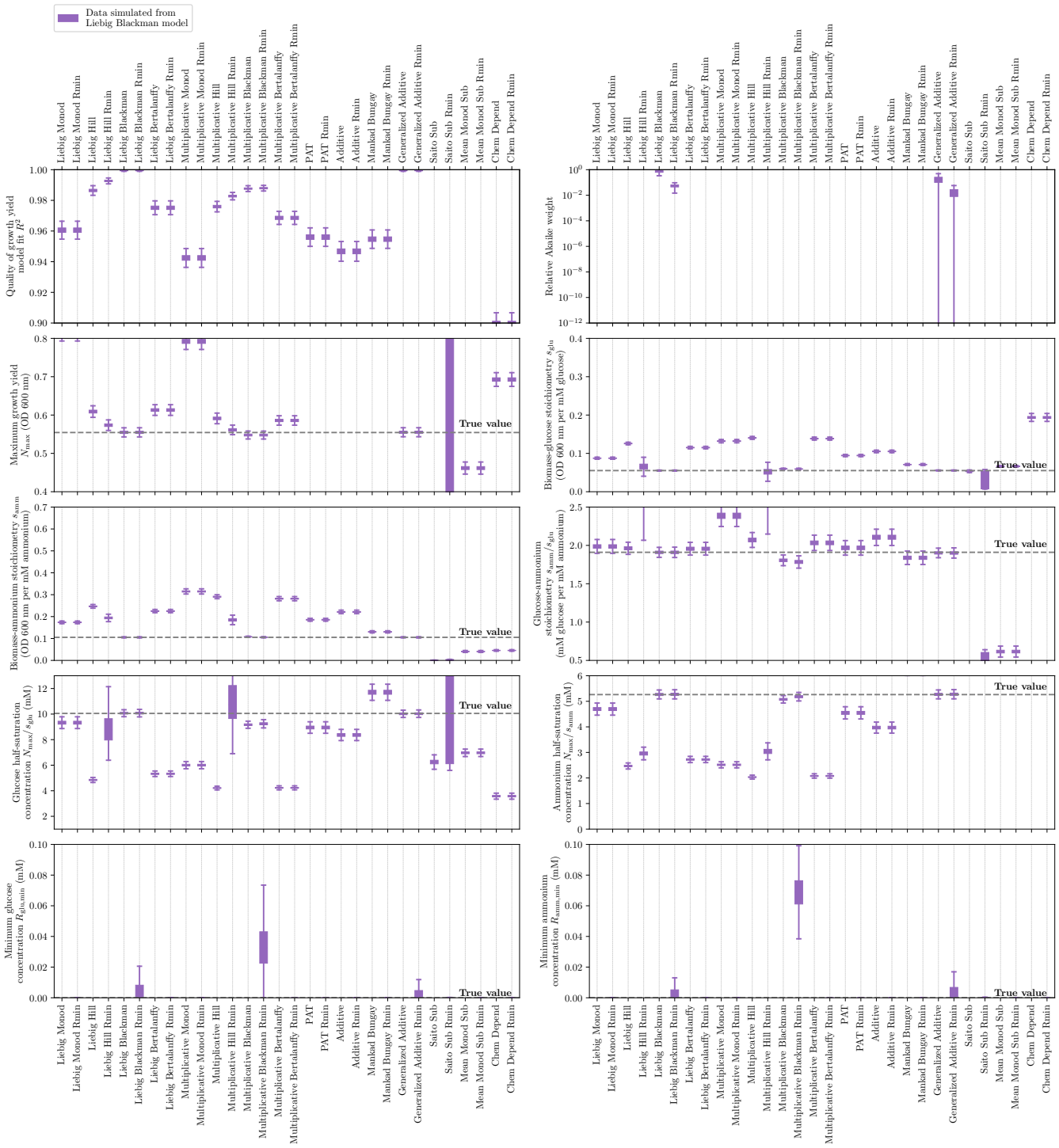

Fig. S27. Fits of simulated (Liebig Blackman model) growth yield scans to models. Same as Fig. S17 but for 10^4 simulations of the Liebig Blackman model (Materials and Methods; Table S1, section S2) with parameters from that model's fit to the experimental growth yield data ($N_{\max} \approx 0.55$ OD, $a_{\mathrm{glu}} \approx 0.055$ OD/mM glucose, $a_{\mathrm{amm}} \approx 0.11$ OD/mM ammonium, $R_{\mathrm{glu,min}} = 0$, and $R_{\mathrm{amm,min}} = 0$; Dataset S2).

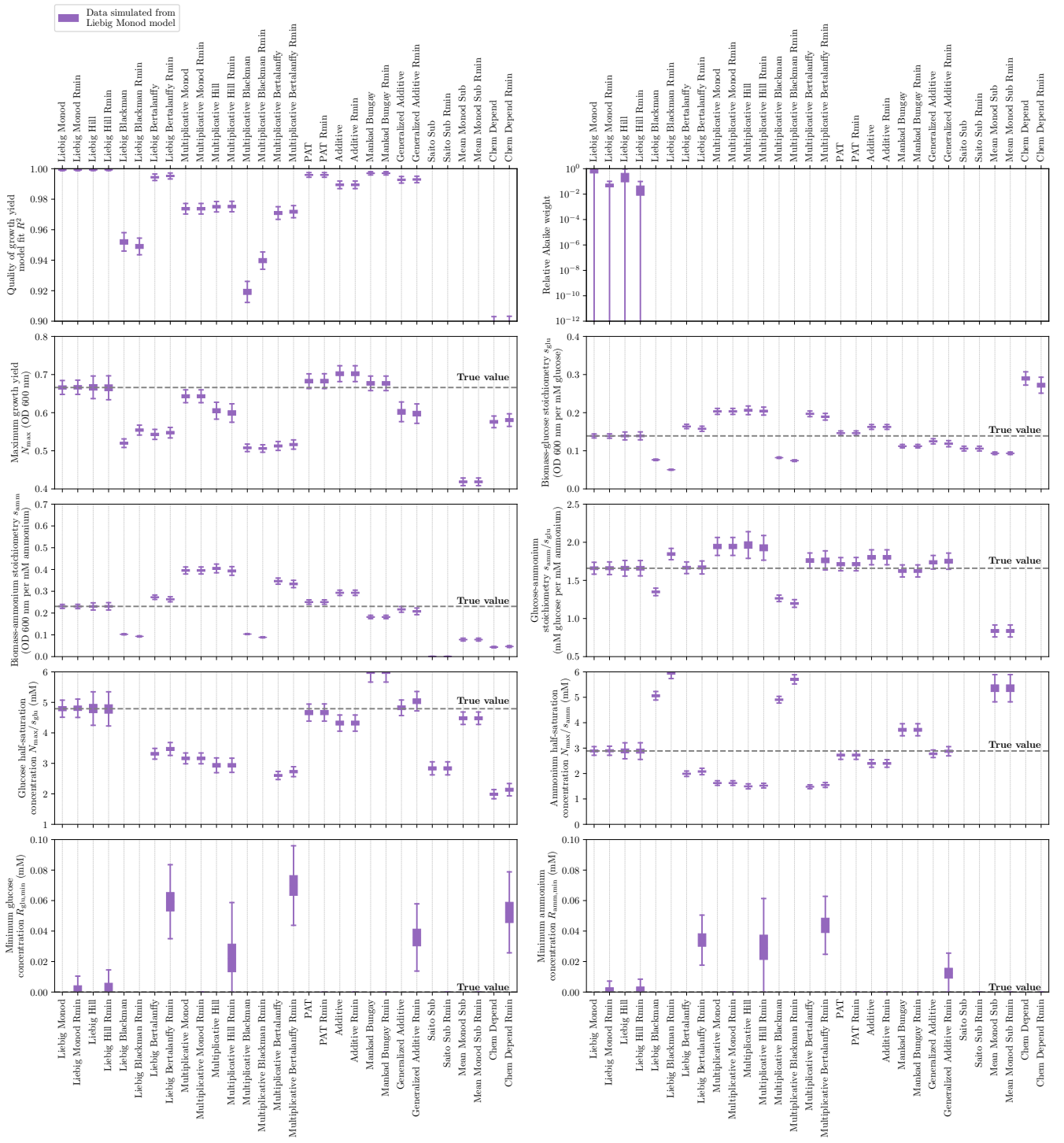

Fig. S28. Fits of simulated (Liebig Monod model) growth yield scans to models. Same as Fig. S17 but for 10^4 simulations of the Liebig Monod model (Materials and Methods; Table S1, section S2) with parameters from that model's fit to the experimental growth yield data ($N_{max} \approx 0.67$ OD, $a_{glu} \approx 0.14$ OD/mM glucose, $a_{amm} \approx 0.23$ OD/mM ammonium, $R_{glu,min} = 0$, and $R_{amm,min} = 0$; Dataset S2).

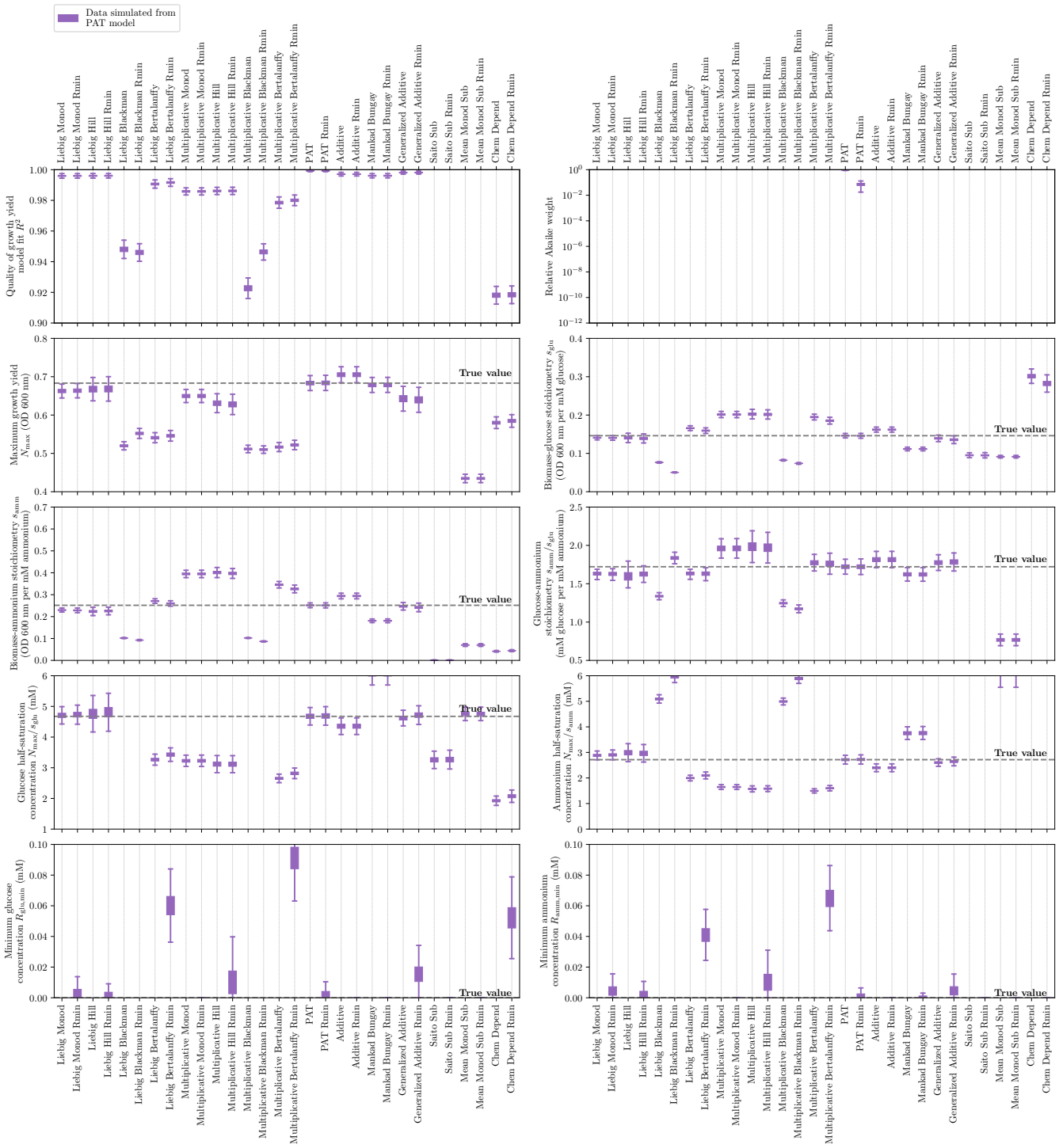

Fig. S29. Fits of simulated (PAT model) growth yield scans to models. Same as Fig. S17 but for 10^4 simulations of the Poisson arrival time model (Materials and Methods; Table S1, section S2) with parameters from that model's fit to the experimental growth yield data ($N_{\max} \approx 0.68$ OD, $a_{\mathrm{glu}} \approx 0.15$ OD/mM glucose, $a_{\mathrm{amm}} \approx 0.25$ OD/mM ammonium, $R_{\mathrm{glu,min}} = 0$, and $R_{\mathrm{amm,min}} = 0$; Dataset S2).

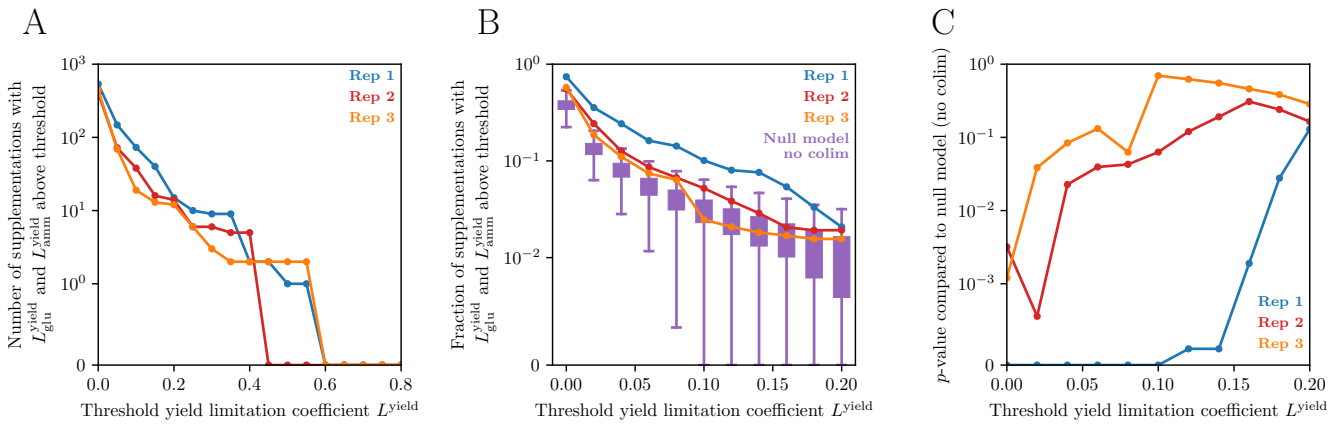

Fig. S30. Testing significance of growth yield colimitation at different thresholds. Same as Fig. S20 but for growth yield.

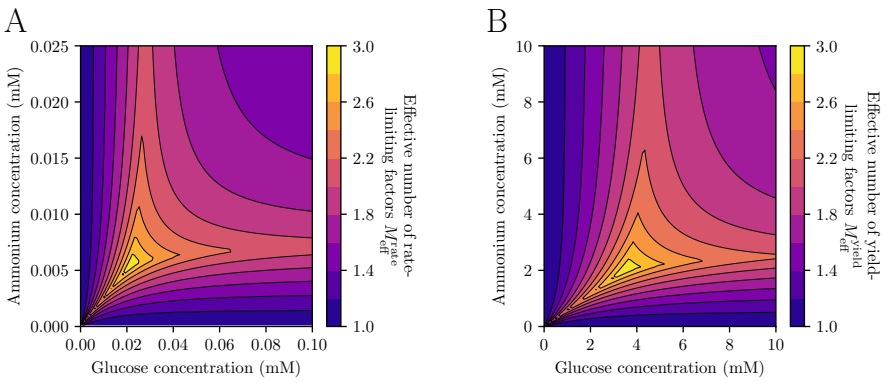

Fig. S31. Effective number of limiting factors for growth rate and growth yield. (A) The effective number of rate-limiting factors as a function of glucose and ammonium concentrations, implied by the model fit to the growth rate scan data in Fig. 2A (Poisson arrival time model with $g_{\max} \approx 0.66$ per hour, $s_{\mathrm{glu}} \approx 23$ per hour per mM glucose, $s_{\mathrm{amm}} \approx 90$ per hour per mM ammonium; $R_{\mathrm{glu,min}} \approx 0.023$ mM, $R_{\mathrm{amm,min}} \approx 0.0039$ mM; Materials and Methods; Dataset S1). (B) The effective number of yield-limiting factors as a function of glucose and ammonium concentrations, implied by the model fit to the growth yield scan data in Fig. S21A (Poisson arrival time model with $N_{\max} \approx 0.68$ OD, $a_{\mathrm{glu}} \approx 0.15$ OD/mM glucose, and $a_{\mathrm{amm}} \approx 0.25$ OD/mM ammonium; Materials and Methods; Dataset S2).

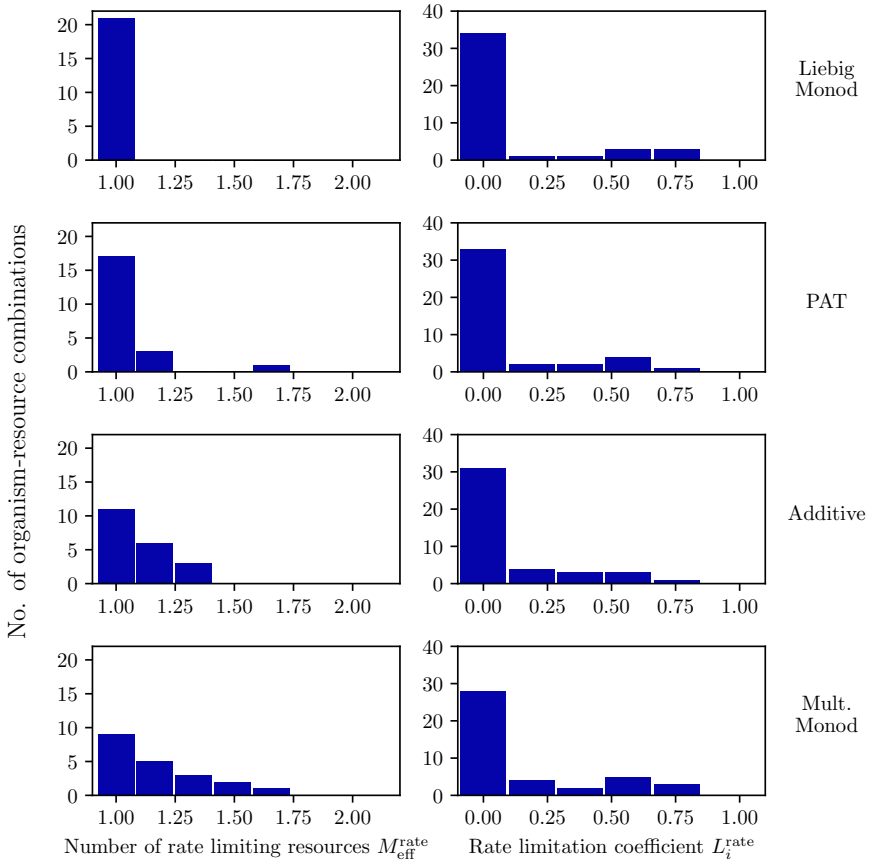

Fig. S32. Histograms of number of rate-limiting resources and rate limitation coefficients for collected organism-resource combinations. Same data as in Fig. 4B,C but plotted as histograms across each example growth rate model (Dataset S3; Table S1, section S2).

SI Dataset S1 (Dataset_S1.xlsx)

Scan of *E. coli* growth rates across glucose and ammonium concentrations. This file includes Tab 1 (growth rates), Tabs 2-4 (raw luminescence data for each of the three replicate experiments), Tab 5 (map of glucose and ammonium concentrations used on the plate), and Tabs 6–9 (summaries of model fits).

SI Dataset S2 (Dataset_S2.xlsx)

Scan of *E. coli* growth yields across glucose and ammonium concentrations. This file includes Tab 1 (growth yields), Tabs 2-4 (raw OD data for each of the three replicate experiments), Tab 5 (map of glucose and ammonium concentrations used on the plate), and Tabs 6–9 (summaries of model fits).

SI Dataset S3 (Dataset_S3.xlsx)

Monod growth data and resource concentration data, collected from the literature.